Handbook on Face Gear Drives With a Spur Involute Pinion

F.L. Litvin and A. Egelja
University of Illinois at Chicago, Chicago, Illinois

J. Tan, D.Y-D. Chen, and G. Heath
The Boeing Company, Mesa, Arizona

20000815 026

March 2000

DTIC QUALITY INSPECTED 4

Since its founding, NASA has been dedicated to the advancement of aeronautics and space science. The NASA Scientific and Technical Information (STI) Program Office plays a key part in helping NASA maintain this important role.

The NASA STI Program Office is operated by Langley Research Center, the Lead Center for NASA's scientific and technical information. The NASA STI Program Office provides access to the NASA STI Database, the largest collection of aeronautical and space science STI in the world. The Program Office is also NASA's institutional mechanism for disseminating the results of its research and development activities. These results are published by NASA in the NASA STI Report Series, which includes the following report types:

- TECHNICAL PUBLICATION. Reports of completed research or a major significant phase of research that present the results of NASA programs and include extensive data or theoretical analysis. Includes compilations of significant scientific and technical data and information deemed to be of continuing reference value. NASA's counterpart of peer-reviewed formal professional papers but has less stringent limitations on manuscript length and extent of graphic presentations.

- TECHNICAL MEMORANDUM. Scientific and technical findings that are preliminary or of specialized interest, e.g., quick release reports, working papers, and bibliographies that contain minimal annotation. Does not contain extensive analysis.

- CONTRACTOR REPORT. Scientific and technical findings by NASA-sponsored contractors and grantees.

- CONFERENCE PUBLICATION. Collected papers from scientific and technical conferences, symposia, seminars, or other meetings sponsored or cosponsored by NASA.

- SPECIAL PUBLICATION. Scientific, technical, or historical information from NASA programs, projects, and missions, often concerned with subjects having substantial public interest.

- TECHNICAL TRANSLATION. English-language translations of foreign scientific and technical material pertinent to NASA's mission.

Specialized services that complement the STI Program Office's diverse offerings include creating custom thesauri, building customized data bases, organizing and publishing research results . . . even providing videos.

For more information about the NASA STI Program Office, see the following:

- Access the NASA STI Program Home Page at *http://www.sti.nasa.gov*

- E-mail your question via the Internet to help@sti.nasa.gov

- Fax your question to the NASA Access Help Desk at (301) 621-0134

- Telephone the NASA Access Help Desk at (301) 621-0390

- Write to:
  NASA Access Help Desk
  NASA Center for AeroSpace Information
  7121 Standard Drive
  Hanover, MD 21076

NASA/CR—2000-209909   ARL–CR–447

U.S. ARMY
RESEARCH LABORATORY

DARPA

Handbook on Face Gear Drives With a Spur Involute Pinion

F.L. Litvin and A. Egelja
University of Illinois at Chicago, Chicago, Illinois

J. Tan, D.Y-D. Chen, and G. Heath
The Boeing Company, Mesa, Arizona

National Aeronautics and
Space Administration

Glenn Research Center

March 2000

Available from

CONTENTS

Introduction

This Handbook is the condensed summary of the results of research that was conducted at the Gear Research Laboratory of the University of Illinois at Chicago, and the Boeing Company in Mesa, Arizona. The research was jointly sponsored by DARPA (Defense Advanced Research Projects Agency) and the Boeing Company Phantom Works, with technical and administrative support by NASA. The research at the Gear Research Laboratory was accomplished under the supervision of Professor F. L. Litvin with participation of Dr. A. Egelja, Dr. C.-L. Hsiao, Dr. J. Lu, Dr. I. Seol., Dr. J.-C. Wang and Dr. Y. Zhang. The results of the research are included in [7], [8], [9], [10], and [11]. Face gear durability test evaluations relating to the above projects were performed at the NASA John H. Glenn Research Center. Results of initial and current testing conducted at the NASA GRC are included in [14] and [15].

Face gear drives were previously a subject of research by Y. S. Davidov [2], Liburkin, Litvin [5], [7], Crown Gear B.V. Company [1] and others. The contents of the Handbook cover the latest developments accomplished at the Gear Research Laboratory and represent the basic information about the design of face gear drives, generation of face gears by cutting and grinding, computerized simulation of meshing and contact, and the application of face gear drives in helicopter transmissions. Although there is much more to be learned about face gear drives, it is felt that they are about to take a prominent place among the gearing options available to drive systems engineers. The advantages they offer in torque splitting arrangements, high ratio capability, and strength will provide the motivation to bring this technology to its full fruition.

Part 1
Face Gear Drives with Intersected Axes

1.1 General Considerations

A face gear drive used for transformation of rotation and torque between intersected axes (fig. 1.1.1) is an alternative one for a spiral bevel gear drive. The driving member of a face gear drive is an involute spur pinion. The bearing contact in a face gear drive is localized (see section 1.3) to avoid the separation of tooth surfaces and edge contact due to misalignment.

The advantages of a face gear drive are:

(1) The possibility to split the torque in a gear transmission, particularly in a helicopter transmission as shown in figs. 1.1.2(b) and 1.1.3. Application of spiral bevel gears for this purpose is less favorable (fig. 1.1.2(a)).

(2) More favorable conditions of transfer of meshing when one pair of teeth is changed for the neighboring one. Due to misalignment, the transfer of meshing in other types of gear drives is accompanied by transmission errors that cause vibration and noise. The advantage of face gear drives is that misalignment does not cause transmission errors at the transfer of meshing, because the involute pinion tooth surfaces are equidistant. However, errors of alignment in a face gear drive may cause a shift in the bearing contact, therefore localization and stabilization of the bearing contact become necessary (see section 1.3).

The design of face gear drives requires the observation of the following conditions:

(1) Avoidance of undercutting and pointing of the face gear teeth.

(2) Favorable relation between the tooth length ' l ' and the diametral pitch P_d.

The structure of a tooth of a face gear generated by a shaper is shown in fig. 1.1.4. The tooth surface is covered by lines L_{2s}, lines of tangency of the face gear 2 with the shaper s. The fillet of the tooth surface of the face gear is generated by the edge of the shaper tooth, and L^* is the line of tangency of both parts of the tooth surface. Undercutting may occur in a cross-section A, and pointing in a cross-section B. Fig. 1.1.5 shows the schematic of a face gear of a non-orthogonal gear drive. The intersected axes of the pinion (or shaper) and the face gear form an angle γ_m that differs from $90°$. Dimensions R_1 and R_2 determine the locations of cross-sections A and B. The tooth length l is determined as:

$$l = R_2 - R_1 \tag{1}$$

A unitless coefficient c is represented as

$$c = lP_d \tag{2}$$

The strength of the teeth depends on c. To obtain $c > 10$, it is recommended to choose the following values:

$$m_{12} = \frac{N_2}{N_1} > 5 \quad , \qquad N_1 \geq \frac{2}{1 - \cos\alpha_o} \quad , \qquad \alpha_o = 25° \tag{3}$$

where N_1 and N_2 are the numbers of teeth in the pinion and the gear, α_o is the nominal pressure angle, and m_{12} is the gear ratio.

1.2 Instantaneous Axis of Rotation, Pitch Cones, Pitch Surfaces

Instantaneous Axis of Rotation

Fig 1.2.1 (a) shows that rotation with angular velocities $\omega^{(1)}$ and $\omega^{(2)}$ is performed between intersected axes $O1$ and $O2$ that form an angle γ. There is such an axis OI that lies in the plane formed by axes of rotation $O1$ and $O2$ that is defined as follows:

(i) At any point M of OI the following vector equation is observed

$$\boldsymbol{\omega}^{(1)} \times \boldsymbol{\rho}_1 = \boldsymbol{\omega}^{(2)} \times \boldsymbol{\rho}_2 \tag{4}$$

Here: ρ_i $(i = 1, 2)$ is the position vector of point M.

(ii) Equation (4) means that

$$\mathbf{v}^{(1)} = \mathbf{v}^{(2)} \tag{5}$$

where $\mathbf{v}^{(i)}$ is the linear velocity of point M in rotation about axis O_i $(i = 1, 2)$.

(iii) Equation (5) yields that

$$\mathbf{v}^{(12)} = \mathbf{v}^{(1)} - \mathbf{v}^{(2)} = 0 \tag{6}$$

This means that the relative linear velocity at a point of the instantaneous axis of rotation OI is equal to zero.

(iv) The *instantaneous axis of rotation OI* forms angles γ_1 and γ_2 with axes of rotation $O1$ and $O2$, respectively (fig. 1.2.1(a)). Here:

$$\cot \gamma_1 = \frac{m_{12} + \cos \gamma}{\sin \gamma} \tag{7}$$

$$\cot \gamma_2 = \frac{m_{21} + \cos \gamma}{\sin \gamma} = \frac{1 + m_{12} \cos \gamma}{m_{12} \sin \gamma} \tag{8}$$

where

$$m_{12} = \frac{N_2}{N_1} = \frac{\sin \gamma_1}{\sin \gamma_2}, \qquad m_{21} = \frac{1}{m_{12}} \tag{9}$$

Pitch Cones

We may consider two cones with apex angles γ_1 and γ_2 that are rotated about axes $O1$ and $O2$ with angular velocities $\omega^{(1)}$ and $\omega^{(2)}$. The relative motion of one cone with respect to the other one is rolling without sliding. This rolling is rotation about the instantaneous axis of rotation with angular velocity:

(i) $\omega^{(12)} = \omega^{(1)} - \omega^{(2)}$

when cone 2 is at rest and cone 1 rolls over cone 2;

(ii) $\omega^{(21)} = \omega^{(2)} - \omega^{(1)} = -\omega^{(12)}$

when cone 1 is at rest and cone 2 rolls over cone 1.

The line of action of angular velocities $\omega^{(12)}$ and $\omega^{(21)}$ coincides with the instantaneous axis of rotation OI. In the case of bevel gears cones 1 and 2 (fig. 1.2.1 (a)) are *the pitch cones*, and they are the basis for determination of the addendum and dedendum cones of the bevel gears.

Pitch Surfaces in a Face Gear Drive

In the case of a face gear drive, the tooth element proportions are determined by application of so called pitch surfaces that differ from the pitch cones. The *pitch surfaces* (fig. 1.2.1(b)) represent a pitch cylinder r_p for the shaper (pinion) and a cone of the apex angle γ for the face gear. Angle γ is equal to the angle formed by the axes of the shaper (pinion) and the face gear. The line of tangency of the pitch surfaces $O'Q$ does not coincide with the instantaneous axis of rotation OI, but intersects it at point P as shown in fig. 1.2.1(b). The pitch surfaces roll over each other only at point P, but roll and slide at any other point of $O'Q$. Radius r_{p1} is the radius of the shaper (pinion) pitch cylinder for a standard shaper (pinion), and is the radius of the operating pitch cylinder of the nonstandard shaper (pinion). Fig. 1.2.2 shows the shaper (pinion) and face gear of a face gear drive with intersected axes. The teeth have a constant height.

The concept of instantaneous axis of rotation in a face gear drive is applied for approximate determination of conditions of pointing (see section 1.7).

1.3   Generation of Face Gears with Localized Bearing Contact

The face gear may be generated by shaping, hobbing, or grinding.

Shaping

The generation is based on simulation of meshing of a shaper and the face gear being generated (fig. 1.3.1). Two approaches for the localization of the bearing contact may be applied.

Approach 1 is based on simulation of meshing by application of a shaper with increased tooth number N_s

$$N_s = N_1 + 1 \sim 3 \tag{10}$$

where N_1 is the pinion tooth number.

We may imagine that the applied shaper and the pinion of the drive are in internal tangency as shown in fig. 1.3.2. The shortest distance B between the axes of the shaper and the pinion is represented as

$$B = r_{ps} - r_{p1} = \frac{N_s - N_1}{2P_d} \tag{11}$$

During the process of generation, the shaper and the gear perform rotation between intersected axes with angular velocities $\omega^{(s)}$ and $\omega^{(2)}$ related as follows

$$\frac{\omega^{(s)}}{\omega^{(2)}} = \frac{N_2}{N_s} \tag{12}$$

The axes of rotation of the shaper and the face gear form an angle $\gamma_m = (180° - \gamma)$ (fig. 1.3.1), where γ is an angle formed by the axes of the pinion and the face gear (fig. 1.2.2). The shaper performs a reciprocating motion in the direction of generatrix of the face gear that is parallel to the shaper axis. The tooth surfaces of the shaper and the face gear are in line contact at every instant. Lines L_{s2} (fig. 1.3.3(a)) are the instantaneous lines of tangency of surfaces Σ_s and Σ_2, the surfaces of the shaper and the face gear.

The shaper tooth surface Σ_s and the pinion tooth surface are also in line contact at every instant. Lines L_{s1} are the instantaneous lines of tangency of surfaces Σ_s and Σ_1 (fig. 1.3.3(b)). The face gear tooth surface Σ_2 and the pinion tooth surface Σ_1 are at every instant in tangency at a point (designated as M in fig. 1.3.3(c)) that is the point of intersection of lines of tangency L_{s2} and L_{s1}.

The approach discussed above allows the bearing contact to be localized as shown in fig. 1.3.4. The bearing contact is formed as a set of instantaneous contact ellipses. The contact of surfaces at a point is spread over an ellipse due to the elastic deformation of tooth surfaces.

More details about the determination of the contact ellipses on the gear tooth surface are given in section 1.8.

Approach 2 is based on the following ideas [9], [12].

(i) The number of teeth of the shaper is the same as the one of the pinion.

(ii) The point contact of the surfaces of the pinion and the face gear is achieved by the modification of the pinion tooth surface. Such a modification is obtained by a varied plunge of the tool that generates the pinion.

Figs. 1.3.5 and 1.3.6 show how the varied plunge of the tool is accomplished by form-grinding (cutting) of the pinion. The axial section of the tool coincides with the involute profile of the pinion. The tool surface is a surface of revolution. During the pinion generation, the tool performs two translational motions (figs. 1.3.5 and 1.3.6): (1) in the direction of the pinion axis, and (2) in the direction of the shortest distance.

Coordinate systems S_1 and S_d, shown in the fig. 1.3.6, are rigidly connected to the pinion and the generating tool. The instantaneous shortest distance E is executed as (fig. 1.3.6)

$$E = E_o - a_d l_d^2 \tag{13}$$

where E_o is the nominal value of the shortest distance, l_d is the displacement along the teeth, a_d is the parabola coefficient of the varied plunge

$$E - E_o = a_d l_d^2 \tag{14}$$

The face gear tooth surface Σ_2 is generated as the envelope to the family of shaper tooth surfaces Σ_s. Surface Σ_s coincides with the theoretical, unmodified pinion tooth surface Σ_1. Surfaces Σ_2 and Σ_s are in line contact, but surfaces Σ_2 and Σ_1 are in point contact because Σ_1 is generated by plunging of the tool.

The modified pinion tooth surface may be generated as well by a hob or a grinding worm that is plunged during the process of generation, similarly to plunging of the form-grinding tool (fig. 1.3.5 and 1.3.6).

The advantages of *Approach 2* for the localization of the bearing contact are as follows:

(i) The possibility to obtain larger dimensions of the contact ellipse since $N_s = N_1$.

(ii) The possibility to compensate the shift of the bearing contact caused by misalignment by an axial displacement of the pinion provided with the modified tooth surface with respect to the face gear.

Hobbing and Grinding

A hob for generating face gears was proposed by E. Miller in patent 2,304,586 (December 8, 1942), titled: *Hob for Generating Crown Gears* (fig. 1.3.7). The main idea of the patent is that the surface of the hob thread can be determined as that generated by the involute profiles of the cross-section of the shaper (fig. 1.3.7). Although the proposed idea of an application of a hob for generation of crown (face) gears was an innovative one, it was not supported with sufficiently detailed investigation of the following topics:

(i) The determination of the exact thread surface of the hob and the determination of deviations of the real surface from the exact one. It should be pointed out that Miller's patent proposed to generate the hob by tooth profiles but not tooth surfaces.

(ii) A method for dressing and manufacturing the hob thread surface.

This was the reason why new ideas that cover grinding and hobbing of face gears were developed. The proposed ideas are as follows:

(1) The shape of the grinding worm (hob) is as shown in fig. 1.3.8.

(2) The worm thread surface can be determined by two alternative approaches:

Approach 1 for Determination of Worm Thread Surface

The worm thread surface Σ_w is the one parameter envelope to the family of the shaper tooth surfaces Σ_s. Surfaces Σ_w and Σ_s are in line contact at every instant. The worm and the shaper perform rotation about crossed axes that form angle λ_w with angular velocities

related as

$$\frac{\omega_w}{\omega_s} = \frac{N_s}{N_w} \tag{15}$$

A single thread worm is applied and $N_w = 1$. The angle λ_w is determined by the relation

$$\sin \lambda_w = \frac{r_{ps}}{N_s r_{pw}} \tag{16}$$

where r_{ps} and r_{pw} are the radii of the pitch cylinders of the shaper and the worm at the mean contact point.

The dressing of the worm is based on simulation of meshing of the worm with an imaginary spur pinion that is identical to the shaper. Fig. 1.3.9 shows a segment of the imaginary spur pinion. The imaginary spur pinion and the shaper complement each other as molding and casting. Contact lines between surfaces Σ_w and Σ_s are shown in fig. 1.3.10. There is a possibility of undercutting of the worm thread surface Σ_w by surface Σ_s. Therefore, the angle of rotation of the worm ϕ_w being in mesh with the dressing tool must be limited. Due to asymmetrical location of contact lines and the limiting line on surface Σ_s, each side of the worm thread surface Σ_w must be ground separately. Due to the low magnitude of the relative velocity in the process of meshing of the worm and the dressing tool, it is difficult to obtain a high quality of the worm thread surface.

Approach 2 for Determination of Worm Thread Surface

This approach was developed by Litvin and Seol and is based on the determination of the worm thread surface Σ_w as the two parameter enveloping of the family of tooth surfaces Σ_2. Surfaces Σ_w and Σ_2 are in point contact at every instant. The two independent parameters of motion are: (i) the angle of rotation of the face gear ϕ_2 being in mesh with the worm, and (ii) the translational motion s along the teeth of the face gear. Parameters ϕ_2 and s are considered as independent although they are related in the real process of generation. However, the relation between ϕ_2 and s does not cause substantial deviations of surface Σ_w from the theoretical one. The angle of rotation of the worm ϕ_w is related with ϕ_2 by the

equation

$$\frac{\phi_w}{\phi_2} = N_2 \tag{17}$$

assuming that *a one-thread worm is applied.*

Dressing of the Worm

A great advantage of the proposed method of dressing is that it is based on application of a dressing disk that is in point contact with the worm thread surface. The grinding disk and the worm thread surface are in point contact at every instant. The mathematically defined worm thread surface Σ_w is generated point by point by the grinding disk. A CNC machine with five degrees of freedom for the continuous installment and tangency of the disk surface relative to the worm thread surface is required. A point of the grinding disk as the candidate point of the tangency must be chosen. The ability to grind the worm thread surface with a plane (applying for this purpose the plane of a disk) is based on the fact that any point of the worm thread surface is an elliptical one. We remind the reader that at various elliptical points of a surface the Gaussian curvature (the product of principal curvatures) is of the same sign.

Generation of the Face Gear Tooth Surface by a Grinding (Cutting) Worm

Once the worm thread surface Σ_w has been created, the generation of the face gear tooth surface can be performed. The generation of the face gear tooth surface Σ_2 by Σ_w is similar to the grinding (cutting) of a spur gear by a worm. The worm and the face gear perform related rotations about crossed axes, the axes of the worm and the face gear. The angles of rotation ϕ_w and ϕ_2 are related by equation (17), assuming that a one-thread worm is applied and that $N_w = 1$.

Surfaces Σ_2 and Σ_w are in point contact and therefore the feed motion of the worm, translation along the direction of face gear teeth must be provided.

1.4 Shaper Tooth Surface

The shaper tooth surfaces are represented in coordinate system S_s (fig. 1.4.1). Plane x_s is the plane of symmetry of the space of the shaper. The variable parameters θ_{ks} ($k = \beta, \gamma$) and u_s are the surface parameters. Parameter u_s is measured in the direction of z_s. Parameters θ_{ks} for the left and the right side profiles are measured in the directions shown in fig. 1.4.1. The constant parameter θ_{os} determines the half of the space width on the base cylinder. It is measured as shown in fig. 1.4.1 and is determined for a standard shaper by the equation

$$\theta_{os} = \frac{\pi}{2N_s} - inv\alpha_o \tag{18}$$

Here: N_s is the number of teeth of the shaper, and α_o is the pressure angle.

The tooth surface and the surface unit normal are represented by the following equations

$$\mathbf{r}_s(u_s, \theta_{ks}) = \begin{bmatrix} \pm r_{bs}[\sin(\theta_{ks} + \theta_{os}) - \theta_{ks}\cos(\theta_{ks} + \theta_{os})] \\ -r_{bs}[\cos(\theta_{ks} + \theta_{os}) + \theta_{ks}\sin(\theta_{ks} + \theta_{os})] \\ u_s \end{bmatrix} \tag{19}$$

$$\mathbf{n}_s = \frac{\dfrac{\partial \mathbf{r}_s}{\partial \theta_{ks}} \times \dfrac{\partial \mathbf{r}_s}{\partial u_s}}{\left| \dfrac{\partial \mathbf{r}_s}{\partial \theta_{ks}} \times \dfrac{\partial \mathbf{r}_s}{\partial u_s} \right|} = \begin{bmatrix} -\cos(\theta_{ks} + \theta_{os})] \\ \mp\sin(\theta_{ks} + \theta_{os})] \\ 0 \end{bmatrix} \tag{20}$$

The upper and the lower signs in the equations (19) and (20) correspond to the left and right side profiles, respectively; r_{bs} is the radius of the base circle.

1.5 Face Gear Tooth Surface

Applied Coordinate Systems

We use the following coordinate systems for derivation of Σ_2 (fig. 1.5.1): $S_s(x_s, y_s, z_s)$ and $S_2(x_2, y_2, z_2)$ that are rigidly connected to the shaper and the face gear; coordinate systems

S_m and S_p that are rigidly connected to the frame of the cutting machine. Coordinate systems S_p is used for simplification of derivations of coordinate transformation. Angle γ_m is the angle between the pinion shaft rotational axis and the face gear shaft rotational axis. It is formed between axes z_m and z_2 and is determined as $\gamma_m = (180° - \gamma)$ (see designation in figs. 1.5.1 $(a), (b)$).

Equations of the face gear tooth surfaces are represented as follows [7]

$$\mathbf{r}_2(u_s, \theta_{ks}, \phi_s) = \mathbf{M}_{2s}(\phi_s)\, \mathbf{r}_s(u_s, \theta_{ks}) \tag{21}$$

$$f(u_s, \theta_{ks}, \phi_s) = r_{bs}(1 - m_{2s}\cos\gamma_m) - u_s m_{2s}\sin\gamma_m \cos(\phi_s + \theta_{os} + \theta_{ks}) = 0 \tag{22}$$

where (22) is the *equation of meshing*.

Matrix $\mathbf{M}_{2s} = \mathbf{M}_{2p}\mathbf{M}_{pm}\mathbf{M}_{ms}$ is represented by the following equation

$$\mathbf{M}_{2s} = \begin{bmatrix} \cos\phi_2\cos\phi_s + \cos\gamma_m\sin\phi_2\sin\phi_s & -\cos\phi_2\sin\phi_s + \cos\gamma_m\sin\phi_2\cos\phi_s & -\sin\gamma_m\sin\phi_2 & 0 \\ -\sin\phi_2\cos\phi_s + \cos\gamma_m\cos\phi_2\sin\phi_s & \sin\phi_2\sin\phi_s + \cos\gamma_m\cos\phi_2\cos\phi_s & -\sin\gamma_m\cos\phi_2 & 0 \\ \sin\gamma_m\sin\phi_s & \sin\gamma_m\cos\phi_s & \cos\gamma_m & 0 \\ 0 & 0 & 0 & 1 \end{bmatrix} \tag{23}$$

where

$$\phi_2 = \phi_s \frac{N_s}{N_2} \tag{24}$$

Vector equation $\mathbf{r}_s(u_s, \theta_{ks})$ is represented by equation (19).

Equations (21) and (22) represent the tooth surfaces of the face gear using three related parameters. Since parameter u_s is a linear one, it can be easily eliminated, and then the tooth surface of the face gear can be defined by two independent parameters as $\mathbf{r}_2(\theta_{ks}, \phi_s)$.

1.6 Avoidance of Undercutting

General Approach.

Avoidance of undercutting of face gear teeth can be achieved by the elimination of singular points of the face gear tooth surface. We remind the reader that at a surface singular point, the surface normal becomes equal to zero [6], [7]. It was proposed and proven in the works [6] and [7], that singular points on the generated surface Σ_2 appear if the following vector equation is observed

$$\mathbf{v}_r^{(s)} + \mathbf{v}^{(s2)} = \mathbf{0} \tag{25}$$

Here: $\mathbf{v}_r^{(s)}$ is the velocity of the contact point on generating surface Σ_s; $\mathbf{v}^{(s2)}$ is the relative velocity of the point of tangency of surface Σ_s with respect to the face gear tooth surface Σ_2.

The differentiated equation of meshing

$$\frac{\partial f}{\partial u_s} \frac{du_s}{dt} + \frac{\partial f}{\partial \theta_{ks}} \frac{d\theta_{ks}}{dt} + \frac{\partial f}{\partial \phi_s} \frac{d\phi_s}{dt} = 0 \tag{26}$$

and vectors equation (25) represent a system of four linear equations in terms of two unknowns: $\dfrac{du_s}{dt}$ and $\dfrac{d\theta_{ks}}{dt}$ considering $\dfrac{d\phi_s}{dt}$ as chosen. The system has a certain solution for the unknowns if the matrix

$$\mathbf{A} = \begin{bmatrix} \dfrac{\partial \mathbf{r}_s}{\partial u_s} & \dfrac{\partial \mathbf{r}_s}{\partial \theta_{ks}} & -\mathbf{v}_s^{(s2)} \\ \dfrac{\partial f_s}{\partial u_s} & \dfrac{\partial f_s}{\partial \theta_{ks}} & -\dfrac{\partial f_s}{\partial \phi_s} \dfrac{d\phi_s}{dt} \end{bmatrix} \tag{27}$$

has the rank $r = 2$.

This yields that four determinants of the third order are equal to zero. The investigation shows that the equality of two of them to zero is equivalent to the existence of the equation of meshing given by equation (22). Therefore, it is necessary to use one of the following two equations

$$\Delta_1 = \begin{vmatrix} \dfrac{\partial x_s}{\partial u_s} & \dfrac{\partial x_s}{\partial \theta_{ks}} & v_{xs}^{(s2)} \\[2mm] \dfrac{\partial z_s}{\partial u_s} & \dfrac{\partial z_s}{\partial \theta_{ks}} & v_{zs}^{(s2)} \\[2mm] f_{u_s} & f_{\theta_{ks}} & f_{\phi_s}\dfrac{d\phi_s}{dt} \end{vmatrix} = 0 \tag{28}$$

$$\Delta_2 = \begin{vmatrix} \dfrac{\partial y_s}{\partial u_s} & \dfrac{\partial y_s}{\partial \theta_{ks}} & v_{ys}^{(s2)} \\[2mm] \dfrac{\partial z_s}{\partial u_s} & \dfrac{\partial z_s}{\partial \theta_{ks}} & v_{zs}^{(s2)} \\[2mm] f_{u_s} & f_{\theta_{ks}} & f_{\phi_s}\cdot\dfrac{d\phi_s}{dt} \end{vmatrix} = 0 \tag{29}$$

Here f_{u_s}, $f_{\theta_{ks}}$, and f_{ϕ_s} are the partial derivatives of the equation of meshing taken with respect to u_s, θ_{ks}, and ϕ_s, respectively. x_s, y_s, and z_s are the coordinates of a point of the shaper surface Σ_s in coordinate system S_s; $(v_{xs}^{(s2)}, v_{ys}^{(s2)}, v_{zs}^{(s2)})$ are the components of the relative velocity in the same coordinate system.

Any of the couple of equations (28) and (29) can be used, and (for example) equation (28) yields the following relation

$$F(u_s, \theta_{ks}, \phi_s) = \frac{\partial x_s}{\partial u_s}\left(\frac{\partial z_s}{\partial \theta_{ks}}f_{\phi_s} - v_{zs}^{(s2)}f_{\theta_{ks}}\right) - \frac{\partial x_s}{\partial \theta_{ks}}\left(\frac{\partial z_s}{\partial u_s}f_{\phi_s} - v_{zs}^{(s2)}f_{u_s}\right)$$
$$+ v_{xs}^{(s2)}\left(\frac{\partial z_s}{\partial u_s}f_{\theta_{ks}} - \frac{\partial z_s}{\partial \theta_{ks}}f_{u_s}\right) = 0 \tag{30}$$

Equation (30) with the equation of meshing (22) and the equations of shaper surface (19) considered simultaneously enable to determine the limiting line L_s on the shaper tooth surface Σ_s (fig. 1.6.1) that will be used for the determination of dimensions of the face gear free of undercutting. Line L_s contains regular points of surface Σ_s, but generates singular points on surface Σ_2. Fig. 1.6.2 shows line of singular points on the face gear tooth surface, generated by line L_s. Dashed portion of the face gear tooth surface must be eliminated in order to avoid undercutting (fig. 1.6.2). In the case of a face gear drive with intersected axes, due to the symmetry of two sides of face gear tooth surfaces, it is sufficient to determine a limiting line L_s for one of two sides of the shaper tooth surfaces.

The point of intersection (T) of line L_s (fig. 1.6.1) with the addendum cylinder of the shaper is a critical point of undercutting. The shaper parameter θ_{ks} that corresponds to the addendum of the shaper is determined by equation

$$\theta_{ks}^* = \frac{\sqrt{r_{as}^2 - r_{bs}^2}}{r_{bs}} \tag{31}$$

where r_{as} and r_{bs} are the radii of the addendum and the base cylinder of the shaper. The coordinates (x_s^*, y_s^*, z_s^*) of point of intersection of the limiting line L_s with the addendum cylinder of the shaper can be determined by using equation (31) and vector equation (19) of the shaper surface. The limiting inner radius of the orthogonal face gear R_1 (fig. 1.1.5) is determined as

$$R_1 = \sqrt{x_2^2 + y_2^2} \tag{32}$$

and the limiting value of the shaper (fig.1.2.2) as

$$L_1 = z_s^* \tag{33}$$

where x_2 and y_2 are the coordinates of the point on the face gear tooth surface obtained from coordinates (x_s^*, y_s^*, z_s^*) by coordinate transformation from S_s to S_2.

If the conditions of non-undercutting are observed, then the fillet surface and the working surface of the face gear are in tangency and their line of tangency is designated by L^* (fig. 1.1.4).

Numerical example: The input data is represented in Table 1

Table 1

INPUT DATA	
Number of teeth of the shaper	$N_s = 20$
Number of teeth of the face gear	$N_2 = 100$
Pressure angle	$\alpha_o = 25°$
Diametral pitch	$P_d = 10\ (1/in)$
Center distance	$E = 0\ (in)$
Intersecting angle	$\gamma_m = 90°$

Using the input data above, the following auxiliary data is obtained:

- Gear ratio $m_{2s} = 0.2$

- Radius of the pitch circle of the shaper $r_{ps} = 1$ (in)

- Radius of the base circle of the shaper $r_{bs} = 0.9063$ (in)

- Radius of the addendum circle of the shaper $r_{as} = 1.125$ (in)

- Surface parameter of the shaper addendum $\theta_{ks}^* = 0.735408$ (rad) (see equation (31))

Procedure of Computations:

Step 1: We use equation of meshing (22), equation (30) and consider as known θ_{ks}^*. Then, we obtain $\phi_s^* = -\ 0.65266(rad)$ and $u_s^* = 4.57089$ (in).

Step 2: We use equations (19) and consider as known θ_{ks}^* and u_s^* obtained above. Then, we obtain the coordinates $x_s^* = -0.16798$ (in) and $y_s^* = -1.11238$ (in) for the critical point T of the shaper $z_s^* = u_s^*$.

Step 3: Using equation (33), we obtain the limiting length of the shaper surface $L_1 = 4.57089$ (in).

Step 4: Using matrix equation (21) and considering as known u_s^*, θ_{ks}^* and ϕ_s^*, we obtain the following coordinates of the critical point on the face gear tooth surface $x_2^* = -0.05747$ (in), $y_2^* = -4.60257$ (in), $z_2^* = -0.98577$ (in).

Then, using equation (32) we obtain the limiting inner radius of the face gear $R_1 = 4.60292$ (in).

1.7 Pointing

Pointing is another negative phenomenon that occurs in the process of generation of the face gear tooth. The top-land of a face gear tooth is not a constant width (fig. 1.1.4). There is an area where width of the top-land becomes equal to zero, which means that the tooth

is pointed. It will cause the weakness of the tooth in that area. One of the design goals is to properly determine the area of pointing and the outer radius R_2 of the face gear blank that will be free of pointing.

Two approaches are proposed for determination of the area of pointing. The first one requires simultaneous consideration of the equations of surfaces of both sides of the face gear tooth and the determination of the area where these two surfaces intersect each other. This approach is discussed in Part 2 of this book. The other one is based on application of the instantaneous axis of rotation and consideration of cross-sections of tooth profiles of the shaper and the face gear [7] and [9]. Both approaches have been applied using the numerical examples, and found to have almost identical results.

Approach 2

It was mentioned earlier that this approach is based on consideration of the cross-sections of tooth surfaces of the shaper and the face gear. Although this alternative approach is only approximate, it does provide results that are very close to the exact ones. In the case of face gear drives with intersected axes, the *instantaneous axis of rotation is used for determination of pointing*, while in the case of the offset face gear drives the axis of meshing is used instead.

This approach is based on the following considerations:

The face gear is generated by a shaper. The axes of rotation of the shaper and the face gear are intersected and they are designated by z_m and z_2, respectively (fig. 1.5.1). The instantaneous axis of rotation is designated by IA_{s2} and the pitch line by $O'P^*$ (fig. 1.7.1). Point P is the pitch point and point I is the current point of the instantaneous axis of rotation.

Fig. 1.4.1 show that $x_s = 0$ is the plane of symmetry of the shaper space. Any cross-sections of the shaper tooth surface by planes that are parallel to x_s and perpendicular to z_m axis represent the same involute curves. Two such planes, Π_1 and Π_2, are shown in fig. 1.7.1. Plane Π_1 intersects the instantaneous axis of rotation IA_{s2} at a point P that belongs

to the axis of symmetry of the cross-section of the space of the shaper. Similarly, plane Π_2 intersects the instantaneous axis of rotation IA_{s2} at a point I. Figs. 1.7.2 and 1.7.3 show points P and I that are the points of intersection of the instantaneous axis of rotation IA_{s2} with Π_1 and Π_2, respectively. A normal to the shaper tooth surface is perpendicular to z_m- axis and therefore it lies in plane Π_i. The common normal to the surfaces of the shaper and the face gear passes through the points P in plane Π_1 and I in plane Π_2. The common tangents to the cross-section profiles form an angle α_o and α, respectively (fig. 1.7.2 and 1.7.3).

Now, assume that plane Π_2 is the plane where the pointing of the cross-section profiles of the face gear occurs. The investigation shows that in the area where pointing is observed, the cross-section profiles of the face gear deviate from the straight lines only slightly. Therefore, it can be assumed that the point K of intersection of the tangents to the profiles (fig. 1.7.3), is actually the point of intersection of the real cross-section profiles of the face gear.

The consideration discussed above enables us to derive the equations for determination of the outer radius R_2 of the face gear for the zone of pointing using the following procedure.

Step 1: Vector equation (fig. 1.7.3)

$$\overline{O_sN} + \overline{NM} + \overline{MK} = \overline{O_sK} \tag{34}$$

yields that:

$$\alpha - \tan\alpha \frac{2P_d r_{ms}}{N_s} = \theta_{os} \tag{35}$$

where θ_{os} is represented by the equation (18) and $r_{ms} = r_{ps} - \dfrac{1}{P_d}$.

Step 2: It is considered that point P belongs to the pitch cylinder of the shaper , and the location of I with respect to P is determined with segments Δl and Δq (fig. 1.7.1). Drawings of figs. 1.7.1, 1.7.2 and 1.7.3 yield

$$\Delta q = O_sI - O_sP = \frac{r_{bs}}{\cos\alpha} - \frac{r_{bs}}{\cos\alpha_o} = \frac{N_s}{2P_d}(\frac{\cos\alpha_o - \cos\alpha}{\cos\alpha}) \tag{36}$$

$$\Delta l = \frac{\Delta q}{\tan \gamma_s} \tag{37}$$

Step 3: The location of plane Π_2 is determined with parameter R_2 in coordinate system S_2 (fig. 1.7.1). Here

$$R_2 = \frac{N_s}{2P_d} \left(\frac{1 + \Delta q}{\tan \gamma_s} \right) \tag{38}$$

$$\tan \gamma_s = \frac{\sin \gamma}{m_{s2} + \cos \gamma} \tag{39}$$

where γ is the crossing angle and m_{s2} is the gear ratio.

Numerical example: The following numerical example illustrates the above approach for the avoidance of pointing. The input data are given in the following table.

Table 2

INPUT DATA	
Number of teeth of the shaper	$N_s = 20$
Number of teeth of the face gear	$N_2 = 100$
Pressure angle	$\alpha_o = 25°$
Diametral pitch	$P_d = 10 \ (1/in)$
Center distance	$E = 0 \ (in)$
Intersecting angle	$\gamma_m = 90°$

Using the input data above, the following auxiliary data is obtained:

- Gear ratio $m_{s2} = 5$

- Radius of the pitch circle of the shaper $r_{ps} = 1.0 \ (in)$

- Angle $\gamma_s = 0.197395 \ (rad)$ (see equation (39))

- Radius of the shaper $r_{ms} = r_{ps} - \dfrac{1}{P_d} = 0.9000 \ (in)$

- Radius of the base circle of the shaper $r_{bs} = 0.9063 \ (in)$

Since $r_{ms} < r_{bs}$ it must be taken for the further calculation that $r_{ms} = r_{bs} = 0.9063 \ (in)$

- Half of the space width on the shaper base cylinder is determined with $\theta_{os} = 0.04856 (rad)$ (see equation (18))

Procedure of Computations Applying Approach 2:

Step 1: We use equation (35), and consider as known: P_d, N_s (from the input data) and r_{ms}, θ_{os} (from the auxiliary data). Then, we solve equation (35) by using subroutine for solution of nonlinear equations, and we obtain angle $\alpha = 0.66791$ (rad) (fig. 1.7.3).

Step 2: We use equations (36) and (37), and consider as known α_o (from the input data), and α obtained in Step 1. Then, we obtain the values $\Delta q = 0.15436$ (in) and $\Delta l = 0.77184$ (in) (fig. 1.7.1).

Step 3: Using equation (38) and considering as known: γ_s (from the auxiliary data), N_s and P_d (from the input data), and Δq from Step 2, we obtain the limiting outer radius of the face gear $R_2 = 5.7718$ (in) (fig. 1.7.1)

1.8 Contact Ellipse

The pinion and the face gear tooth surfaces are in point contact at every instant. Due to elasticity of tooth surfaces, the contact is spread over an elliptical area. The center of symmetry of the instantaneous contact ellipse coincides with the theoretical point of tangency (fig. 1.3.4). The goal is to determine the orientation and dimensions of the contact ellipse in the tangent plane to the contacting surfaces. This can be accomplished considering as known: the principal curvatures of two contacting surfaces, the angle σ between the unit vectors $\mathbf{e}_I^{(1)}$ and $\mathbf{e}_I^{(2)}$ which are the principal directions of the surfaces (fig. 1.8.1), and the elastic deformation δ of the surfaces at the point of tangency. Note that the ratio between the major and minor axes of the contact ellipse does not depend on the elastic deformation δ. The elastic deformation depends on the load and it is considered as known from the experimental data.

It is easy to determine directly the principal curvatures and the directions for the spur involute pinion surface. In the case of non-modified spur involute pinion (*see Approach 1 for localization of bearing contact*), the curvatures are given by

$$\kappa_I^{(1)} = -\frac{1}{\theta_p r_{b_p}}$$
$$\kappa_{II}^{(1)} = 0 \tag{40}$$

where θ_p is the pinion surface parameter and r_{b_p} is the radius of the base circle of the pinion. In the case when the pinion surface is modified (*see Approach 2 for localization of bearing contact*) the expressions for the pinion curvatures are more complex.

The problem of determination of principal curvatures and the directions of the face gear tooth surface requires more complex derivations. A simplified approach to the solution of this problem is based on direct relations between the principal curvatures of the shaper-tooth surface and the generated face gear surface [7] (the determination of the principle curvatures of a face gear tooth surface is performed numerically and requires an algorithm given in [7]).

The principal curvatures of the spur involute shaper are given by

$$\kappa_I^{(1)} = -\frac{1}{\theta_s r_{b_s}}$$
$$\kappa_{II}^{(1)} = 0 \tag{41}$$

where θ_s is a shaper surface parameter and r_{b_s} is the radius of the base circle of the shaper. Note that r_{b_s} and r_{b_p} are different because the number of teeth of the shaper and the pinion are not the same (*see Approach 1 for localization of bearing contact*).

The determination of the instantaneous contact ellipse is based on the following equations:

$$g_i = \kappa_I^{(i)} - \kappa_{II}^{(i)} \tag{42}$$

$$\kappa_\Sigma^{(i)} = \kappa_I^{(i)} + \kappa_{II}^{(i)} \tag{43}$$

$$\cos 2\alpha^{(1)} = \frac{g_1 - g_2 \cos 2\sigma}{\sqrt{(g_1^2 - 2g_1 g_2 \cos 2\sigma + g_2^2)}} \tag{44}$$

$$\sin 2\alpha^{(1)} = \frac{g_2 \sin 2\sigma}{\sqrt{(g_1^2 - 2g_1 g_2 \cos 2\sigma + g_2^2)}} \tag{45}$$

$$2a = 2\left|\frac{\delta}{A}\right|^{1/2} \quad , \quad 2b = 2\left|\frac{\delta}{B}\right|^{1/2} \tag{46}$$

where

$$A = \frac{1}{4}\left[\kappa_\Sigma^{(1)} - \kappa_\Sigma^{(2)} - \sqrt{(g_1^2 - 2g_1 g_2 \cos 2\sigma + g_2^2)}\right] \tag{47}$$

$$B = \frac{1}{4}\left[\kappa_\Sigma^{(1)} - \kappa_\Sigma^{(2)} + \sqrt{(g_1^2 - 2g_1 g_2 \cos 2\sigma + g_2^2)}\right] \tag{48}$$

Here (fig. 1.8.1) $\alpha^{(1)}$ is the angle that is formed by axis η of the contact ellipse with the unit vector $\mathbf{e}_I^{(1)}$ of the principal directions on surface Σ_1; σ is the angle formed by unit vectors $\mathbf{e}_I^{(1)}$ and $\mathbf{e}_I^{(2)}$ of the principal directions of the contacting surfaces; $2a$ and $2b$ are the axes of the contact ellipse; δ is the elastic deformation; $\kappa_I^{(i)}$ and $\kappa_{II}^{(i)}$ are two principal curvatures of the tooth surface i.

1.9 Algorithms for Simulation of Meshing and Contact

Simulation of meshing and contact is a significant test of the technology and quality of the gears. The computer programs that are developed for simulation of meshing and contact are named TCA (tooth contact analysis). The main idea of TCA is based on simulation of continuous tangency of tooth surfaces being in mesh.

Assuming that the surfaces are in point contact, TCA is directed at the determination of:

(i) transmission errors (caused by errors of assembly)

(ii) the path of contact (its shape and stability)

(iii) the bearing contact as the set of instantaneous contact ellipses

It is assumed that the equations of the gear tooth surfaces are known and that the location and orientation of gear axes are given. To simulate the errors of assembly (misalignment), the location and orientation of gear axes of rotation (shown in figs. 1.9.1 $(a), (b), (c)$ and (d)) differ from the ones designated for gear generation. These errors of assembly are represented by ΔE (change of center distance between gear and the pinion axes), $\Delta \gamma$ (change of crossing angle), and Δq (the axial displacement of the face gear).

For TCA the following algorithm is applied.

Assume that three coordinate systems S_1, S_2, and S_f are rigidly connected to the pinion, the face gear and the frame, respectively.

Step 1: We represent in S_1 and S_2 the tooth surfaces of the pinion and the face gear and the surface unit normals by the following vector functions

$$\mathbf{r}_i(u_i, \theta_i) \in C^2 \ , \quad \frac{\partial \mathbf{r}_i}{\partial u_i} \times \frac{\partial \mathbf{r}_i}{\partial \theta_i} \neq 0 \ , \quad (u_i, \theta_i) \in E_i \quad (i = 1, 2)$$

$$\mathbf{n}_i(u_i, \theta_i) = \frac{\dfrac{\partial \mathbf{r}_i}{\partial u_i} \times \dfrac{\partial \mathbf{r}_i}{\partial \theta_i}}{\left| \dfrac{\partial \mathbf{r}_i}{\partial u_i} \times \dfrac{\partial \mathbf{r}_i}{\partial \theta_i} \right|} \tag{49}$$

Note: The unit normal to the pinion tooth surface is represented by vector function $\mathbf{n}_1(\theta_1)$.

Step 2: Consider that the pinion tooth surface Σ_1 is rotated about the fixed axis z_f (fig. 1.9.1(a)). Thus, the pinion tooth surface is represented in S_f by

$$\mathbf{r}_f^{(1)}(u_1, \theta_1, \phi_1') = \mathbf{M}_{f1}(\phi_1') \mathbf{r}_1(u_1, \theta_1) \tag{50}$$

and its unit normal by

$$\mathbf{n}_f^{(1)}(\theta_1, \phi_1') = \mathbf{L}_{f1}(\phi_1') \mathbf{n}_1(\theta_1) \tag{51}$$

The face gear tooth surface is rotated about another fixed axis z_e (fig. 1.9.1 (d)). The location and orientation of coordinate systems S_e, S_d, and S_q with respect to S_f enables us to simulate the errors of alignment. Note that all errors of assembly (misalignment) are

referred to the face gear. Finally, we may represent in S_f gear tooth surface Σ_2 and the surface unit normal as

$$\mathbf{r}_f^{(2)}(\phi_s, \theta_s, \phi_2') = \mathbf{M}_{f2}\mathbf{r}_2(\theta_s, \phi_s) = \mathbf{M}_{fq}\mathbf{M}_{qd}\mathbf{M}_{de}\mathbf{M}_{e2}\mathbf{r}_2(\theta_s, \phi_s) \tag{52}$$

and

$$\mathbf{n}_f^{(2)}(\phi_s, \theta_s, \phi_2') = \mathbf{L}_{f2}\mathbf{n}_2(\theta_s, \phi_s) \tag{53}$$

Matrices $\mathbf{L}ij$ are the 3×3 transformation matrices, obtained by elimination of the last row and column in 4×4 homogeneous transformation matrix $\mathbf{M}_{ij}$.

Step 3: The continuous tangency of tooth surfaces is represented by the following conditions (fig. 1.9.2)

$$\mathbf{r}_f^{(1)}(u_1, \theta_1, \phi_1') = \mathbf{r}_f^{(2)}(\phi_s, \theta_s, \phi_2') \tag{54}$$

$$\mathbf{n}_f^{(1)}(\theta_1, \phi_1') = \mathbf{n}_f^{(2)}(\phi_s, \theta_s, \phi_2') \tag{55}$$

where ϕ_1' and ϕ_2' are the angles of rotation of the pinion and the face gear being in mesh; u_1, θ_1 are pinion surface parameters and ϕ_s, θ_s are the face gear surface parameters. Note that ϕ_1' and ϕ_2' are different from the angles of rotation ϕ_s and ϕ_2 that were considered in meshing of the shaper and the face gear.

Vector equation (54) yields three independent scalar equations, but equation (55) yields only two independent scalar equations because

$$\left|\mathbf{n}_f^{(1)}\right| = \left|\mathbf{n}_f^{(2)}\right| = 1 \tag{56}$$

Therefore, vector equations (54) and (55) yield the following system of only five independent equations

$$f_i(u_1, \theta_1, \phi_1', \phi_s, \theta_s, \phi_2') = 0 \qquad (i = 1, .., 5) \tag{57}$$

It is assumed that

$$\{f_1, f_2, f_3, f_4, f_5\} \in C^1 \tag{58}$$

Step 4: The pinion - gear tooth surfaces are in point contact at every instant since the contact has been localized. Let us assume that the system of equations (57) is satisfied at point M_o by the set of parameters

$$P^o = (u_1^o, \theta_1^o, \phi_1^{'o}, \phi_s^o, \theta_s^o, \phi_2^{'o}) \tag{59}$$

Since we have 5 equations in 6 unknowns, in order to solve this system, we choose one of the parameters, say ϕ_2', as the input one.

The system of nonlinear equations (57) may be solved in the neighborhood of P^o if the following inequality is satisfied [7].

$$\Delta_5 = \frac{D(f_1, f_2, f_3, f_4, f_5)}{D(u_1, \theta_1, \phi_1', \phi_s, \theta_s)} \neq 0 \tag{60}$$

The solution of equations (57) is obtained by the following functions

$$u_1(\phi_2'), \ \theta_1(\phi_2'), \ \phi_1'(\phi_2'), \ \phi_s(\phi_2'), \ \theta_s(\phi_2') \tag{61}$$

The solution of the system of equations (57) is a continuous iterative process.

(More details about the application of TCA for the case when the localization of bearing contact is achieved due to different numbers of teeth of the shaper and the pinion are given in the book "Gear Geometry and Applied Theory" by F. L. Litvin; section 17.11 [7])

The results of computation for simulation of the bearing contact and the paths of contact are illustrated in figs. 1.9.3(a), (b) and (c) (*using Approach 1 for localization of bearing contact*).

Approach 2 for localization of the bearing contact (with modified pinion tooth surface) requires different setup of coordinate systems used for TCA. More details are given in Part 2 (Offset Face Gear Drives).

Transmission Errors

The transmission errors are represented by the equation

$$\Delta\phi_2' = \phi_2' - \frac{N_1}{N_2}(\phi_1' - \phi_1^*) \tag{62}$$

In the equation above we designate with ϕ_1^* the value of ϕ_1' that corresponds to $\phi_2^* = 0$, that is the initial value of ϕ_2' (the position error). The value of ϕ_1^* can be determined from the numerical function $\phi_1'(\phi_2')_{\phi_2'=0}$. The linear function $\dfrac{N_1}{N_2}(\phi_1' - \phi_1^*)$ represents the ideal transmission function of the face gear. The analysis of transmission errors caused by misalignment yields the conclusion that face gear drives are not sensitive to misalignment. Using *Approach 1 for localization of bearing contact*, it was found that the level of transmission errors is equal to zero even for a misaligned face gear drive. In the case of *Approach 2 for localization of bearing contact (with the crowned pinion)*, the transmission errors for misaligned gear drives are on the order of 1/3 of an arc second, which is negligibly small (fig.1.9.4). This is an advantage of the face gear drives in comparison with other gear drives that are used for transformation of power between intersected or crossed axes.

Part 2
Offset Face Gear Drives (crossed axes)

2.1 General Considerations

In this part, a face gear drive used for transformation of rotation and torque between crossed axes is considered (fig. 2.1.1). This drive, called an *Offset Face Gear Drive*, is an alternative for the hypoid gear drive.

The discussion is limited to the offset face gear drive with crossing angle $\gamma = 90°$ (orthogonal face gear drive). The driving member of an offset face gear drive is an involute spur pinion and the driven member is a face gear. The pinion and the face gear rotate about axes z_s and z_2 with angular velocities ω_s and ω_2, respectively (fig. 2.1.2). The axes of rotation are crossed as shown in figs. 2.1.1 and 2.1.2; E is the shortest distance between the axes of rotation of the gear and the pinion.

Generation of a face gear was covered in *Part 1, Section 1.3*. The same methods of generation are applied in the case of the drive with crossed axes. The surface of the generating shaper $\mathbf{r}_s(u_s, \theta_{ks})$ and its unit normal $\mathbf{n}_s(\theta_{ks})$ are given in *Part 1* by equations (19) and (20).

Due to offset E of the shaper, the tooth surfaces of the generated gear will not be symmetric (fig. 2.1.3) as they are in the case of the face gear drive with intersected axes (fig. 1.1.4). Generated surfaces of the *orthogonal* offset face gear are represented by the following equations

$$\mathbf{r}_2(u_s, \theta_{ks}, \phi_s) = \mathbf{M}_{2s}(\phi_s)\,\mathbf{r}_s(u_s, \theta_{ks}) \tag{63}$$

$$f(u_s, \theta_{ks}, \phi_s) = r_{bs} - u_s m_{2s} \cos(\phi_s \pm (\theta_{os} + \theta_{ks})) = 0 \tag{64}$$

Here and below the upper and the lower signs correspond to the surfaces that are generated by the shaper involute surfaces $\gamma - \gamma$ and $\beta - \beta$, respectively (fig. 1.4.1).

Equation (64) is the *equation of meshing*, and $\mathbf{M}_{2s} = \mathbf{M}_{2a}\mathbf{M}_{ah}\mathbf{M}_{hs}$ is the transformation matrix represented by

$$\mathbf{M}_{2s}(\phi_s) = \begin{bmatrix} \cos\phi_2 \cos\phi_s & -\cos\phi_2 \sin\phi_s & -\sin\phi_2 & E\cos\phi_2 \\ -\sin\phi_2 \cos\phi_s & \sin\phi_2 \sin\phi_s & -\cos\phi_2 & -E\sin\phi_2 \\ \sin\phi_s & \cos\phi_s & 0 & 0 \\ 0 & 0 & 0 & 1 \end{bmatrix} \tag{65}$$

Here ϕ_s and ϕ_2 are the angles of rotation of the shaper and the face gear, respectively, and they are related by the following equation

$$\phi_2 = \phi_s \frac{N_s}{N_2} \tag{66}$$

After transformation, we represent face gear tooth surfaces (Σ_2) as follows:

$$\mathbf{r}_2(\phi_s, \theta_{ks}) = \begin{bmatrix} r_{bs}[\cos\phi_2(\sin\xi_{ks} \mp \theta_{ks}\cos\xi_{ks}) - \dfrac{\sin\phi_2}{m_{2s}\cos\xi_{ks}} + \dfrac{E}{r_{bs}}\cos\phi_2] \\ -r_{bs}[\sin\phi_2(\sin\xi_{ks} \mp \theta_{ks}\cos\xi_{ks}) + \dfrac{\cos\phi_2}{m_{2s}\cos\xi_{ks}} + \dfrac{E}{r_{bs}}\sin\phi_2] \\ -r_{bs}(\cos\xi_{ks} \pm \theta_{ks}\sin\xi_{ks}) \end{bmatrix} \tag{67}$$

where

$$\xi_{ks} = \phi_s \pm (\theta_{ks} + \theta_{os}) \qquad k = (\gamma, \beta) \tag{68}$$

E is the *shortest center distance* (figs. 2.1.1 and 2.1.2), and the following design recommendation for the magnitude of E should be observed (increasing E beyond this limit on a face gear drive with crossed axes will cause an increase in friction by sliding and an increase in the dimensions of the face gear drive)

$$|E| \leq \frac{mN_2}{4} = \frac{d_2}{4} \tag{69}$$

N_2 is the number of teeth of the face gear and m is the *module* that is represented by

$$m = \frac{1}{P_d} \tag{70}$$

The bearing contact of the offset face gear drive is localized using the same principles as in the case of the face gear drive with intersected axes (see section 1.3).

The design of offset face gear drives requires the observation of following conditions:

(1) Avoidance of undercutting and pointing of the face gear teeth.

Due to the asymmetry of the face gear tooth surfaces, the critical value of the inner radius R_1, where the undercutting of each surface occurs, must be determined. Then the dimension of the blank used for manufacturing of the face gear is determined using the larger (more critical) value of the inner radius R_1. The research results show that, for a positive offset $(E > 0)$ (fig. 2.1.2), the critical shaper profile is $\beta - \beta$ (fig. 1.4.1), and it is the opposite for negative offset $(E < 0)$.

Pointing of the *offset face gear tooth* is determined by using two approaches. The first one requires simultaneous consideration of the equations of surfaces of both sides of the face gear tooth and the determination of the area "B" (fig. 2.1.3), where these two surfaces intersect each other. The other one is based on the consideration of the *axis of meshing* and cross-sections of tooth profiles of the shaper and the face gear. Both approaches are explained in detail in the following sections.

(2) Favorable relation between the tooth length " l " and the diametral pitch P_d.

The structure of a tooth of the offset face gear generated by a shaper is shown in fig. 2.1.3.

The fillets of two tooth surfaces of the face gear that are generated by the top edge of the shaper tooth are not the same size (fig. 2.1.3). Having a large value for the coefficient "c", represented by the equation (2), it becomes possible to eliminate the part of the face gear tooth that has a larger fillet. The elimination of the fillet surface will enable to give the tooth of the face gear a more uniform and favorable structure, but in the same time it will reduce the value of "c".

2.2 Axes of Meshing

In this section the concept of axes of meshing for approximate determination of conditions of pointing of the face gear is considered. The idea of axes of meshing proposed and developed in [6], [7] and [9] is based on the following considerations:

(1) The relative motion of gears between crossed axes may be represented by a manifold of correlated vectors $\omega^{(I)}$ and $\omega^{(II)}$, instead of vectors $\omega^{(1)}$ and $\omega^{(2)}$, that represent the angular velocities of gear rotation about the gear axes z_f and z_2 (fig. 2.2.1).

(2) Now, we can consider a sub-manifold of vectors $\omega^{(I)}$ and $\omega^{(II)}$ that satisfies the requirement that a common normal to gear tooth surfaces Σ_s and Σ_2 intersects the lines of action of $\omega^{(I)}$ and $\omega^{(II)}$ (fig. 2.2.2).

(3) The location and orientation of two axes of meshing may be represented by parameters $X^{(i)}$, $K^{(i)}(i = I, II)$, where

$$K^{(i)} = \frac{\omega_z^{(i)}}{\omega_y^{(i)}} \tag{71}$$

is the direction of the axis of meshing.

Only three out of four parameters are independent, and one, say $X^{(I)}$, can be chosen deliberately. This means that in the general case there is an infinite number of correlated axes of meshing that can be chosen for each point of tangency of surfaces Σ_s and Σ_2.

(4) There is a particular case when parameters $X^{(i)}$, $K^{(i)}$ of axes of meshing do not depend on the location of contact point of surfaces Σ_s and Σ_2. Such axes of meshing exist only in particular cases and one of them is the case when one of the mating surfaces is a helicoid whose axis coincides with the axis of gear rotation. In that case, the orientation and location of axes of meshing are constant in the process of meshing and the common normal to Σ_s and Σ_2 intersects both axes of meshing.

(5) In the case of face gear drives with crossed axes, the applied shaper is a spur gear that is considered as a particular case of a helicoid with the screw parameters $p_s = \infty$.

In *the orthogonal offset face gear drive* the driving member is an involute spur pinion. Based on the fact that the involute spur surface is a particular case of an involute helicoid when the screw parameter of helicoid $p_s = \infty$, it is clear that the two axes of meshing exist. The location and orientation of axes of meshing (fig. 2.2.3) for *the orthogonal offset face gear drive* are determined by the following equations [6]

$$K^{(I)} = \frac{E}{p_s} - \frac{1}{m_{2s}} \tag{72}$$

$$X^{(I)} = 0 \tag{73}$$

$$K^{(II)} = 0 \tag{74}$$

$$X^{(II)} = -E + \frac{p_s}{m_{2s}} \tag{75}$$

Parameters $K^{(i)}(i = I, II)$ designate the directions of the axes of meshing, E is the shortest center distance, p_s is the screw parameter and $m_{2s} = \frac{N_s}{N_2}$ is the gear ratio.

Axis of meshing $I - I$ lies in plane $x_h^{(I)} = 0$ (fig. 2.2.3), and according to equations (72) and (73) its location and orientation is determined as follows

$$X^{(I)} = 0 \tag{76}$$

$$K^{(I)} = -\frac{1}{m_{2s}} \tag{77}$$

Axis of meshing $II - II$ is parallel to z_h but lies in a plane $x_h^{(II)}$ that approaches to infinity along negative direction of x_h (fig. 2.2.3). Its location and orientation are determined by

$$X^{(II)} = -\infty \tag{78}$$

$$K^{(II)} = 0 \tag{79}$$

Note that the axes of meshing can be used as an alternative approach for the derivation of equation of meshing that was represented earlier by (64).

2.3 Pointing

Tooth pointing was described in *Part 1, section 1.7.* In this section two approaches for determination of tooth pointing are examined in detail.

Approach 1 for Avoidance of Pointing

Pointing is determined considering the intersection of two opposite surfaces of the face gear. Before we proceed with the determination of pointing, let us consider some characteristics of the involute curves (surfaces).

The pitch circle is the reference dimension for tooth element proportions. The initial point of the shaper involute curve belongs to the base circle of radius

$$r_{bs} = r_{ps} \cos \alpha_o \qquad (80)$$

where α_o is the pressure angle of the rack cutter that can be used for generation of the involute curve. The value of addendum circle of a standard shaper is determined as

$$r_{as} = r_{ps} + \frac{1.25}{P_d} \qquad (81)$$

where P_d $\left(\frac{1}{in}\right)$ is the diametral pitch.

We have to consider two cases of generation of the face gear addendum surface:

Case 1: The addendum of the face gear surface is generated as conjugated to the dedendum involute surface of the face gear. This becomes possible when the radius r_{ms} of the shaper (fig. 2.3.1) satisfies the inequality $r_{ms} > r_{bs}$, where

$$r_{ms} = r_{ps} - \frac{1}{P_d} \qquad (82)$$

Case 2: The addendum surface of the face gear consists of two sub-surfaces if $r_{ms} < r_{bs}$ as shown in fig. 2.3.1. One of the sub-surfaces is generated as conjugated one to the dedendum involute surface of the shaper, and the other sub-surface is generated by the fillet surface of the shaper. Equations (80) and (82) yield $r_{ms} \geq r_{bs}$ if $N_s \geq \dfrac{2}{1 - \cos \alpha_o}$. In the case when

$N_s \leq \dfrac{2}{1 - \cos \alpha_o}$ and two sub-surfaces of the face gear addendum surfaces are generated, we will determine the conditions of face gear pointing taking that $r_{ms} = r_{bs}$.

To determine the exact point on the face gear surface where pointing will occur, the following is considered:

In general, the intersection of two surfaces is a line. For determination of pointing of the face gear tooth, the goal is to find an exact point on the line of intersection of the face gear tooth surfaces. Such a point lies in the plane tangent to the cylinder of radius r_{ms} and belongs to the top (addendum) of face gear tooth. Therefore, the following equality for *the orthogonal face gear drive* can be applied for each of the two sides of the face gear tooth.

$$z_{2_k} = -r_{ms} \qquad (k = \gamma, \beta) \qquad (83)$$

The subscripts β and γ are used for the designations of the surfaces of the face gear Σ_2 that are generated by the shaper surfaces β and γ, respectively

Substituting equation (83) into equation of face gear tooth surfaces (67), we obtain

$$\theta_{ks} = \pm \left(\frac{r_{ms}}{r_{bs} \sin \xi_{ks}} - \cot \xi_{ks} \right) \qquad (84)$$

where ξ_{ks} is represented earlier by (68).

Now, using equation (68), we obtain the following equations for the motion parameter ϕ_{ks}

$$\phi_{ks} = \xi_{ks} \mp (\theta_{ks} + \theta_{os}) \qquad (k = \gamma, \beta) \qquad (85)$$

The face gear motion parameter $\phi_{2_{(\gamma, \beta)}}$ is expressed in terms of ϕ_{ks} as

$$\phi_{2k} = \phi_{ks} m_{2s} \qquad (k = \gamma, \beta) \qquad (86)$$

where m_{2s} is the gear ratio.

Equation (67) yields

$$
\begin{aligned}
x_{2_k} &= r_{bs}[\cos \phi_2 (\sin \xi_{ks} \mp \theta_{ks} \cos \xi_{ks}) - \frac{\sin \phi_2}{m_{2s} \cos \xi_{ks}} + \frac{E}{r_{bs}} \cos \phi_2] \\
y_{2_k} &= -r_{bs}[\sin \phi_2 (\sin \xi_{ks} \mp \theta_{ks} \cos \xi_{ks}) + \frac{\cos \phi_2}{m_{2s} \cos \xi_{ks}} + \frac{E}{r_{bs}} \sin \phi_2]
\end{aligned}
\qquad (87)
$$

where $(k = \gamma, \beta)$.

In order to obtain intersection of the surfaces, the following conditions are considered

$$x_{2\beta} = x_{2\gamma}$$
$$y_{2\beta} = y_{2\gamma}$$
(88)

Note, using the procedure described above, the system of two nonlinear equations in two unknowns is obtained.

$$f_1(\xi_\beta, \xi_\gamma) = 0$$
$$f_2(\xi_\beta, \xi_\gamma) = 0$$
(89)

The system of equations (89) is solved numerically by the developed computer program applying the subroutine for the solution of system of nonlinear equations. Then the coordinates of intersection of two face gear tooth surfaces are determined, and the outer limiting radius R_2 of the face gear blank (fig. 1.1.5) is determined as

$$R_2 = \sqrt{x_2^2 + y_2^2}$$
(90)

where x_2 and y_2 are the coordinates of the point on the face gear tooth surface where pointing occurs.

Numerical example:

This numerical example illustrates the approach for determination of pointing, represented above. The input data is represented in Table 3

Table 3

INPUT DATA	
Number of teeth of the shaper	$N_s = 20$
Number of teeth of the face gear	$N_2 = 100$
Pressure angle	$\alpha_o = 25°$
Diametral pitch	$P_d = 10\ (1/in)$
Center distance	$E = 1\ (in)$
Crossing angle	$\gamma_m = 90°$

Using above input data, the following auxiliary data is obtained:

- Gear ratio $m_{s2} = 5$

- Radius of the pitch circle of the shaper $r_{ps} = 1.0$ (in)

- Radius of the shaper $r_{ms} = r_{ps} - \dfrac{1}{P_d} = 0.9000$ (in)

- Radius of the base circle of the shaper $r_{bs} = 0.9063$ (in)

Since $r_{ms} < r_{bs}$ it must be taken for the further calculation $r_{ms} = r_{bs} = 0.9063$ (in)

Procedure of Computations

Step 1: Equation (83) yields $z_{2\gamma,\beta} = 0.9063$ (in).

Step 2: Equation (84) is used, and it is considered that the values for $\xi_{\beta s}$ and $\xi_{\gamma s}$ are given by the initial guess. Note that this procedure is the iterative one and the initial guess must be provided. At the last step of iteration we have that $\theta_{\gamma s} = 0.33954$ (rad), and $\theta_{\beta s} = 0.35289$ (rad).

Step 3: Using equation (85), and considering as known: ξ_{ks} (from the initial guess), θ_{ks} (from the previous step) and θ_{os} (from the auxiliary data) the following values for ϕ_{ks} are calculated: $\phi_{\gamma s} = 0.26655$ (rad), and $\phi_{\beta s} = -0.27704$ (rad).

Step 4: Equation (86) and the known value of m_{s2} yield $\phi_{\gamma 2} = 0.05309$ (rad), and $\phi_{\beta 2} = -0.05541$ (rad).

Step 5: Then, equation (87) gives the following values for the coordinates of the gear surfaces where pointing occurs: $x_{2\gamma,\beta} = 1.0014$ (in) and $y_{2\gamma,\beta} = -5.77414$ (in).

Equation (90) gives the following exact solution for the limiting outer radius of the face gear $R_2 = 5.86034$ (in).

Approach 2 for Avoidance of Pointing

It was mentioned earlier that this approach is based on consideration of the cross-sections of tooth profiles of the shaper and the face gear. This is an alternative approximate approach, but the results that are provided by this approach are very close to the exact one. In the case of face gear drives with intersected axes, the instantaneous axis of rotation is used for

determination of pointing, while in the case of the offset face gear drives the axis of meshing is used instead.

This approach is based on the following considerations:

(1) Drawing of fig. 1.4.1 shows that $x_s = 0$ is the plane of symmetry of the shaper space. At a position of the shaper when $\phi_s = 0$, coordinate system S_s coincides with S_h (fig. 2.1.2) and the axis of meshing $I - I$ (fig. 2.2.3) belongs to the plane $x_s = 0$.

(2) Any cross-sections of the shaper tooth surface by planes that are parallel to x_s and perpendicular to the z_s- axis represent the same involute curves. Two such planes, Π_1 and Π_2, are shown in fig. 2.3.2(a). Plane Π_i intersects the axis of meshing $I - I$ at a point P_i that belongs to the axis of symmetry of the cross-section of the space of the shaper. Figs. 2.3.2(b) and 2.3.3 show points P_1 and P_2 that are the points of intersection of the axis of meshing $I - I$ and planes Π_1 and Π_2, respectively.

(3) A normal to the shaper tooth surface is perpendicular to the z_s- axis and therefore it lies in plane Π_i. In accordance to the definition of the axes of meshing, the common normal to the surfaces of the shaper and the face gear passes through the point of axis of meshing P_i $(i = 1, 2)$. Points of tangency of the shaper and the face gear profiles in plane Π_1 are M_1, M_2, and N_1 and N_2 in plane Π_2 (figs. 2.3.2(b) and 2.3.3). The common tangents to the cross-section profiles form an angle α_o and α, respectively.

(4) Now, assume that plane Π_2 is the plane where the pointing of the cross-section profiles of the face gear occurs. The investigation shows that in the area where pointing is observed, the cross-section profiles of the face gear only slightly deviate from the straight lines. Therefore, it can be assumed that point K (fig. 2.3.3) of the intersection of the tangents to the profiles is the point of intersection of the real cross-section profiles of the face gear.

(5) The consideration discussed above enables us to derive the equations for determination of the outer radius R_2 of the face gear for the zone of pointing using the following procedure.

Step 1: Vector equation (fig. 2.3.3)

$$\overline{O_sA} + \overline{AN_1} + \overline{N_1K} = \overline{O_sK} \tag{91}$$

yields that

$$\alpha - \tan\alpha\,\frac{2P_d r_{ms}}{N_s} = \theta_{os} \tag{92}$$

where θ_{os} is represented by the following equation

$$\theta_{os} = \frac{\pi}{2N_s} - inv\alpha_o \tag{93}$$

In the above equation α_o is the pressure angle of the shaper involute tooth.

Step 2: It is considered that point P_1 belongs to the pitch cylinder of the shaper, and the location of P_2 with respect to P_1 is determined with segments Δl and Δq (fig. 2.3.2(a)).

Drawings of figs. 2.3.2 and 2.3.3 yield

$$\Delta q = O_sP_2 - O_sP_1 = \frac{r_{bs}}{\cos\alpha} - \frac{r_{bs}}{\cos\alpha_o} = \frac{N_s}{2P_d}\Big(\frac{\cos\alpha_o - \cos\alpha}{\cos\alpha}\Big) \tag{94}$$

$$\Delta l = \frac{\Delta q}{\tan\gamma_s} \tag{95}$$

Step 3: The location of plane Π_2 is determined with parameter L_2 (fig. 2.3.2(a)), where

$$L_2 = \frac{r_p + \Delta q}{\tan\gamma_s} = \frac{N_s\cos\alpha_o}{2P_d\cos\alpha\tan\gamma_s} \tag{96}$$

where

$$\tan\gamma_s = \frac{\sin\gamma}{m_{s2} + \cos\gamma} \tag{97}$$

In this equation γ is the crossing angle and $m_{s2} = \dfrac{N_2}{N_s}$ is the gear ratio in meshing of the face gear and the shaper.

Finally, the outer radius R_2 of the face gear is determined as

$$R_2 = \sqrt{E^2 + L_2^2} \tag{98}$$

Numerical example:

This numerical example illustrates the approach for determination of pointing, represented above. The input data is represented in Table 3

Using the input data, the following auxiliary data is obtained:

- Gear ratio: $m_{s2} = 5$

- Radius of the pitch circle of the shaper $r_{ps} = 1.0 \ (in)$

- Angle $\gamma_s = 0.197395 \ (rad)$ (see equation (97))

- Radius of the shaper $r_{ms} = r_{ps} - \dfrac{1}{P_d} = 0.9000 \ (in)$

- Radius of the base circle of the shaper $r_{bs} = 0.9063 \ (in)$

Since $r_{ms} < r_{bs}$ it must be taken for the further calculation $r_{ms} = r_{bs} = 0.9063 \ (in)$

- · Half of the space width on the shaper base cylinder is determined with $\theta_{os} = 0.04856 (rad)$ (see equation (93))

Procedure of Computations

Step 1: We use equation (92) and consider as known the following parameters of the equation: P_d, N_s (from the input data), and r_{ms}, θ_{os} (from the auxiliary data). Then, by solving equation (92) using the subroutine for solution of nonlinear equations we obtain angle $\alpha = 0.6679 \ (rad)$ (fig. 2.3.3).

Step 2: We use equations (94) and consider as known from the input data α_o, and α obtained in Step 1. Then, we obtain $\Delta q = 0.15436 \ (in)$ (fig. 2.3.2(a))

Step 3: Using equation (96) and considering as known γ_s, r_{ps} (from the input data) and Δq from Step 2, we obtain the length $L_2 = 5.7718 \ (in)$ (fig. 2.3.2(a))

Step 4: We use equations (98) and consider as known offset E (from the input data), and L_2 obtained in Step 3. Then, we obtain the radius of the face gear, where pointing occurs as $R_2 = 5.8578 \ (in)$.

2.4 Localization of Bearing Contact and Simulation of Meshing

Two approaches for localization of the bearing contact in an offset face gear drive have been applied.

Approach 1

This approach is based on the consideration that the pinion and the generating shaper have different numbers of teeth. This approach has already been discussed in detail in *Part 1* for the case of the face gear drive with intersected axes, and therefore it is only briefly represented in this section.

Applied coordinate systems Two movable coordinate systems S_1 and S_2 are rigidly connected to the pinion and the gear (fig. 2.4.1 $(a), (b)$). Fixed coordinate systems S_h, S_f and S_a are rigidly connected to the frame. Henceforth, we will consider that all errors of alignment are referred to the gear, and the location and the orientation of the pinion are not affected by the errors of alignment. Auxiliary coordinate systems S_r and S_q are applied to simulate the change of shortest center distance and the crossing angle. The pinion performs rotation about the $z_f - axis$ while the gear performs rotation about the $z_q - axis$, and their angles of rotation are designated as ϕ_1' and ϕ_2' (figs. 2.4.1 $(a), (b)$). Parameter $B = r_{ps} - r_{pp}$ represents the distance between the axes of the shaper and the pinion, and it depends on $\Delta N = N_s - N_p$.

Now, applying the *Algorithm for simulation of meshing and contact* (described in *Part 1*, section 1.9), and considering the equations of continuous tangency (54) and (55) of the pinion and the face gear tooth surfaces, we can obtain the coordinates of contact points on the gear surfaces.

Since the tangency of the surfaces must be considered in a fixed coordinate system, for this purpose we may choose the coordinate system S_f. Then, the vector equations of the gear and the pinion tooth surfaces $(\mathbf{r}_i)$, as well as their unit normals $(\mathbf{n}_i)$ have to be represented

in S_f. The transformation matrix for coordinate transformation from the pinion to the fixed coordinate system $\mathbf{M}_{f1}$(equation (50)), and the transformation matrix for coordinate transformation from the gear to the fixed coordinate system $\mathbf{M}_{f2}$ (equation (52)), are given by

$$\mathbf{M}_{f1}(\phi_1') = \begin{bmatrix} \cos\phi_1' & -\sin\phi_1' & 0 & 0 \\ \sin\phi_1' & \cos\phi_1' & 0 & 0 \\ 0 & 0 & 1 & 0 \\ 0 & 0 & 0 & 1 \end{bmatrix} \tag{99}$$

and

$$\mathbf{M}_{f2}(\phi_2') = \mathbf{M}_{fa}\mathbf{M}_{ar}\mathbf{M}_{rq}\mathbf{M}_{q2} = \begin{bmatrix} \cos\phi_2' & -\sin\phi_2' & 0 & -(E+\Delta E) \\ \sin\Delta\gamma\sin\phi_2' & \sin\Delta\gamma\cos\phi_2' & \cos\Delta\gamma & B \\ -\cos\Delta\gamma\sin\phi_2' & -\cos\Delta\gamma\cos\phi_2' & \sin\Delta\gamma & 0 \\ 0 & 0 & 0 & 1 \end{bmatrix} \tag{100}$$

The set of contact points represents the *contact path*. The contact paths and contact ellipses for aligned and misaligned offset face gear drives are shown in figs. 2.4.2(a), (b) and (c).

Approach 2

This approach modifies the pinion tooth surface, instead of the face gear tooth surface, by means of a varied plunging of the tool used to generate the pinion (see section 1.3). This section covers simulation of meshing and contact of aligned and misaligned offset face gear drives with modified pinion tooth surfaces.

The modified tooth surfaces of the pinion are represented by the following equation

$$\mathbf{r}_p(u_p, \theta_p) = \begin{bmatrix} \pm r_{bp}[\sin(\theta_p + \theta_{op}) - \theta_p\cos(\theta_p + \theta_{op})] \\ -r_{bp}[\cos(\theta_p + \theta_{op}) + \theta_p\sin(\theta_p + \theta_{op})] + au_p^2 \\ u_p \end{bmatrix} \tag{101}$$

Face gear tooth surfaces generated by unmodified shaper tooth surfaces are represented by equation (67).

Applied coordinate systems   Two movable coordinate systems S_1 and S_2 are rigidly connected to the pinion and the gear (fig. 2.4.3 $(a), (b)$). Fixed coordinate systems S_f, S_m and S_a are rigidly connected to the frame. Again, it is considered that all errors of alignment are referred to the face gear. Auxiliary coordinate systems S_r and S_q are applied to simulate misalignment. The pinion and the face gear perform rotation about the z_f- and $z_q - axes$, and their angles of rotations are designated as ϕ_1' and ϕ_2' (figs. 2.4.3 $(a), (b)$). Parameter u_o (fig. 2.4.3 (a)) represents the distance between the axis of rotation of the face gear and the location of the origin of the pinion coordinate system. The magnitude of u_o that corresponds to the location of the contact path in the middle of the face gear tooth length is determined as

$$u_o = \sqrt{\left(\frac{R_1 + R_2}{2}\right)^2 - E^2} \tag{102}$$

Here R_1 and R_2 are the inner and outer radii of the face gear, obtained from the conditions of non-undercutting and pointing, and E is the shortest center distance.

Choosing another magnitude of u_o, that differs from the one determined above, we can change the location of the bearing contact on the face gear tooth surface.

We use coordinate system S_f to consider the tangency of the contacting surfaces. Then the vector equations of the gear and the pinion tooth surfaces $(\mathbf{r}_i)$ as well as their unit normals $(\mathbf{n}_i)$ have to be represented in S_f. The transformation matrix from the pinion to the fixed coordinate system $(\mathbf{M}_{f1})$ is given by

$$\mathbf{M}_{f1}(\phi_1') = \begin{bmatrix} \cos\phi_1' & -\sin\phi_1' & 0 & 0 \\ \sin\phi_1' & \cos\phi_1' & 0 & 0 \\ 0 & 0 & 1 & u_o \\ 0 & 0 & 0 & 1 \end{bmatrix} \tag{103}$$

The face gear tooth surface is represented by equation (67). To represent this surface in a fixed coordinate system, we use the following transformation matrix

$$
\mathbf{M}_{f2}(\phi_2') = \mathbf{M}_{fa}\mathbf{M}_{ar}\mathbf{M}_{rq}\mathbf{M}_{q2} = \begin{bmatrix} \cos\phi_2' & -\sin\phi_2' & 0 & -(E+\Delta E) \\ \sin\Delta\gamma\sin\phi_2' & \sin\Delta\gamma\cos\phi_2' & \cos\Delta\gamma & 0 \\ -\cos\Delta\gamma\sin\phi_2' & -\cos\Delta\gamma\cos\phi_2' & \sin\Delta\gamma & 0 \\ 0 & 0 & 0 & 1 \end{bmatrix}
$$

(104)

Having the gear surfaces represented in a fixed coordinate system and applying the described *Algorithm for simulation of meshing and contact* (Part 1, section 1.9), we can obtain the set of contact points and contact ellipses. The contact path for an ideal gear drive (gear drive without assembly errors) as well as contact paths for gear drives with simulated misalignment are represented in fig. 2.4.4(a), (b), (c).

An analysis of the results for approach 2, when a pinion with a modified tooth surface is applied, shows that the magnitude of the transmission errors (represented by equation (62)) is not equal to zero, as was the case when an unmodified pinion tooth surface was applied. However, the magnitude of these transmission errors for a misaligned offset face gear drive does not exceed 3 arc seconds. This leads us to the conclusion that face gear drives are not sensitive to misalignments if the localization of the bearing contact is performed by the application of an involute pinion with a modified surface and the same number of teeth as the generating shaper. This approach helps to reduce the shift of the bearing contact caused by misalignment as shown in fig. 2.4.4(a), (b), (c).

Part 3
Applications for Face Gear Drives

3.1 Design Uses for Face Gears in Aerospace Applications

Boeing has investigated several candidate aerospace applications for face gears. Use of face gears in helicopter transmissions has been the main area of investigation, with preliminary conceptual designs for several different main rotor transmission configurations having been completed to date. Most of these concepts involve taking advantage of face gears configured to split engine input torque entering the transmission as shown in figs. 1.1.2 and 1.1.3. Additional face gear arrangements were conceived for nacelle transmissions in tilt rotor aircraft, counter-rotating NOTAR® fan gear boxes used in helicopter antitorque systems (see fig. 3.1.1), lift fan propulsion gear boxes and turbo-prop gear boxes for jet aircraft. Face gears can be used in many angular-drive applications for which bevel gears (straight or spiral bevel) are currently used. The exception to this is with gear boxes having ratios lower than 3.5 to 1, as face gears don't offer a significant advantage over conventional gears at lower reduction ratios. The application of face gears in several split torque concepts is unique, as bevel gears cannot be used in these configurations, with details of this to be described later.

3.2 Comparisons of Face Gears with Bevel Gears

Face gears have several differences with bevel gears which should be examined. Standard face gear pinions are conventional involute spur gears, which are inexpensive to procure when compared with bevel gears. The spur pinion has no sensitivity to axial location and only low sensitivity to radial location. As a result of this, it is not necessary to install the pinion at a

precise mounting distance, as is the case with bevel gear installations. This reduces assembly costs and allows easy field installations of new spur pinions into gearboxes if required. Also, no axial force is generated on the spur pinion as it meshes with the face gear. This removes the requirement for larger bearings to handle thrust, bearings which are always required for bevel gears. The face gear member of the set also tolerates small misalignments well, and the misalignments cause less transmission error than in other gear forms. Like a bevel set, the motion of a face gear set attains true conjugate action, resulting in constant velocity shaft rotation. Basic geometric differences between these gears and bevel gears are readily apparent, as can be seen by referring to the face gear teeth shown in figs. 1.1.1 and 1.1.3. For the gear member of a face gear set, teeth become narrower along the top land of the tooth as one progresses from the inside diameter (I.D.) of the gear to the outside diameter (O.D.), and teeth widen as one goes along the tooth bottom from I.D. to O.D.. In short, the face gear tooth has an increasing pressure angle along its length from I.D. to O.D.. The height of the face gear teeth stays constant along their length, so that both pinion and gear members operate along a constant base circle. In contrast, bevel gear teeth increase in both height and width along the tooth length from I.D. to O.D.. Face gear teeth are only slightly curved (nearly straight), both along their length and along their height, whereas spiral bevel teeth curve significantly along both height and length.

Regarding tooth widths, the length of face gear teeth are limited by conditions of tooth undercutting near the I.D. and tooth pointing near the O.D.. The I.D. must be greater than the diameter at which undercutting would otherwise occur, and the O.D. must be smaller than the diameter at which pointing would normally occur (although the O.D. can be left somewhat larger if the top land is chamfered to remove the pointed area as shown in fig. 3.2.1). In comparison, the length of bevel gear teeth is similarly limited as a percentage of the outer come distance, although for an equal set of basic design parameters, more bevel gear tooth length than face gear tooth length is usually available after applying the limiting criteria noted above.

3.3 Split Torque Face Gear Arrangements

One of the biggest advantages for using face gears is when they are applied in torque splitting arrangements. When face gear designs are configured to allow input torque to be divided equally from a single pinion into two face gears, the sizes of the gears involved can be reduced substantially. This is because gear volume is proportional to the square of gear diameter, while torque-carrying capacity of gearing is proportional to lower order determinants of gear diameter (depending on whether bending or compressive stress evaluations are being used). Therefore, if torque is reduced by approximately one-half (based on the actual percentage of torque split between the gears) for a load-carrying gear, the weight of the gear can be reduced by more than one-half, due to the square relationship of weight to gear diameter. Face gears have unique advantages over other types of angular-drive gearing when used in specific torque splitting configurations. Two of these configurations for which this is the case are shown in figs. 3.3.1 & 3.3.2. In particular, other types of existing gears cannot be configured to provide an input pinion driving through angles other than ninety degrees to two gears simultaneously. This is true whether the two driven gears face each other with one directly above the other as shown in fig. 3.3.1, or if they are facing each other in a staggered arrangement as shown in fig. 3.3.2. Bevel gears form cones if the pitch lines of the gear teeth are projected out until they reach a single apex. If the shaft angle in a three member set of one pinion driving two gears is not equal to ninety degrees (either greater or less than ninety degrees), one of the members would have to have a cone that funnels inward (concave shape). Bevel gears cannot be cut or ground to yield a funneled cone shape, due to manufacturing limitations. Face gears are not restricted by this manufacturing limitation. Also, split torque designs are almost always used in conjunction with a requirement to achieve high reduction ratios, and face gears operate better than bevel gears at these higher ratios (see section 3.1).

3.4 Design Considerations for Face Gear Usage

Special Design Considerations

The face gear design process includes some special considerations required to allow the use of these gears. Basically, implementation of face gears into designs where bevels are typically used is limited only by the requirement to use larger reduction ratios wherever face gears are employed. On a more detailed level, though, several tooth geometric considerations must be taken into account during the design process. The conditions of tooth undercutting and tooth pointing mentioned previously in section 3.2 must be avoided. This is accomplished by first determining at what inside radius of the gear the condition of undercutting would occur, and at what outside radius of the gear the condition of tooth pointing would occur. To determine these for a prospective design, the numbers of gear and pinion teeth, the diametral pitch, the shaft angle, and the approximate amount of tooth crowning desired must be entered as variables into known equations. Limit values for directions along both the pitch angle and normal to the shaft centerline can be obtained. The available tooth face width can also be obtained (also along both directions as above) from the difference between these values. Once the face width is known, this information is considered in the gear stress analysis along with the other design parameters. The inner and outer radius values are utilized in design envelope considerations as well as bearing sizing and support arrangements.

Stress Considerations

At the present time, no substantiated stress formulas are available for sizing face gear sets in the same manner as traditional bevel or spur gear sets. Preliminary methods for analyzing face gears have been developed at both UIC and Boeing, using a combination of Finite Element Analysis (FEA) and modifications to existing spur gear formulas to calculate tooth bending and tooth contact stresses for face gear sets. The analysis assumes, with

substantiation from FEA, that the spur pinion is the weaker (in bending) of the two gears in the set. Based on the FEA of models of face gear tooth geometry, it appears that the spur pinion in a face gear set has approximately 1/3 less tooth bending stress than that of an identical spur pinion mated with a spur gear under the same loading conditions. This is apparently due in large part to the greater contact ratio of the face gear set vs. a standard spur set. In the traditional spur gear set, the pinion sees the load being alternately carried by one then two teeth, whereas with a face gear set the load is carried by two or three teeth in an alternating manner. Tooth compressive or contact stresses appear to be in the same range as those currently found in spur gear sets, and it remains to be seen how they will compare to spur, helical, and bevel gears after long term testing. A good discussion of the subject of face gear stress analysis can be found in the paper "Design, Analysis, and Testing Methods for a Split-Torque face gear Transmission" [13]. Durability tests are currently underway at the NASA John H. Glenn Research Center to generate vibration and SN curve data for carburized and ground face gears. These tests will also determine the characteristics of the face gear tooth contact pattern during installation and operation. A good summary of the most recent NASA GRC test investigations can be found in the paper "Evaluation of Carburized and Ground Face Gears" [14]. A significant number of these durability tests have yet to be run, and until these tests are completed, or at least much more complete, all formulas created and used to estimate face gear stresses and lives are subject to revision, and must be considered preliminary.

References

[1] Basstein, G. and Sijtstra, A., "New Developments in Design, Manufacturing and Applications of Cylkro-(Face) Gears", A.G.M.A. Technical Paper, 93FTM7, October 1993.

[2] Davidov, S.Ya., "Non-Involute Gears", Mashgiz, 1950.

[3] Favard, J., "Course of Local Differential Geometry", Gauthier-Villars, 1957.

[4] Korn, G.A. and Korn, T.M., "Mathematical Handbook for Scientists and Engineers", 2nd edition, McGraw-Hill, New York, 1968.

[5] Litvin, F.L., "Theory of Gearing", Nauka, 1968, (in Russian).

[6] Litvin, F.L., "Theory of Gearing", NASA Reference Publication 1212, 1988.

[7] Litvin, F.L., "Gear Geometry and Applied Theory", Prentice Hall, Englewood Cliffs, NJ, 1994.

[8] Litvin, F.L., Chen, J.-S., Seol, I., Kim, D.H., Lu, J., Zhao, X., Egelja, A., and Wang, A. G., "Computerized Design and Generation of Gear Drives with Localized Bearing Contact and Low Level of Transmission Errors", Proceedings of International Conference on Gears, Dresden, Germany, April 22 - 24, NR. 1230, pp. 63-82, 1996.

[9] Litvin, F.L., Egelja, A., Tan, J., and Heath, G., "Computerized Design, Generation and Simulation of Meshing of Orthogonal Offset Face-Gear Drive with a Spur Involute Pinion with Localized Bearing Contact", Mechanism and Machine Theory, in press.

[10] Litvin, F.L., Wang, J.-C., Chen, Y.-J., Bossler, R.B., Heath, G., and Lewicki, D.J., "Face-Gear Drives: Design, Analysis and Testing for Helicopter Transmission Applications", A.G.M.A. paper, 92TFM.

[11] Litvin, F.L., Zhang, Y., Wang, J.-C., Bossler, R.B., and Chen, Y.-J., "Design and Geometry of Face-Gear Drives", ASME J. Mechanical Design, 114: pp. 642-647, 1992(c).

[12] Litvin, F.L. and Kim, D.H., "Computerized Design, Generation and Simulation of Meshing of Involute Spur Gears With Localized Bearing Contact and Reduced Level of Transmission Errors", Transactions of ASME, Vol. 119: pp. 96-100, 1997.

[13] Chen, Y.D. and Bossler, R.B., "Design, Analysis, and Testing Methods for a Split Torque Face-Gear Transmission", A.I.A.A. paper 95-3051, July 1995.

[14] Lewicki, D.G., Handschuh, R.F., Heath, G.F., and Sheth, V., "Evaluation of Carburized and Ground Face Gears", Proceedings of the 55th American Helicopter Society International Forum, May 1999, pp. 723-731. (Also NASA TM-1999-209188, Army Research Laboratory Report ARL-TR-1998)

[15] Litvin, F.L., Wang, J.-C., Bossler, R.B., Lewicki, D.J., Heath, G.F., and Chen, Y.-J., "Application of Face Gear Drives in Helicopter Transmissions", ASME Journal of Mechanical Design, Vol. 116(3), September 1994, pp. 672-676.
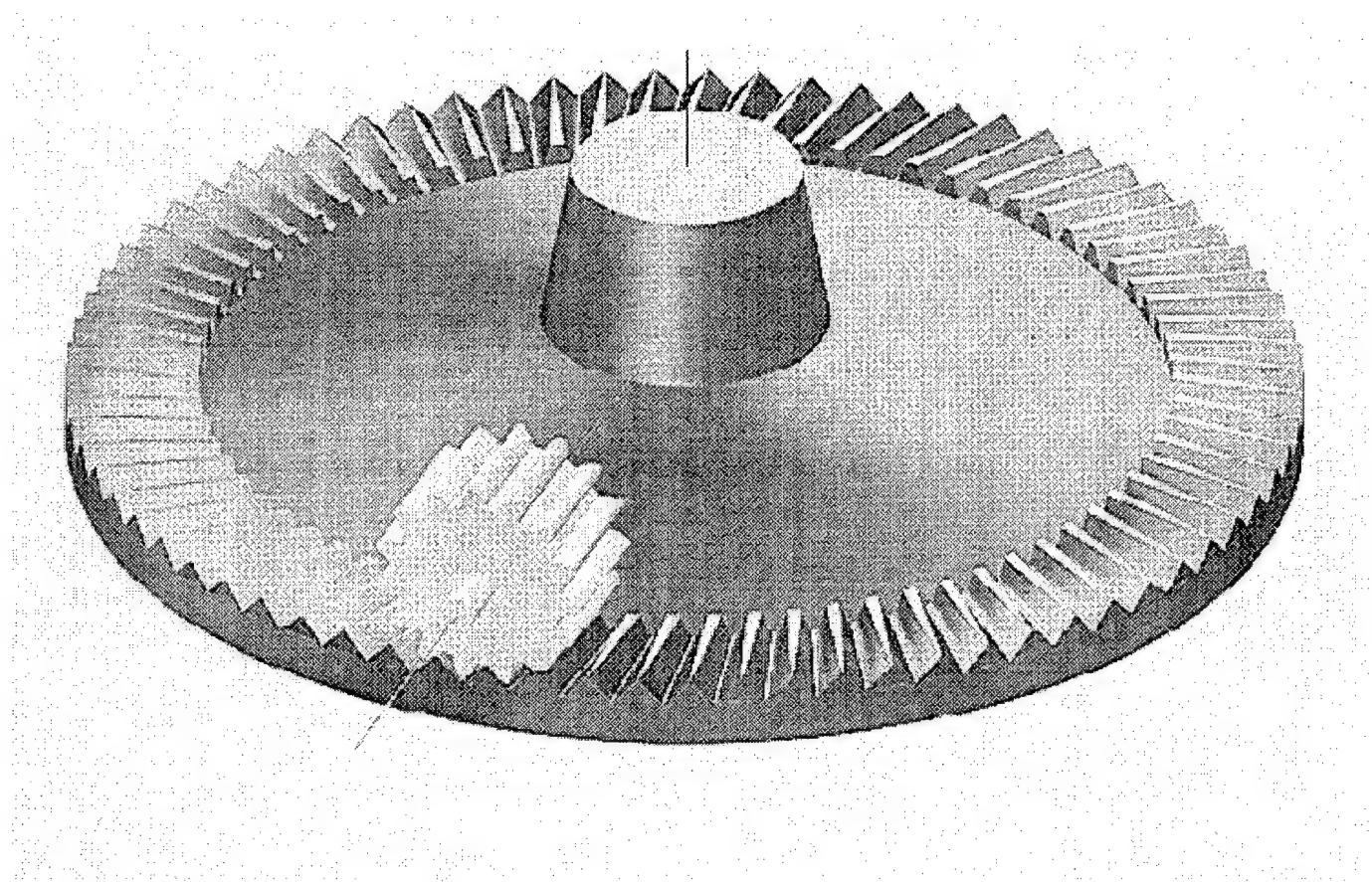
Fig. 1.1.1   Face-gear drive with intersecting axes

(a)

Combining gear

Spiral bevel pinions

Spiral bevel gears

Engine shaft

(b)

Combining gear

Face-gears

Engine shaft
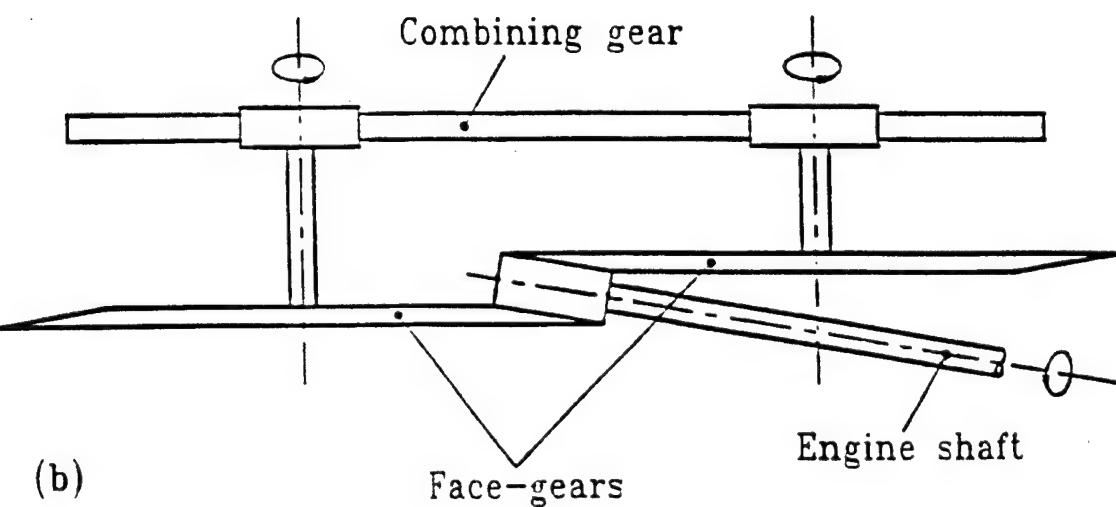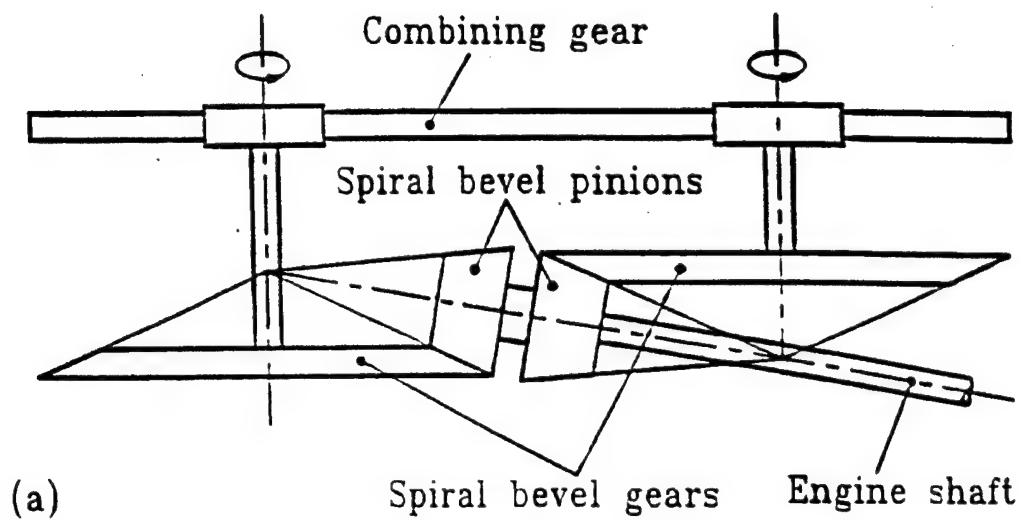
Fig. 1.1.2 Examples of torque split

54
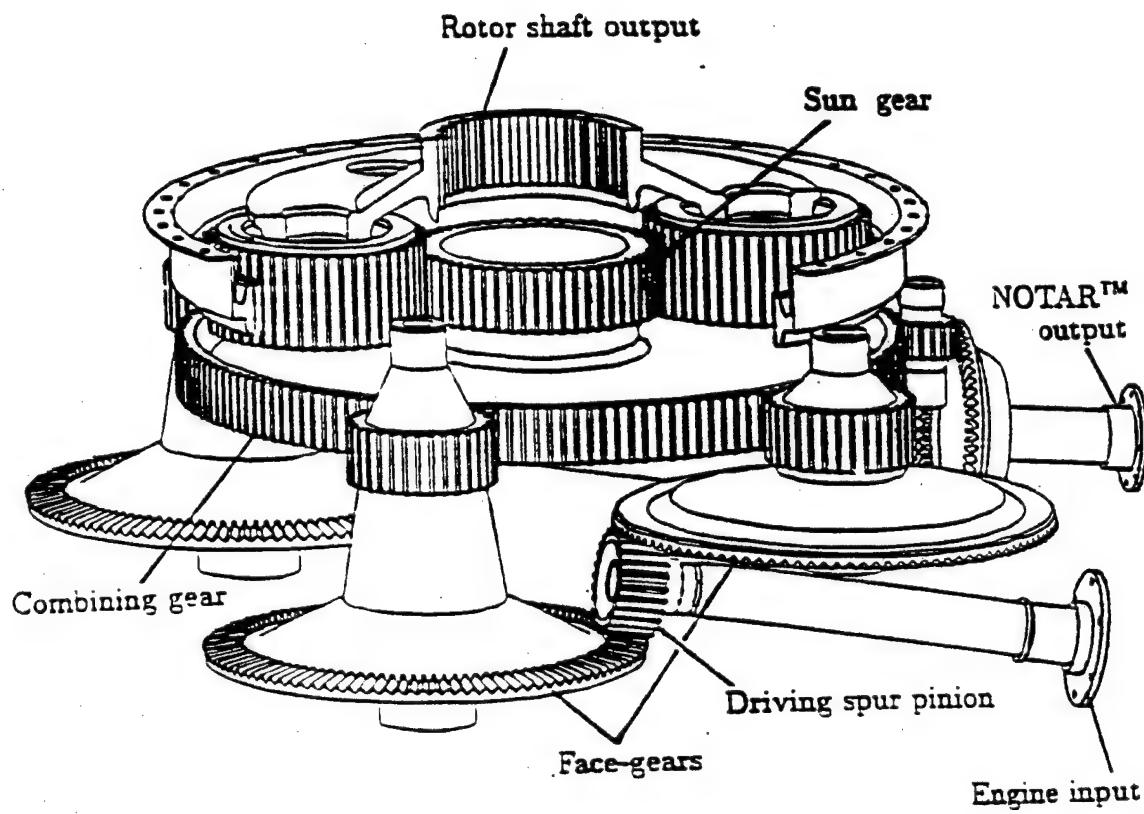
Fig. 1.1.3   Helicopter transmission with a face-gear drive
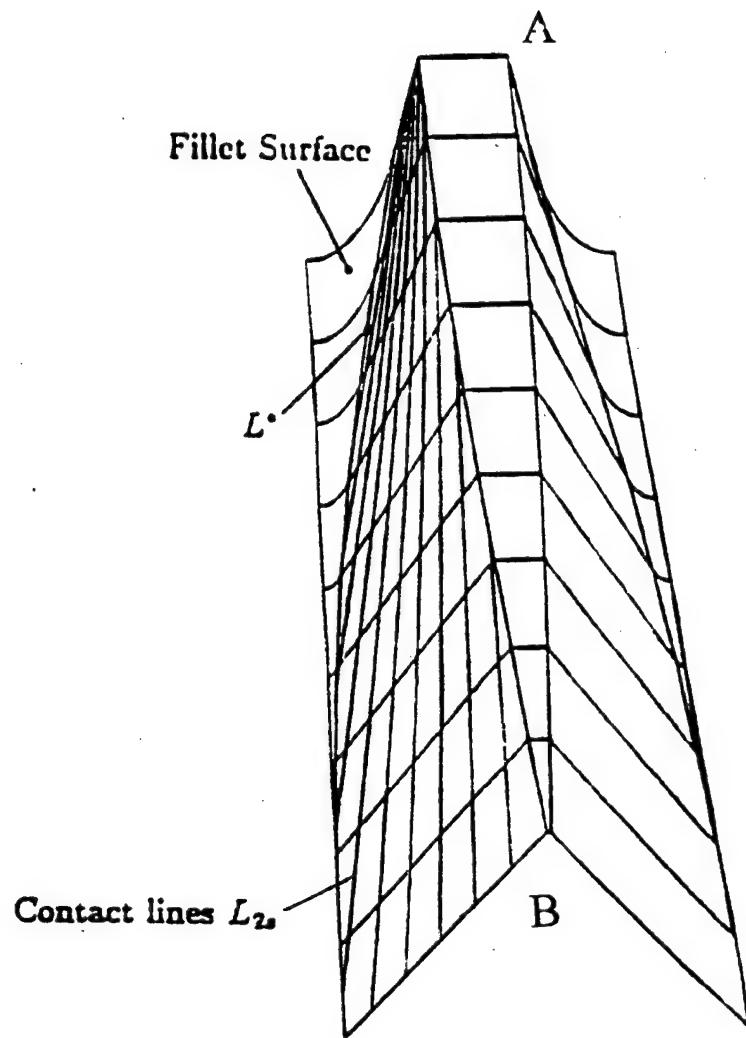
Fig. 1.1.4   Face-gear tooth of the gear drive with intersected axes
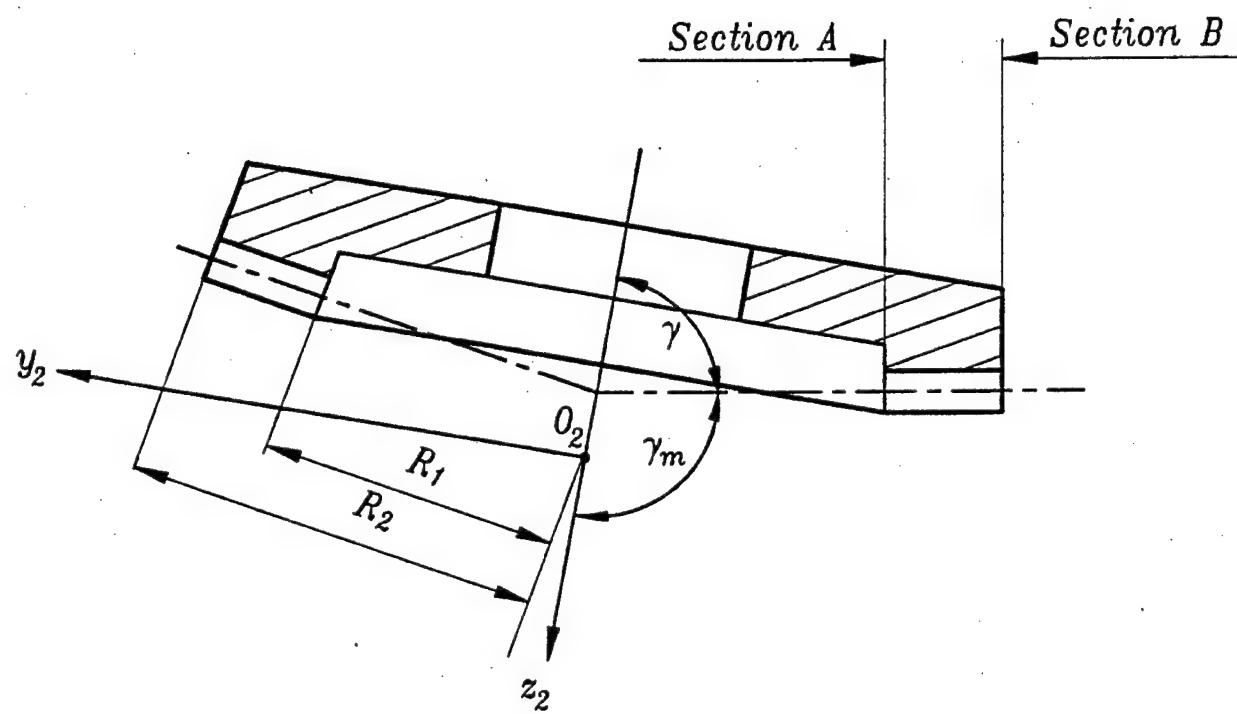
Fig. 1.1.5   Schematic of a face gear
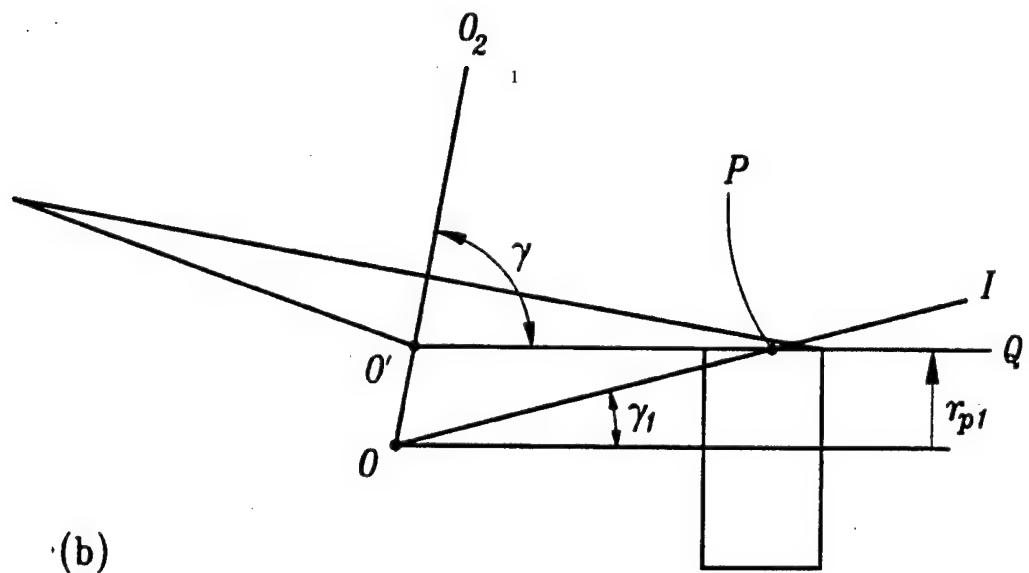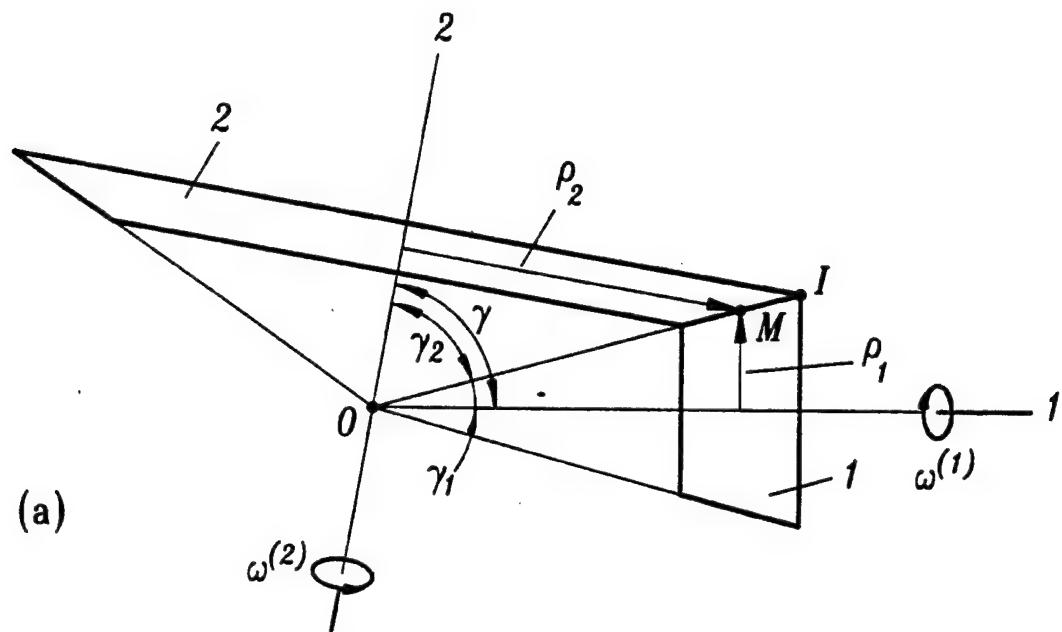
Fig. 1.2.1 Instantaneous axis of rotation OI, pitch cones with pitch angles γ_1 and γ_2, pitch surfaces as a cylinder r_p and cone of angle γ
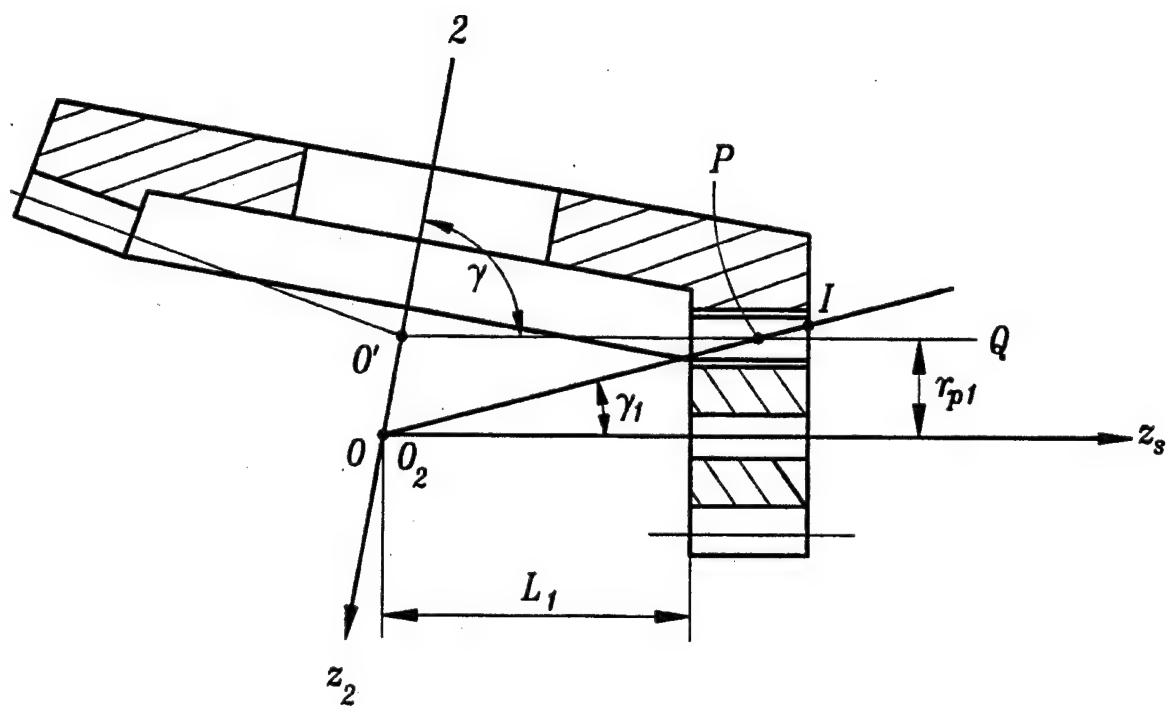
Fig. 1.2.2   Shaper (pinion) and the face gear
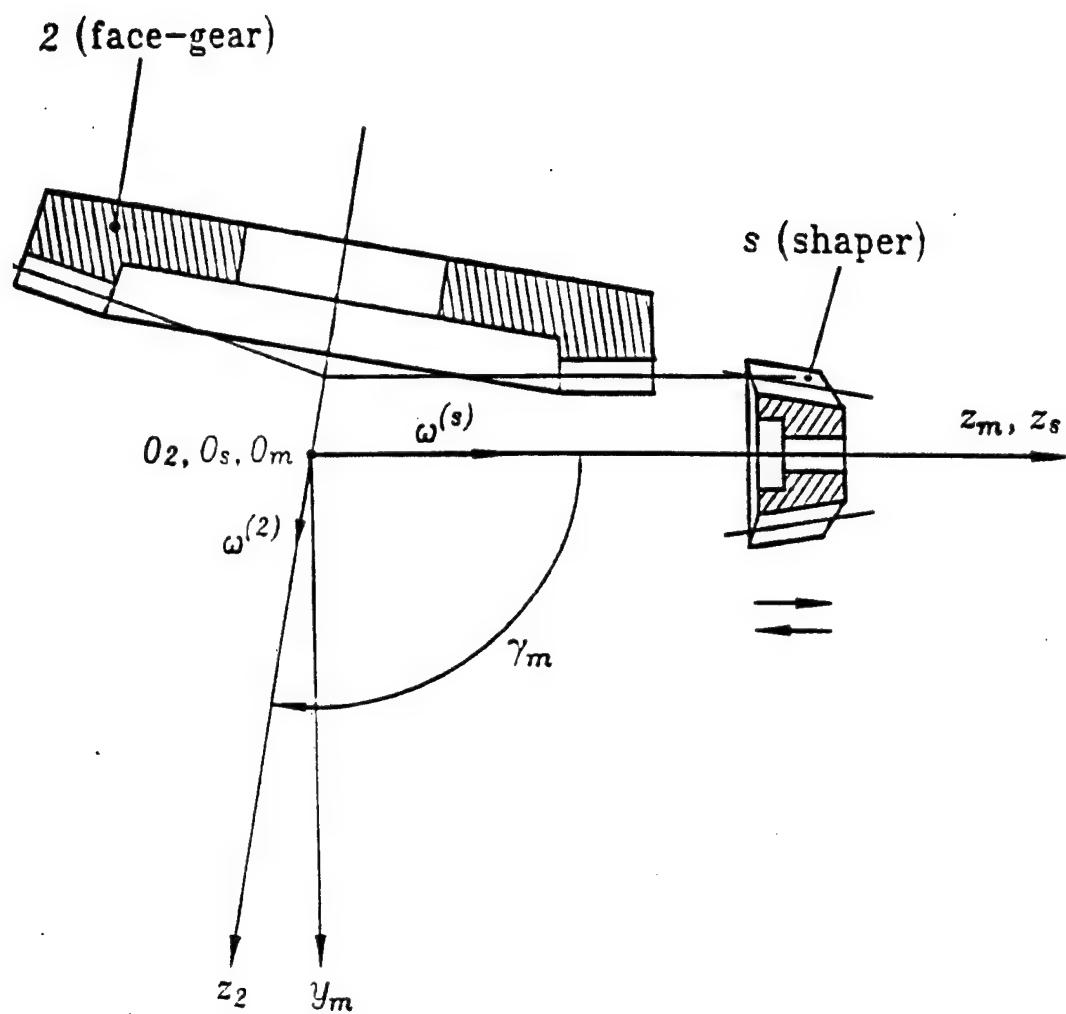
Fig. 1.3.1   Generation of face gear by a shaper
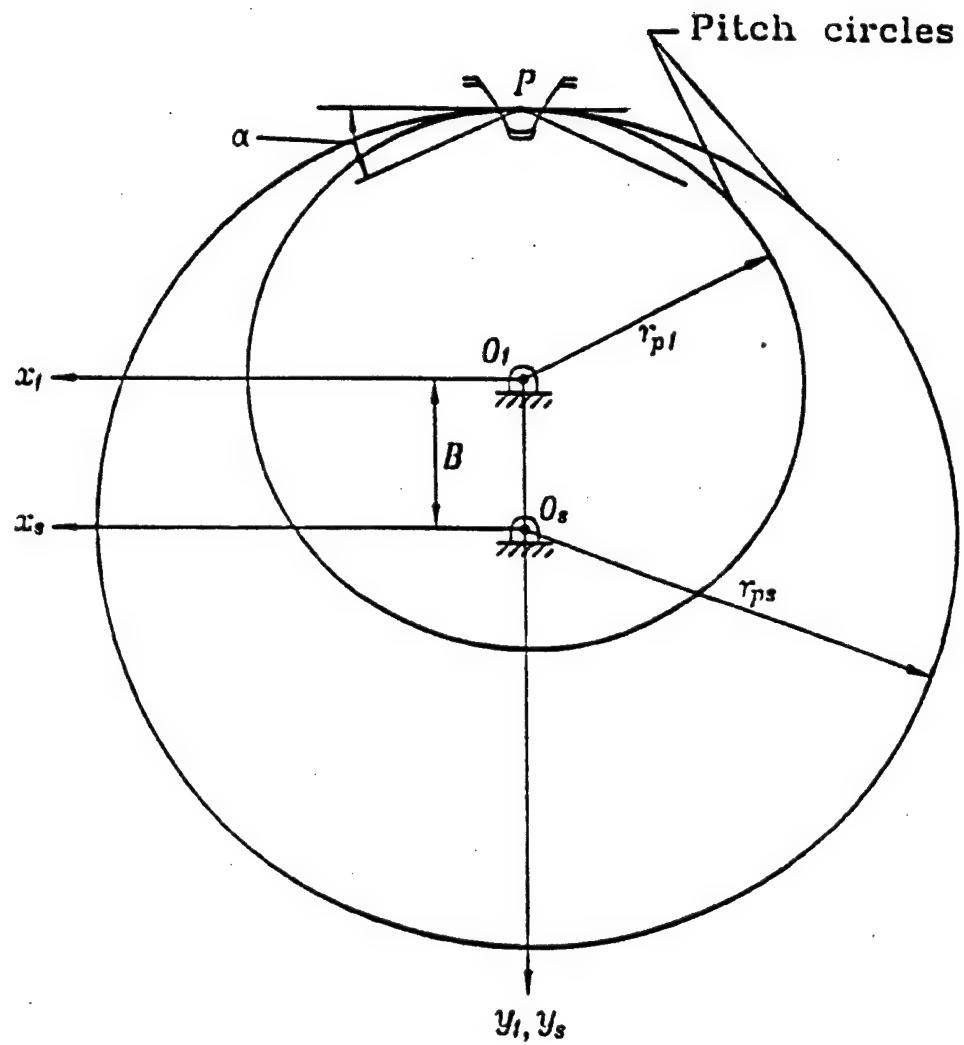
Fig. 1.3.2   Imaginary tangency of the shaper and the pinion of the drive
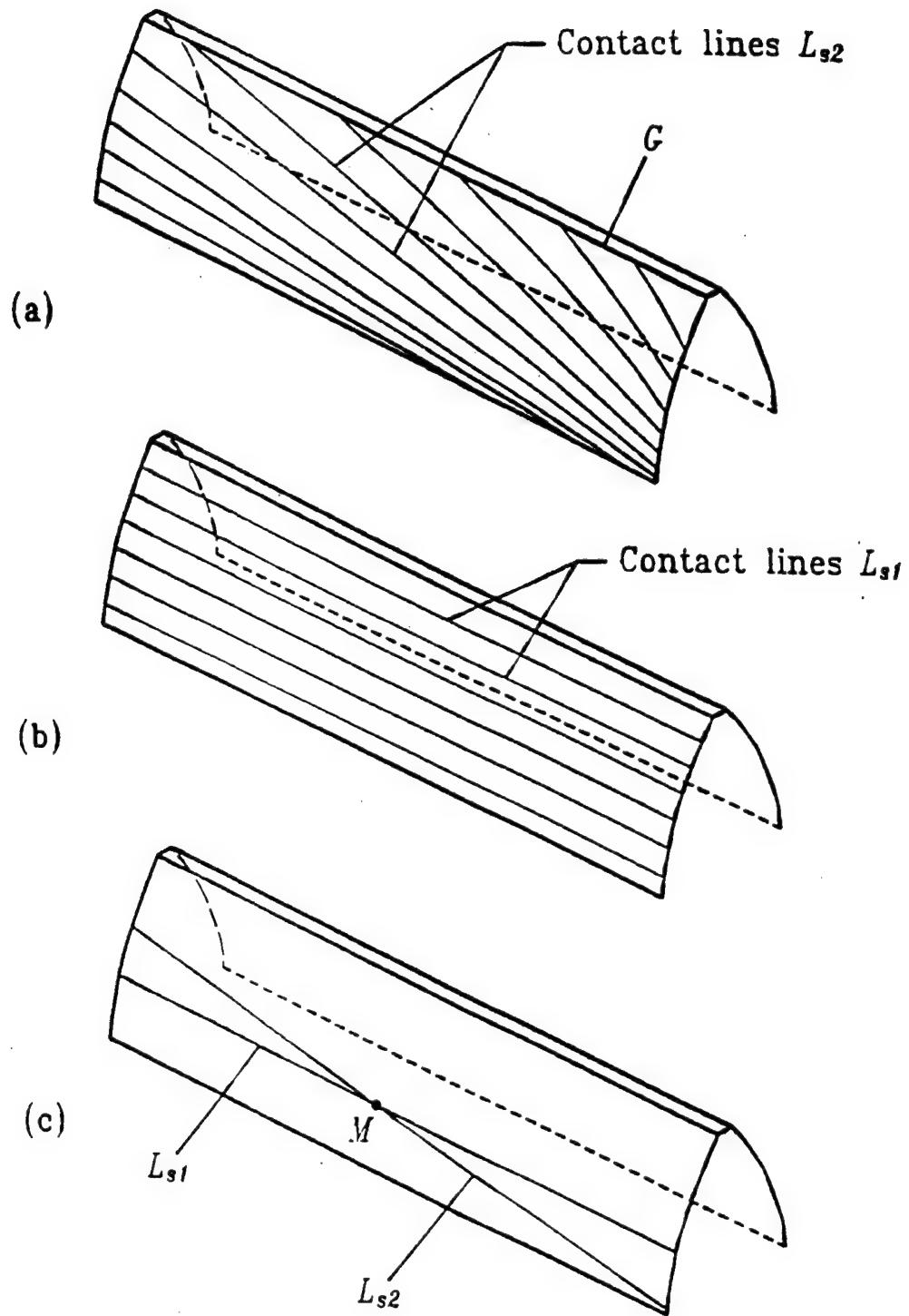
Fig. 1.3.3 Contact lines on shaper tooth surface

Major axis of contact ellipse
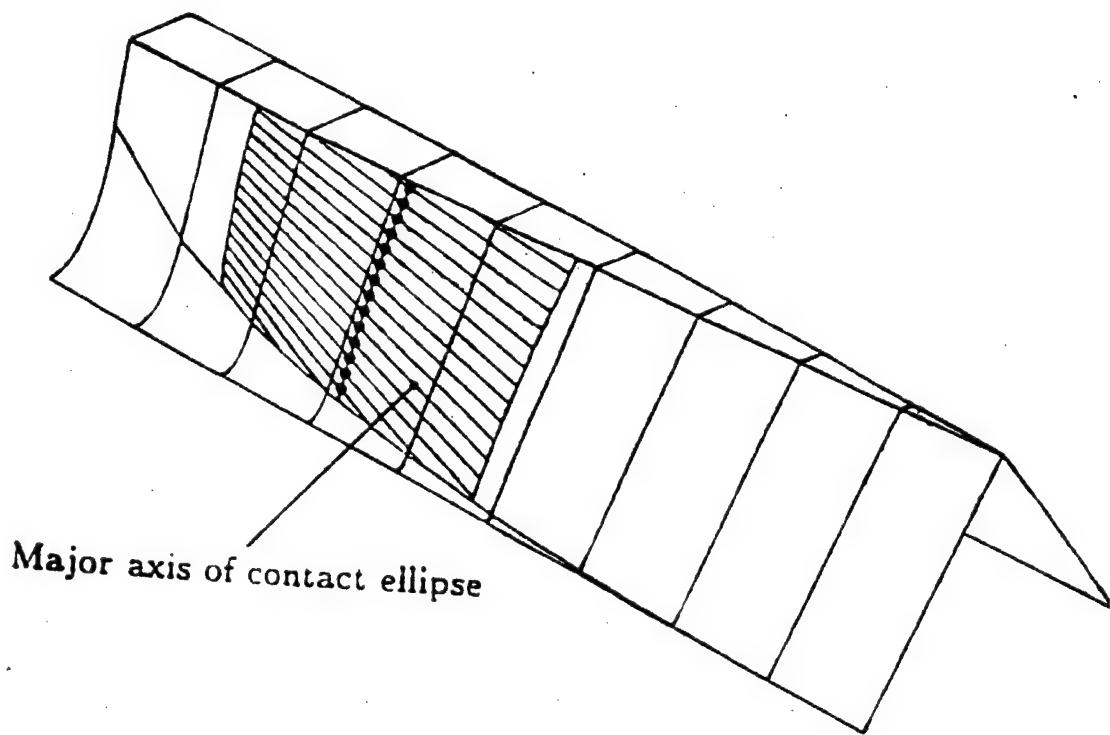
Fig. 1.3.4   Localized bearing contact
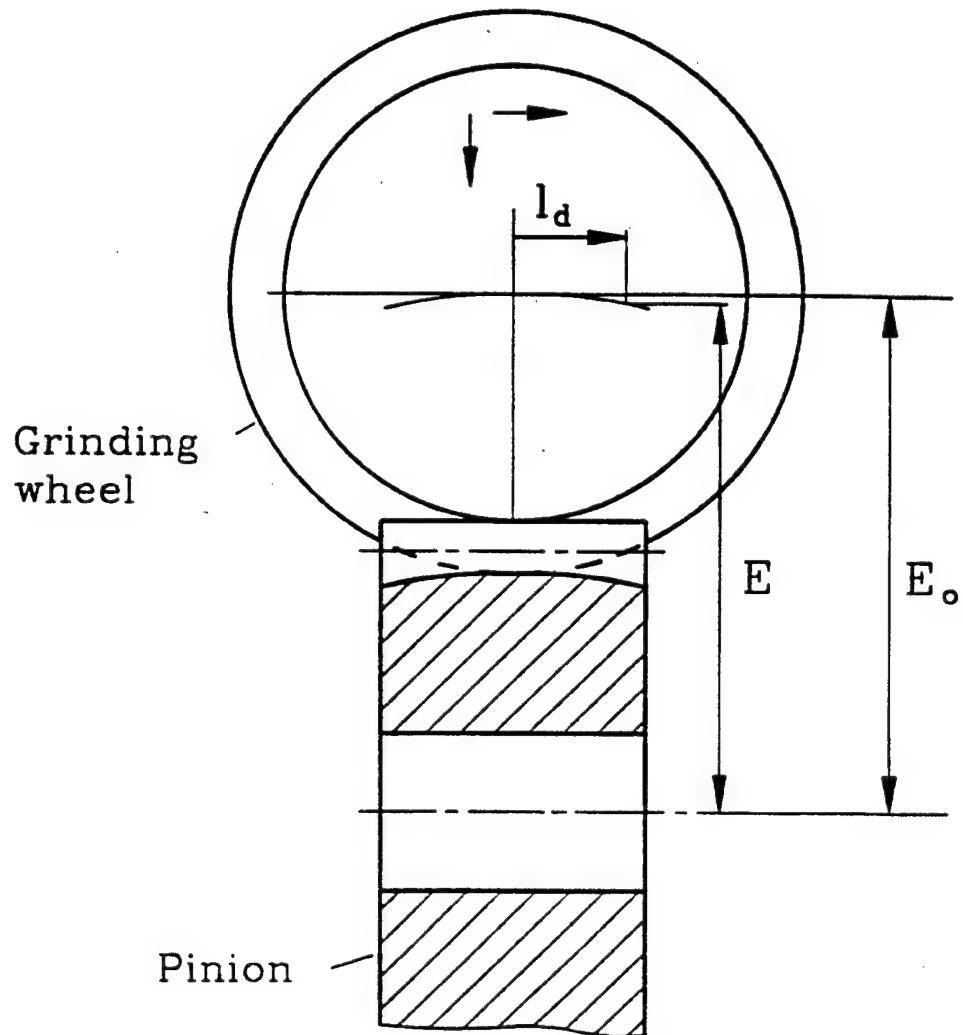
Fig. 1.3.5   Form grinding of the pinion with plunging of the grinding disk
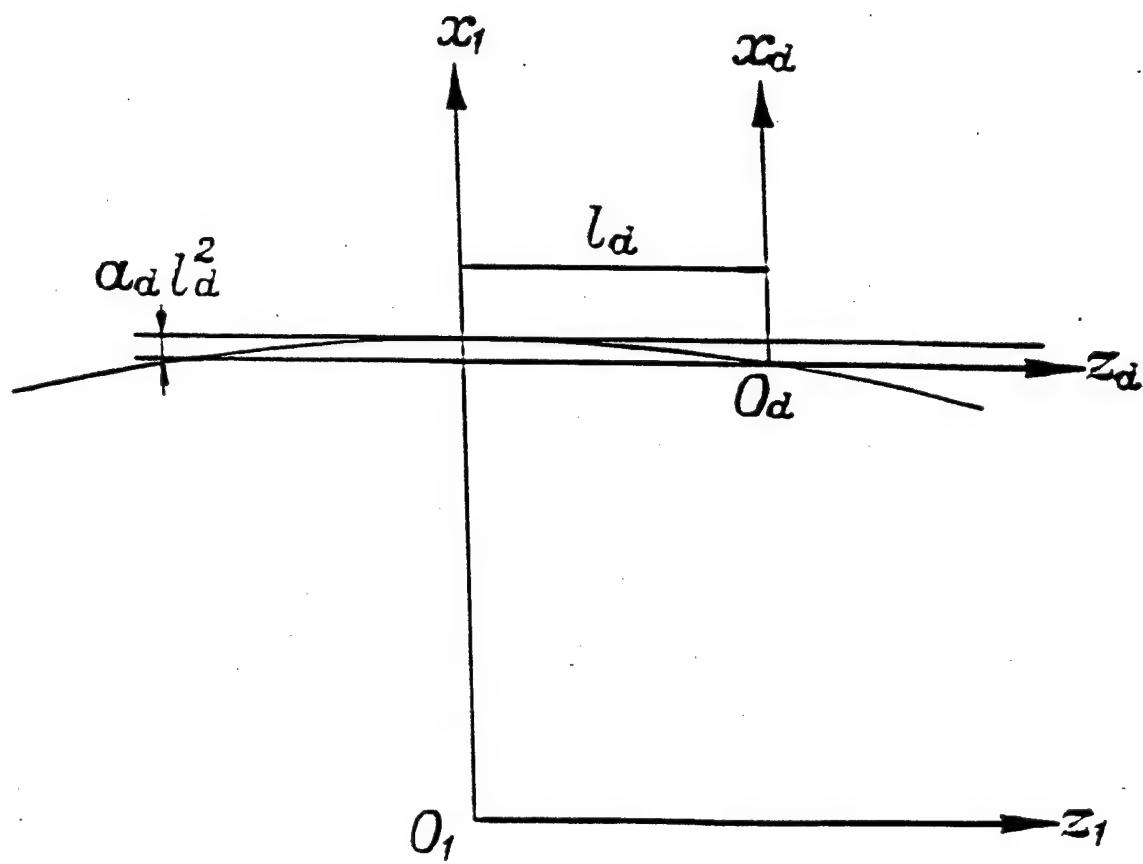
Fig. 1.3.6 Coordinate systems applied for generation of the pinion by plunging

65
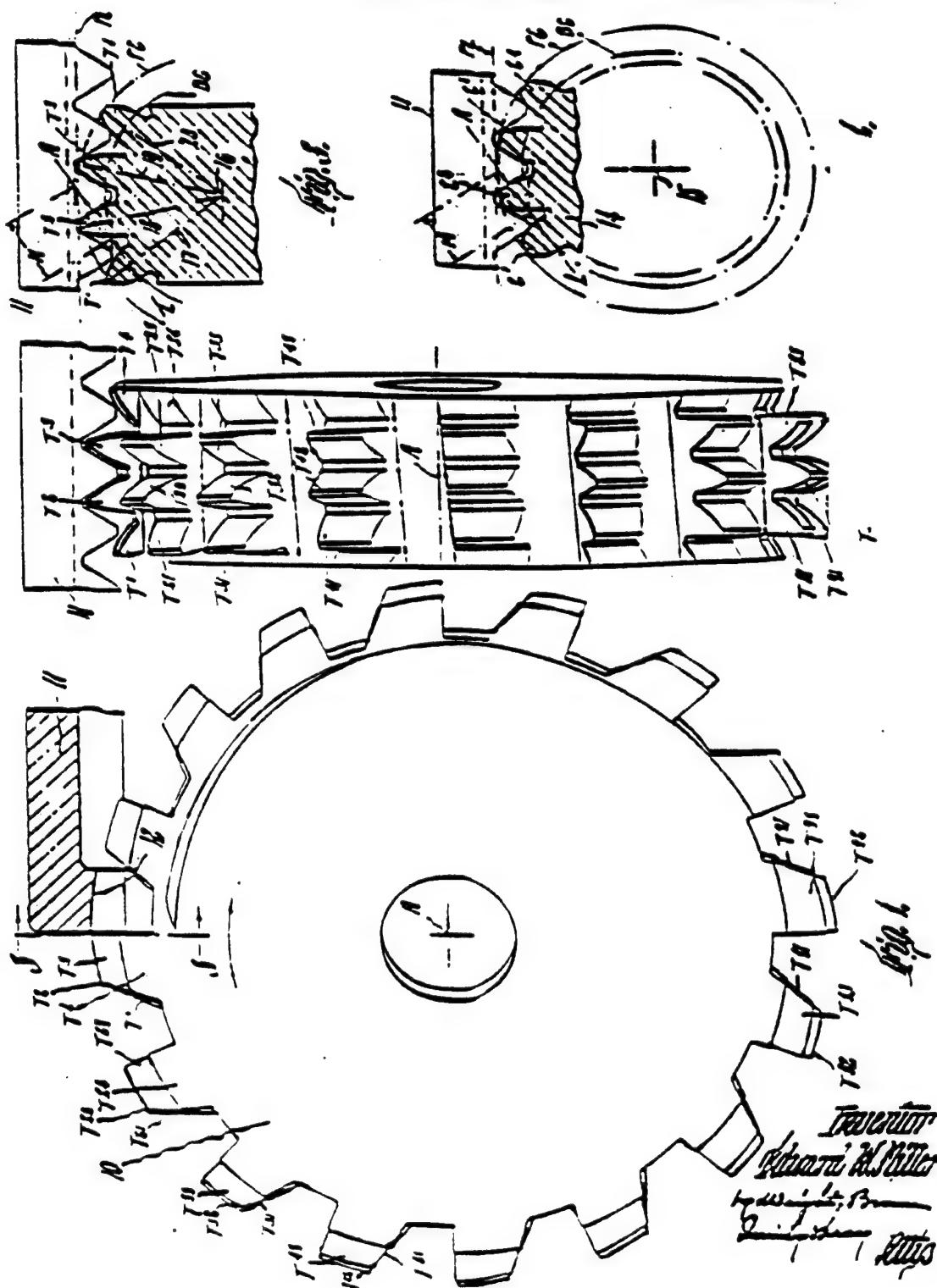
Fig. 1.3.7   Grinding worm proposed by E. W. Miller
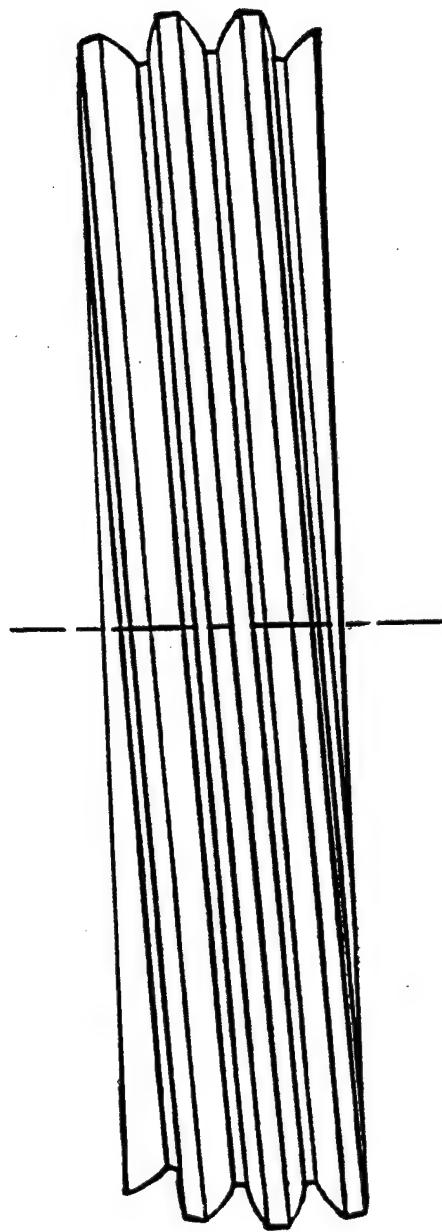
Fig. 1.3.8 Grinding worm proposed by F. L. Litvin et al.
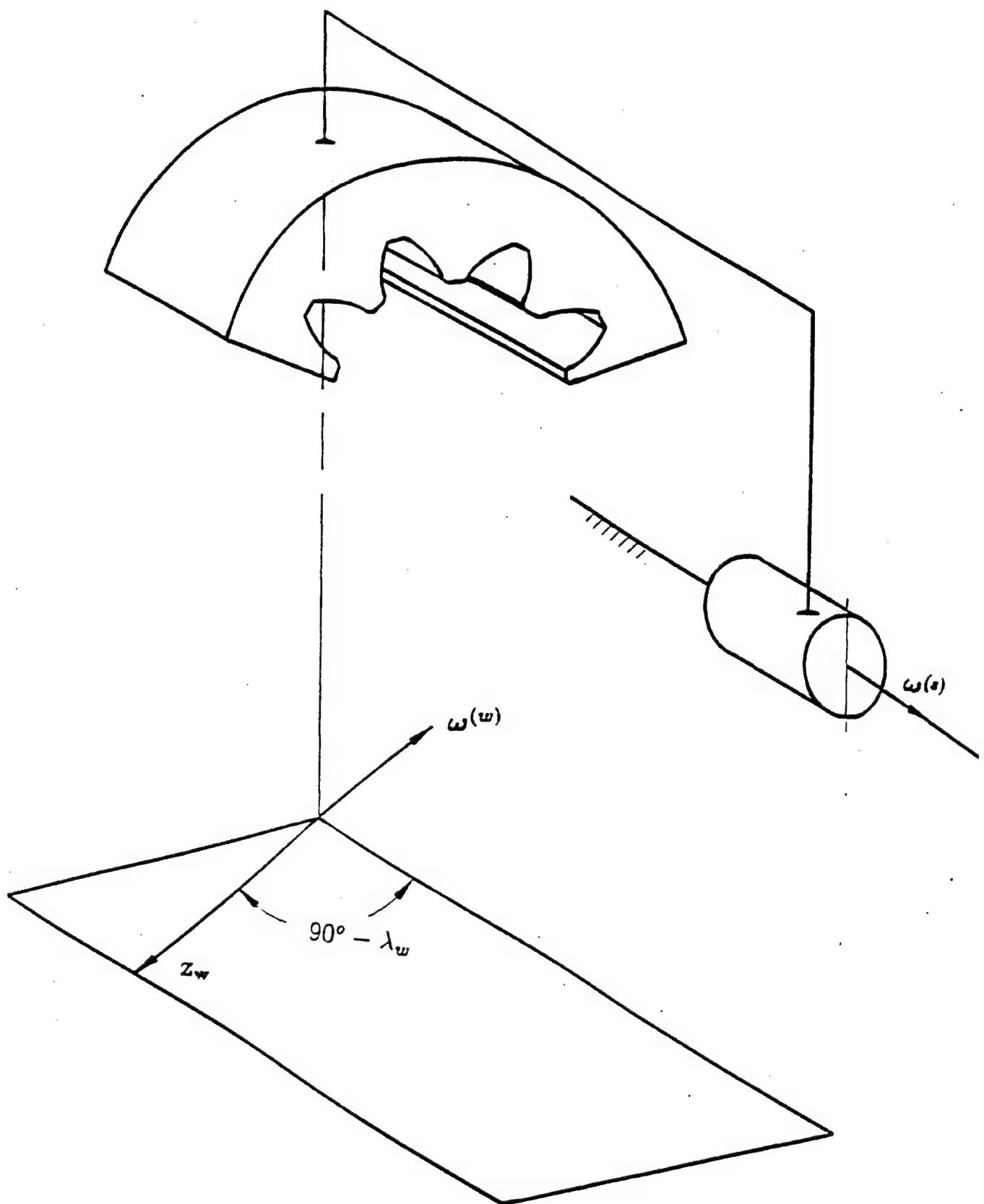
Fig. 1.3.9   Dressing of the worm
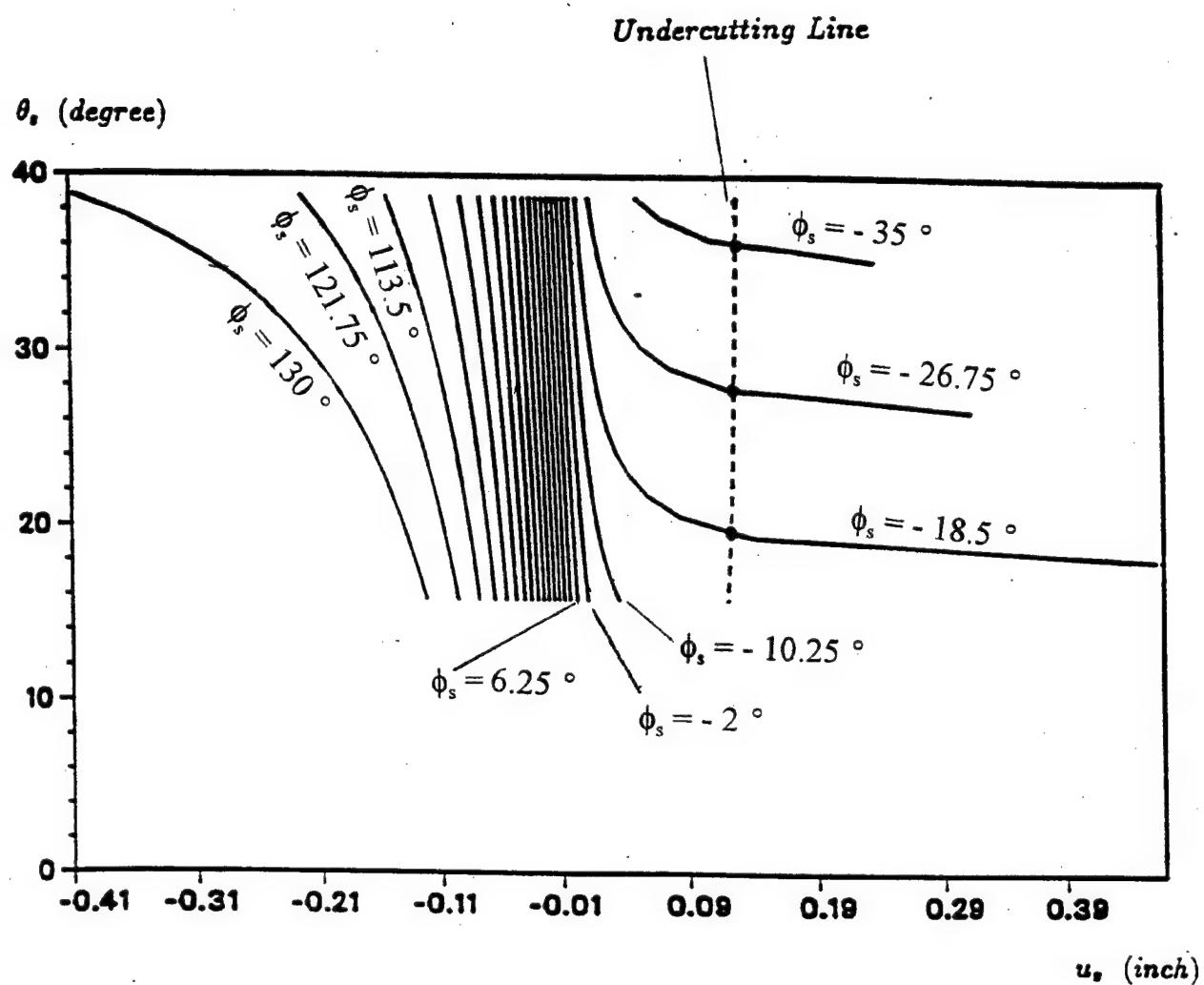
Fig. 1.3.10   Contact lines and undercutting line of dressing shaper with $N_s = 28$, $\alpha_n = 27.5°$, $E_{sw} = 2.6799$ (in); driving side
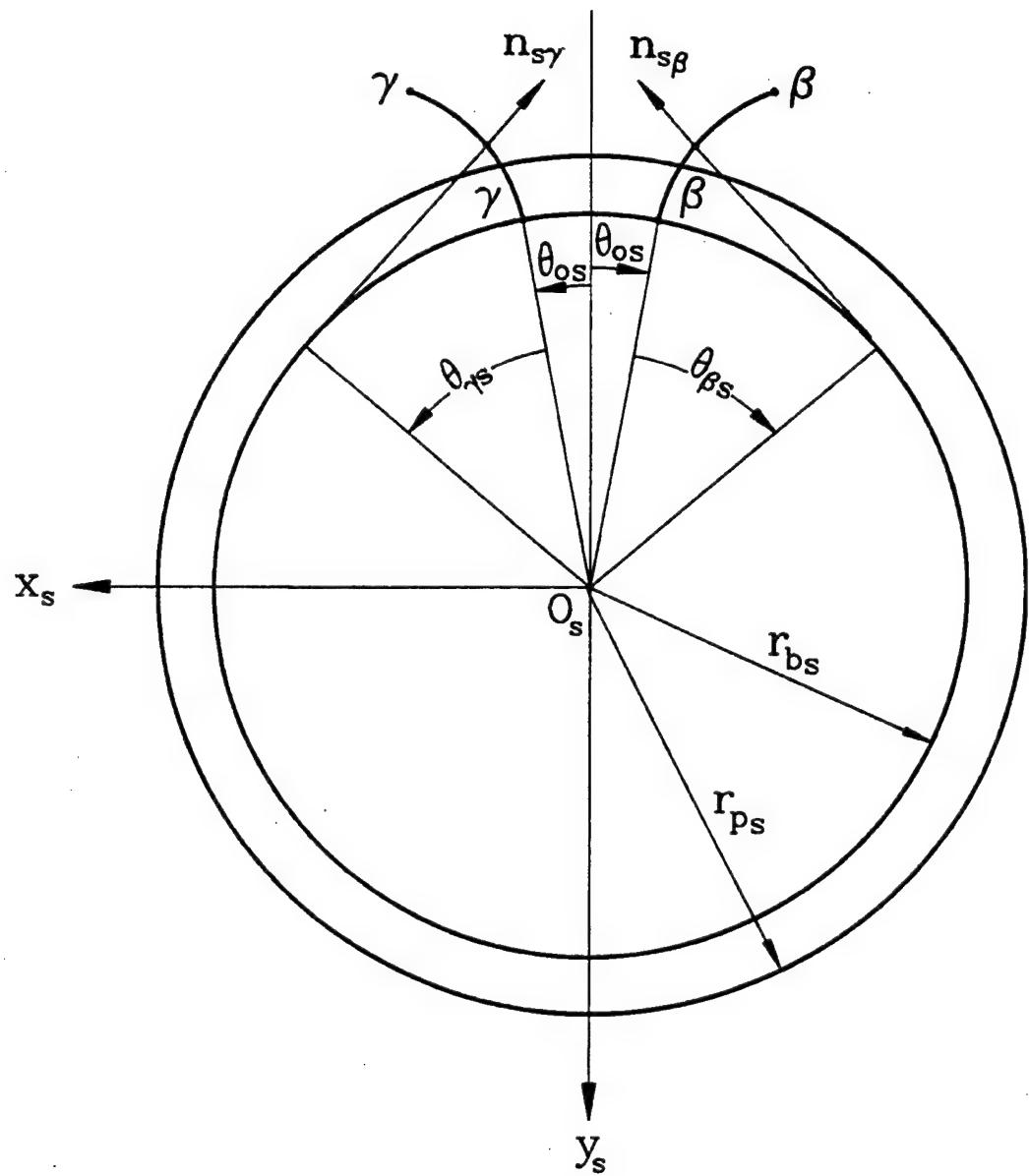
Fig. 1.4.1   Tooth profiles of the shaper
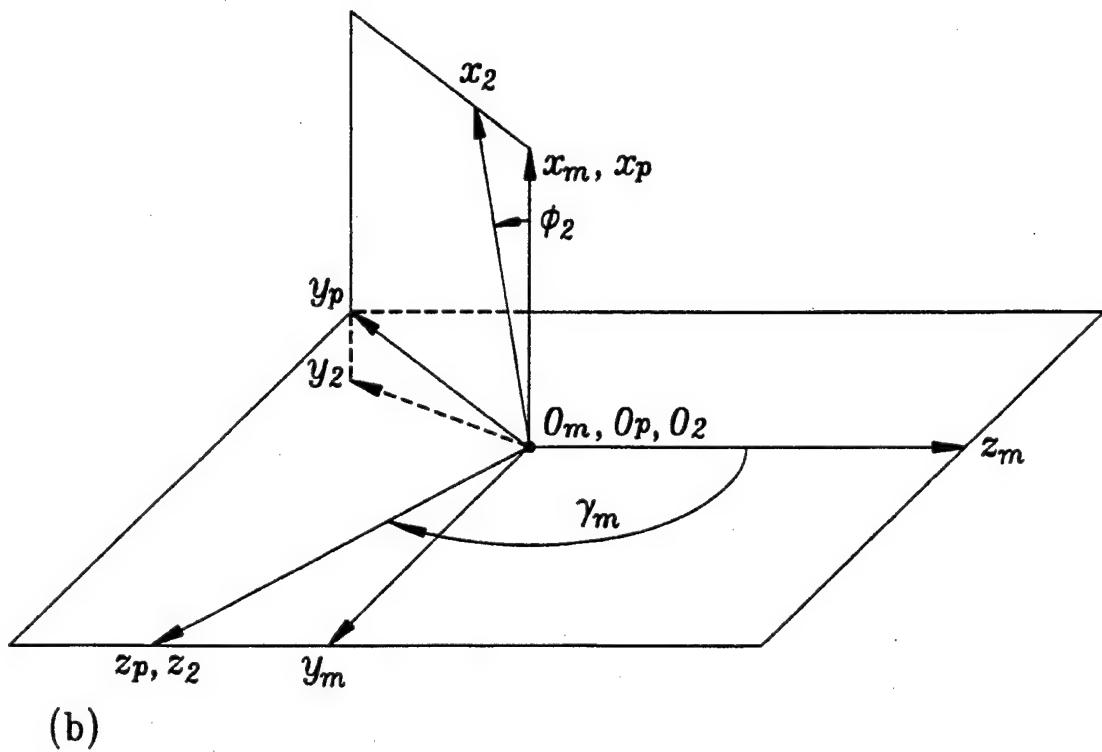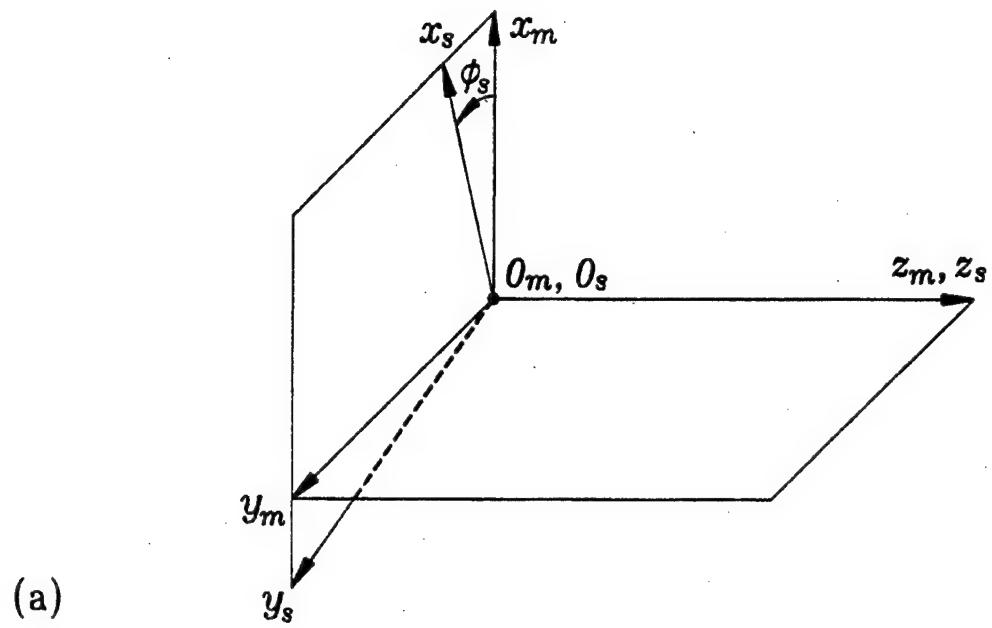
Fig. 1.5.1 Applied coordinate systems for generation of the face gear

71
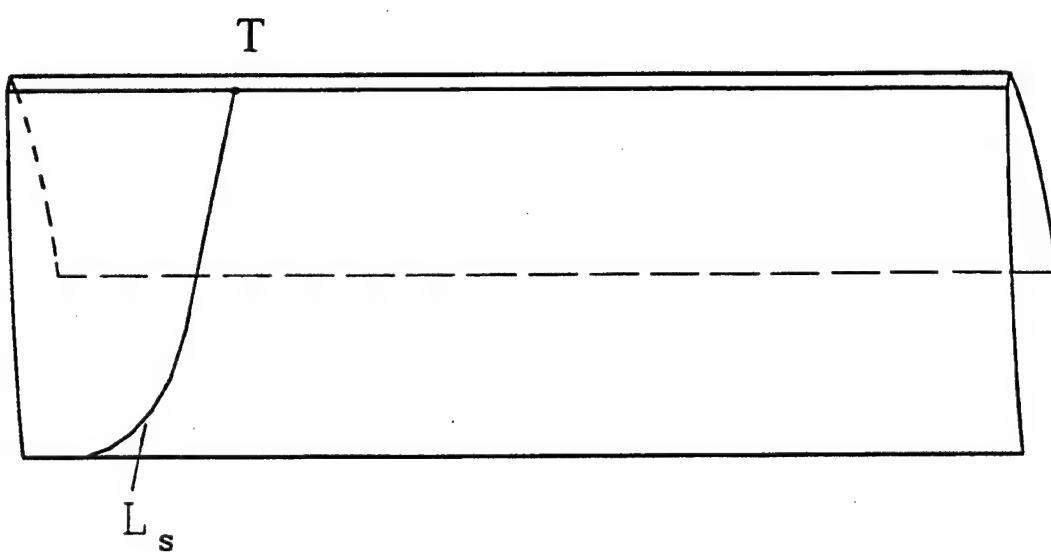
Fig. 1.6.1   Limiting line L_s on the shaper tooth surface

Line of singular points
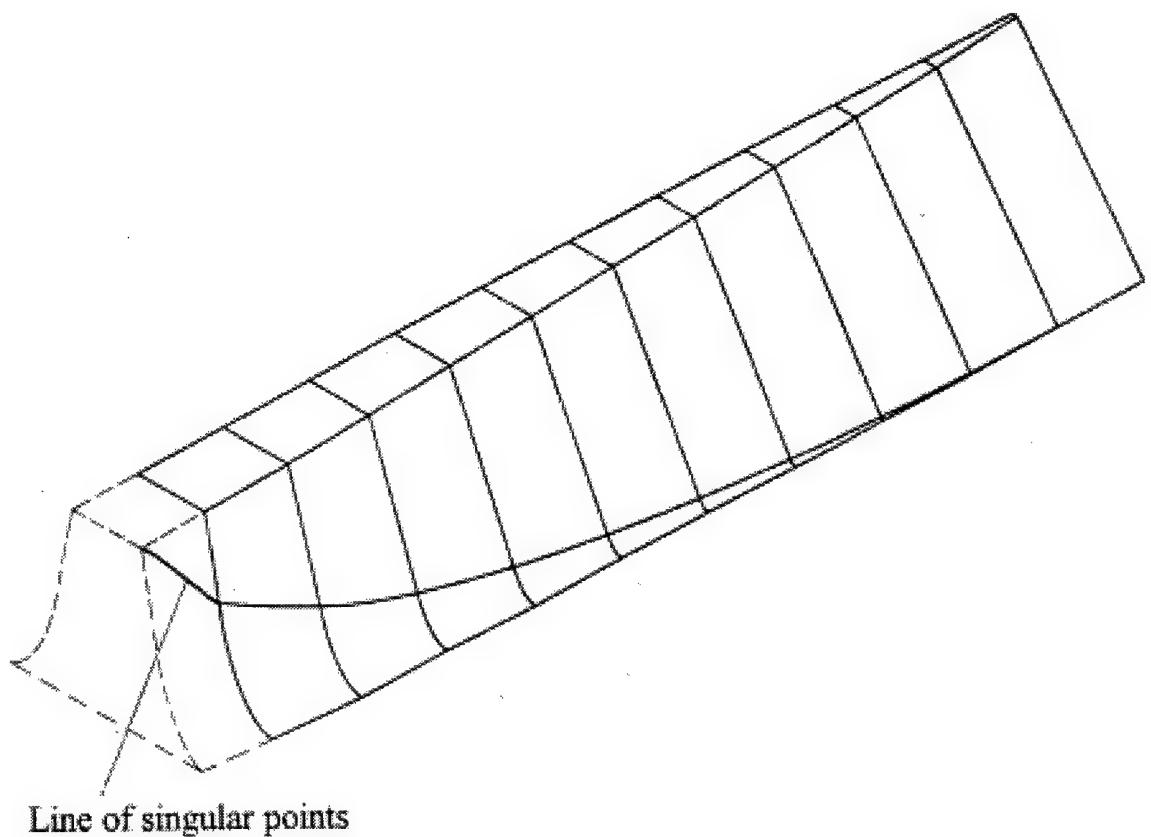
Fig. 1.6.2 Line of singular points on the face-gear tooth surface
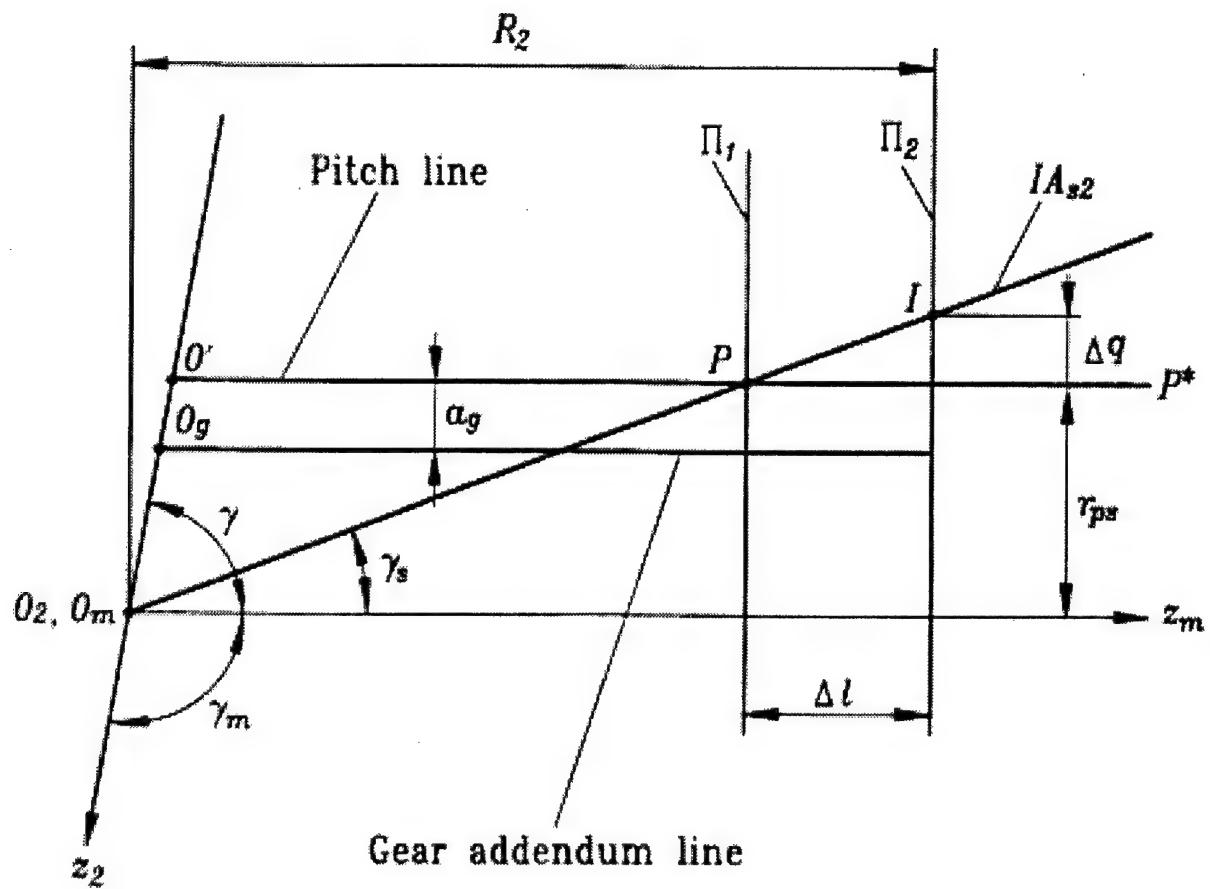
Fig. 1.7.1   For derivation of tooth pointing
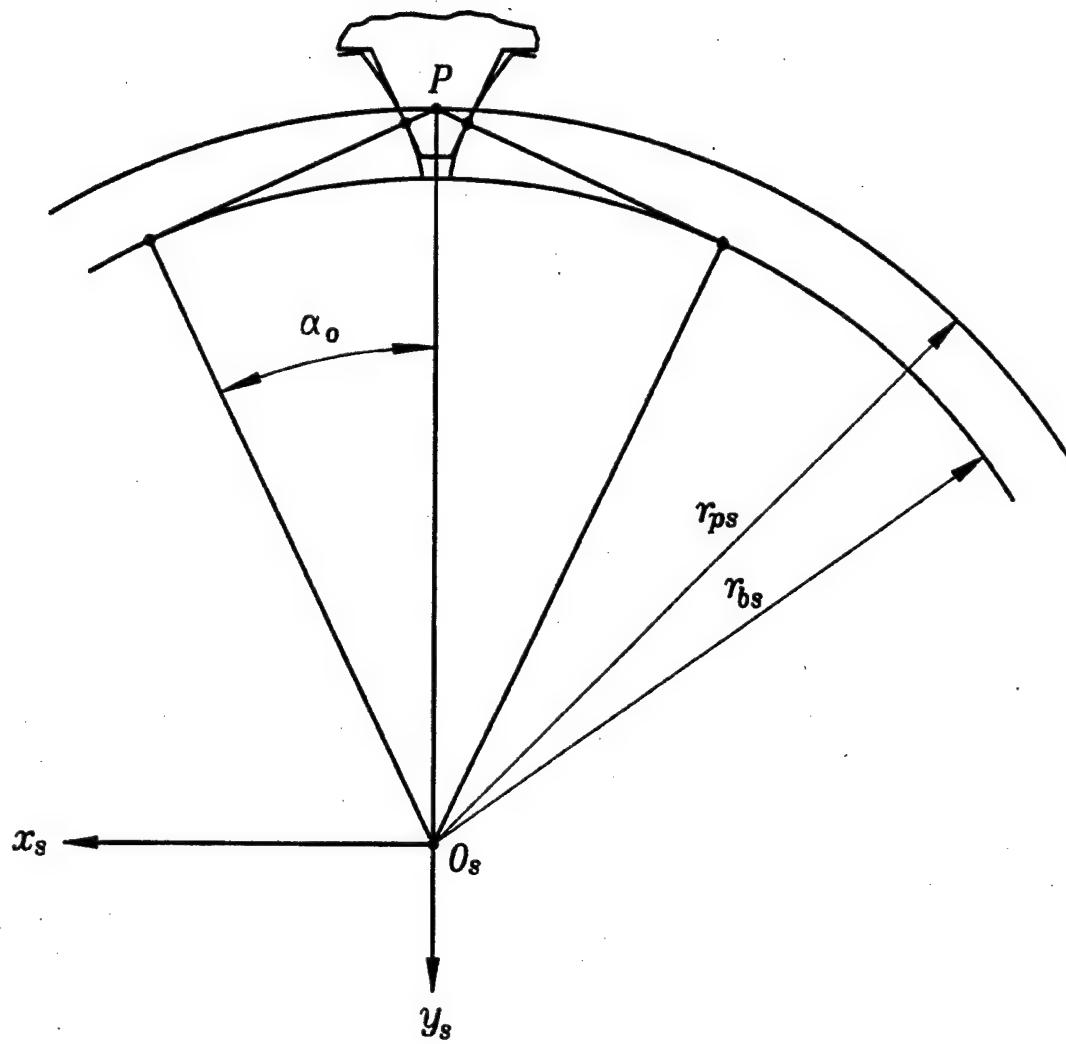
Fig. 1.7.2   Cross section of face gear and shaper by plane II_1
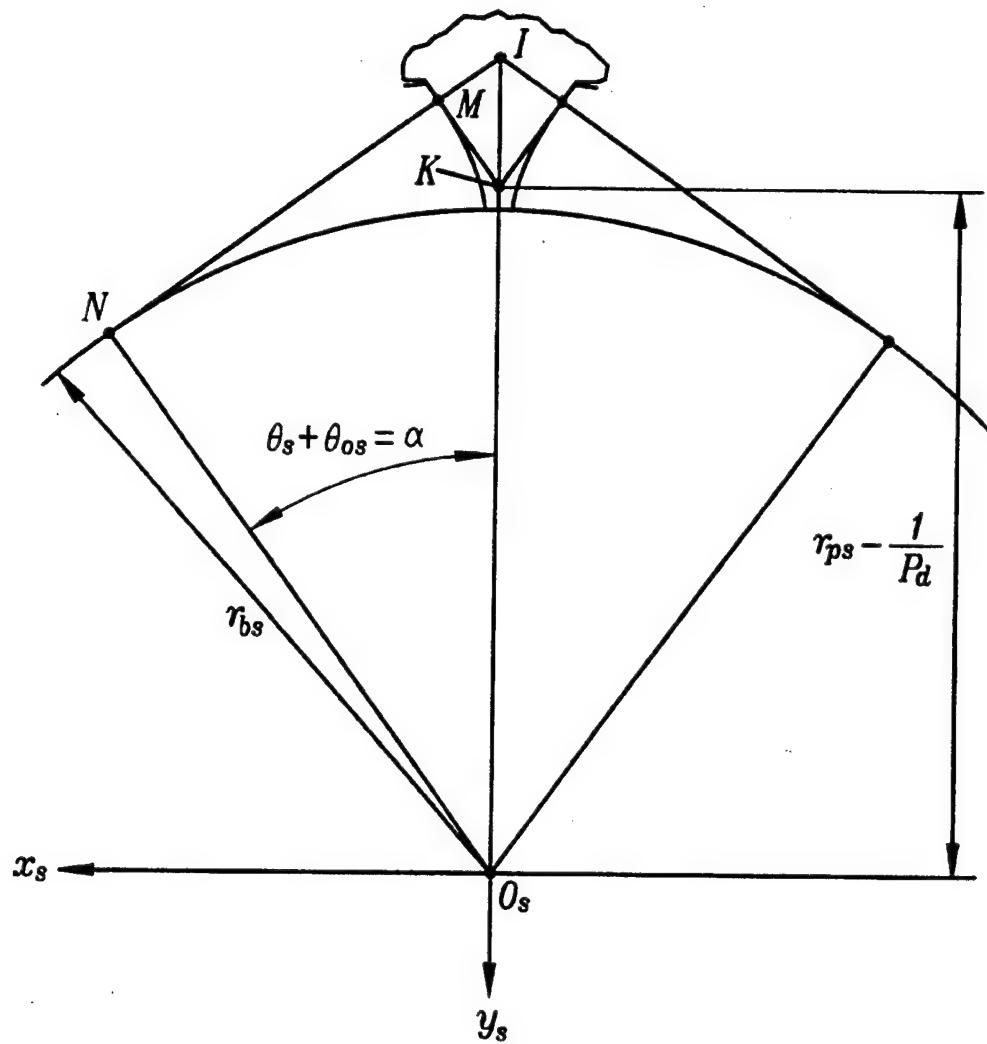
Fig. 1.7.3 Cross section of face gear and shaper by plane II$_2$
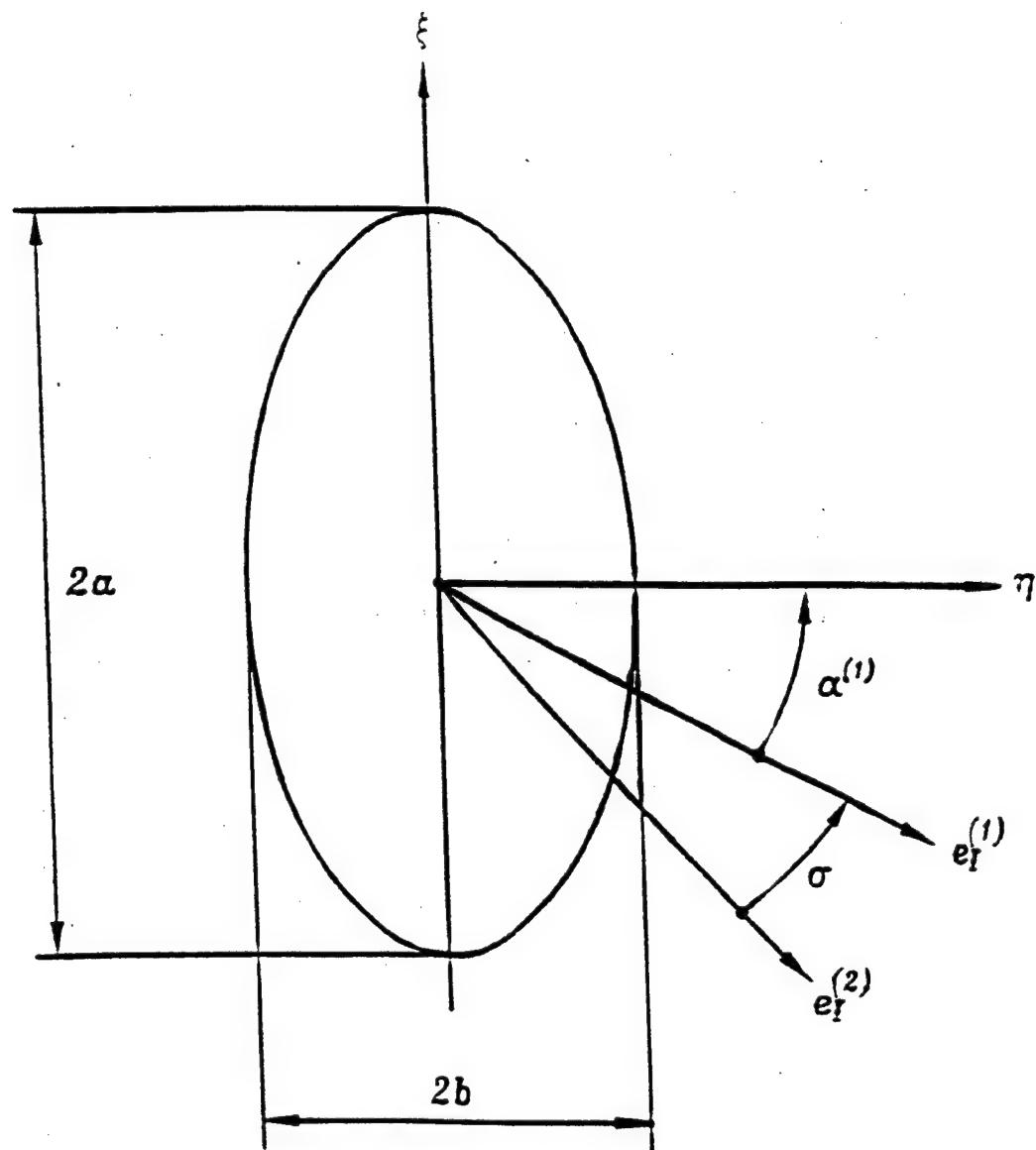
Fig. 1.8.1   Orientation and dimensions of contact ellipse
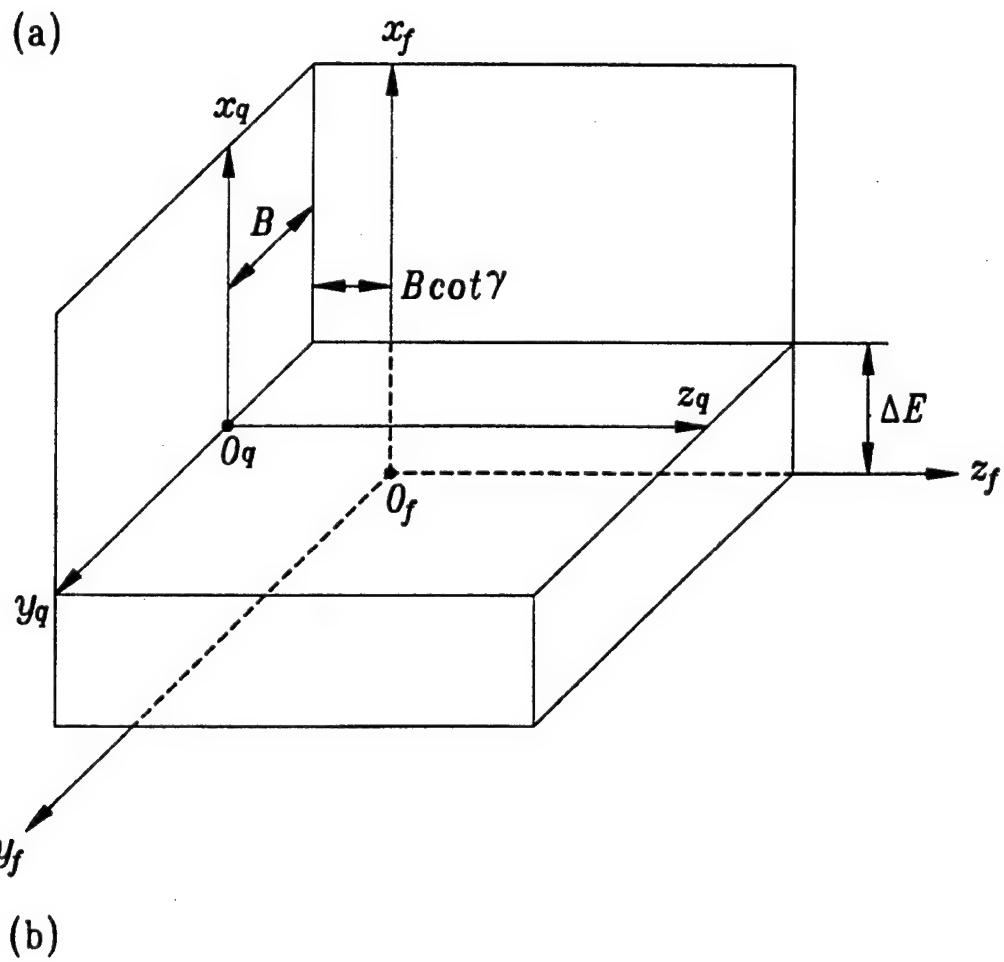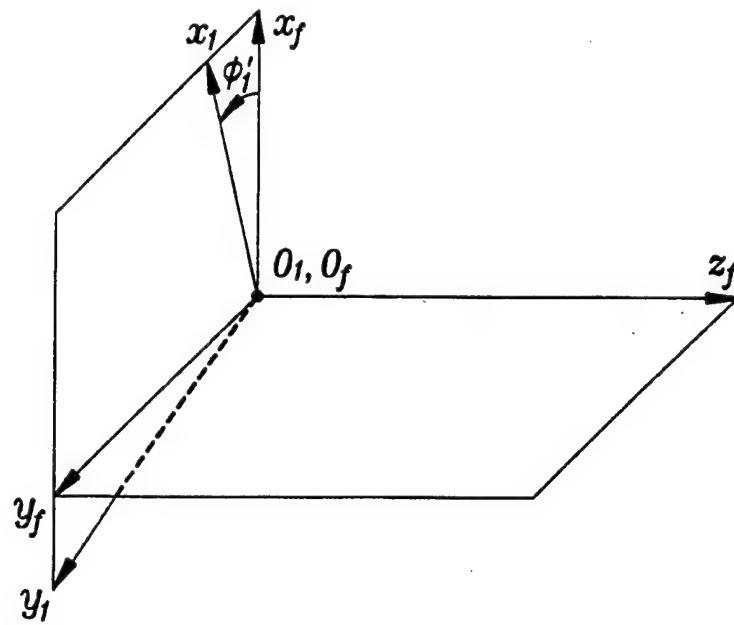
Fig. 1.9.1 (a), (b)   Coordinate systems applied for simulation of meshing
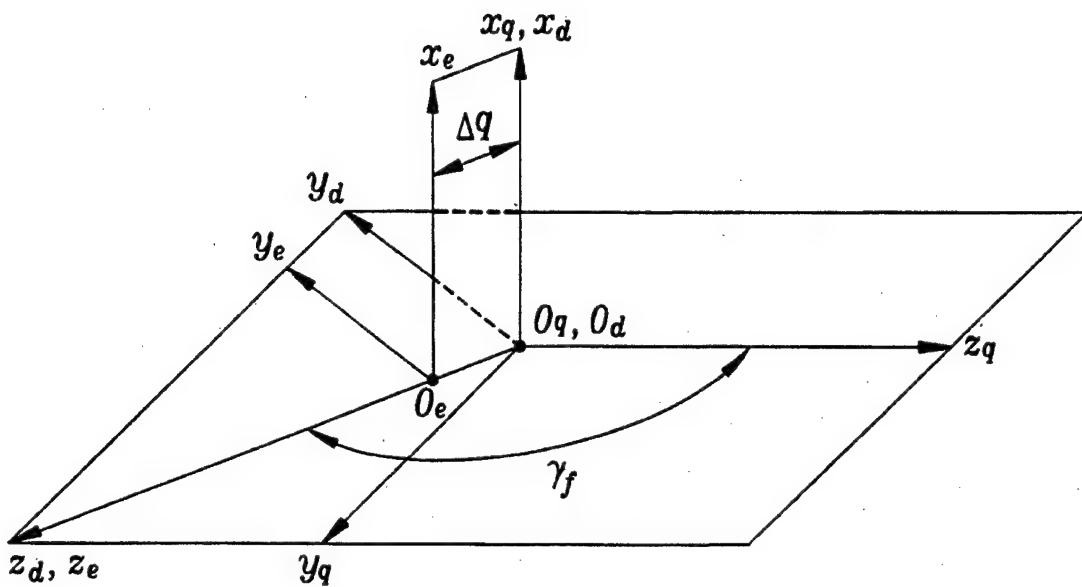
(c)
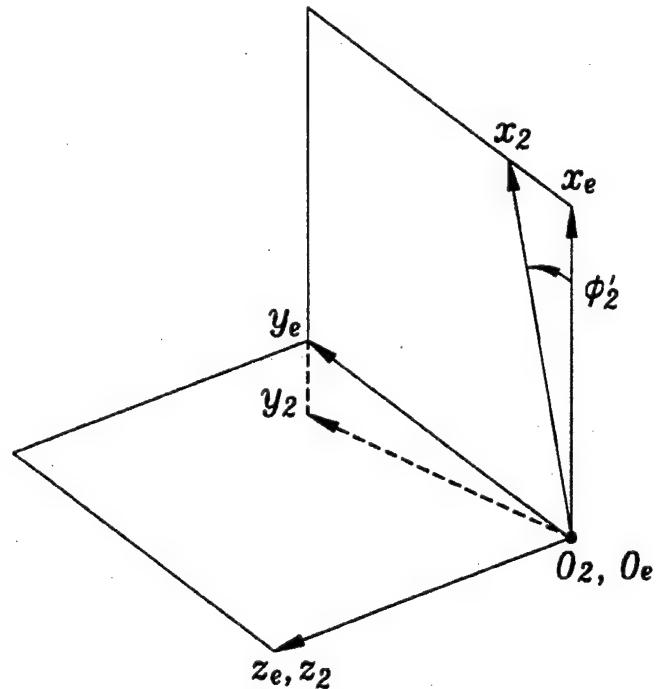
(d)

Fig. 1.9.1 (c), (d)   Coordinate systems applied for simulation of meshing
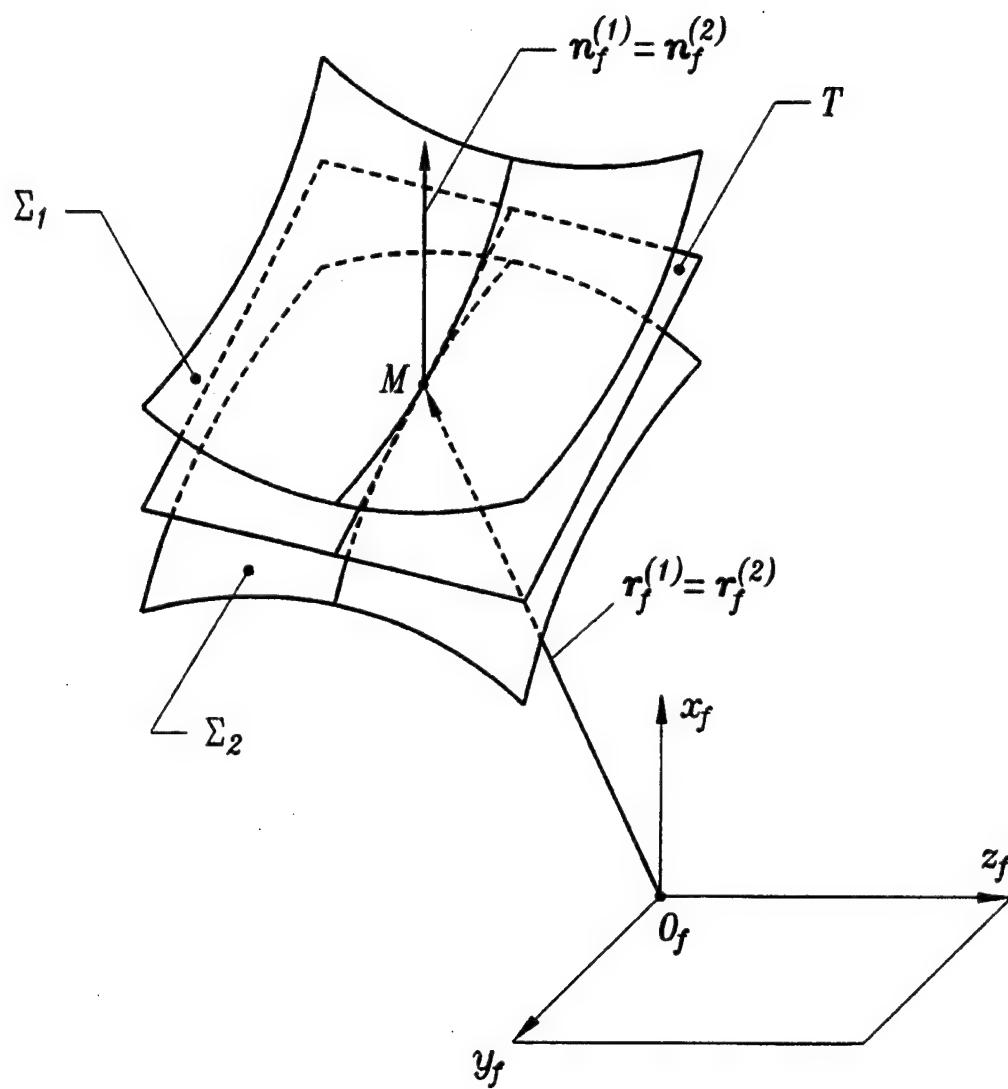
Fig. 1.9.2 Tangency of surfaces in ideal gear train

(a) $(\Delta N = 3, \Delta E = 0.1 \text{ mm})$

(b) $(\Delta N = 3, \Delta q = 0.2 \text{ mm})$

(c) $(\Delta N = 3, \Delta \gamma = 0.05°)$
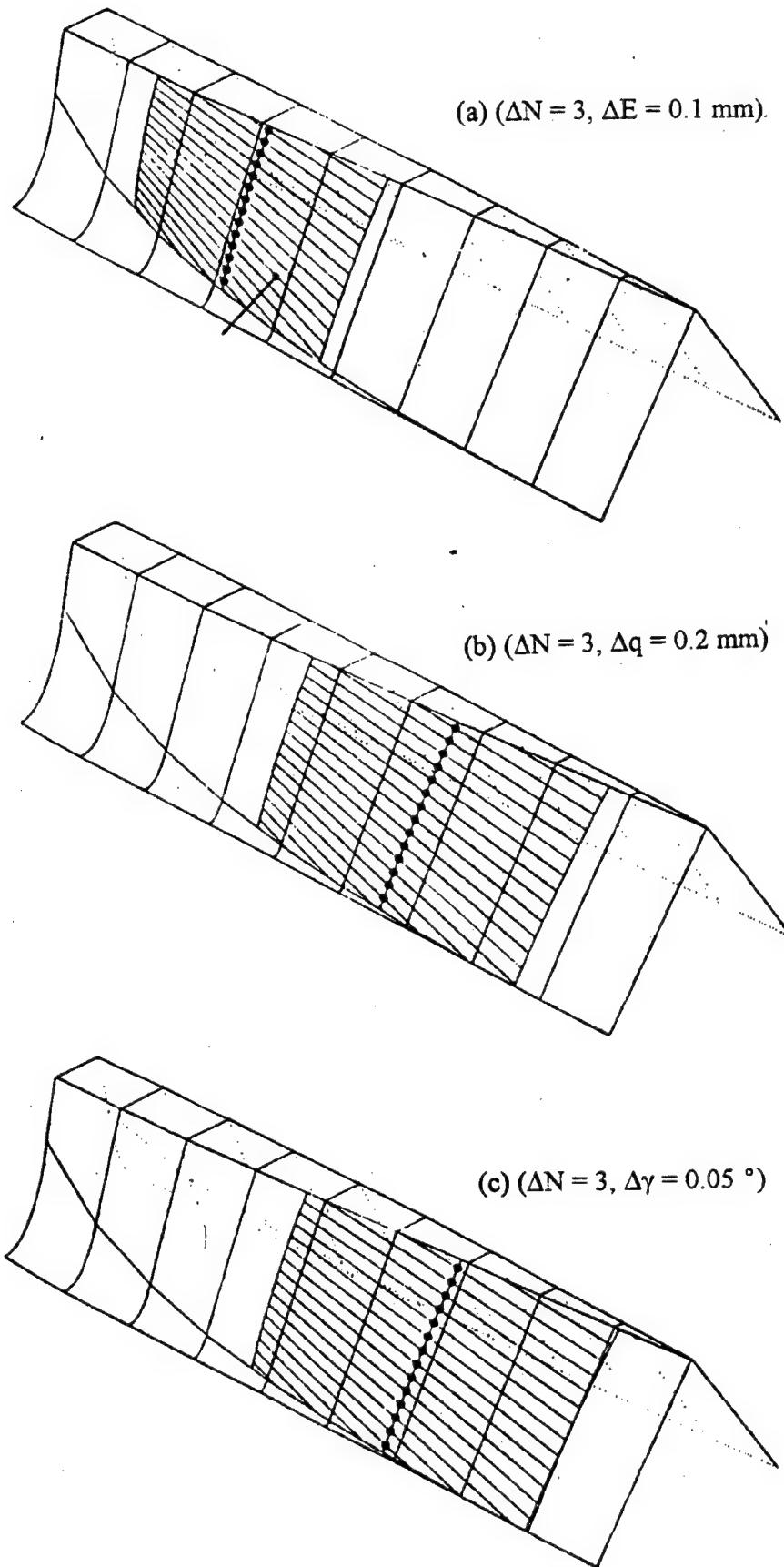
Fig. 1.9.3   Face gear tooth: localized bearing contact
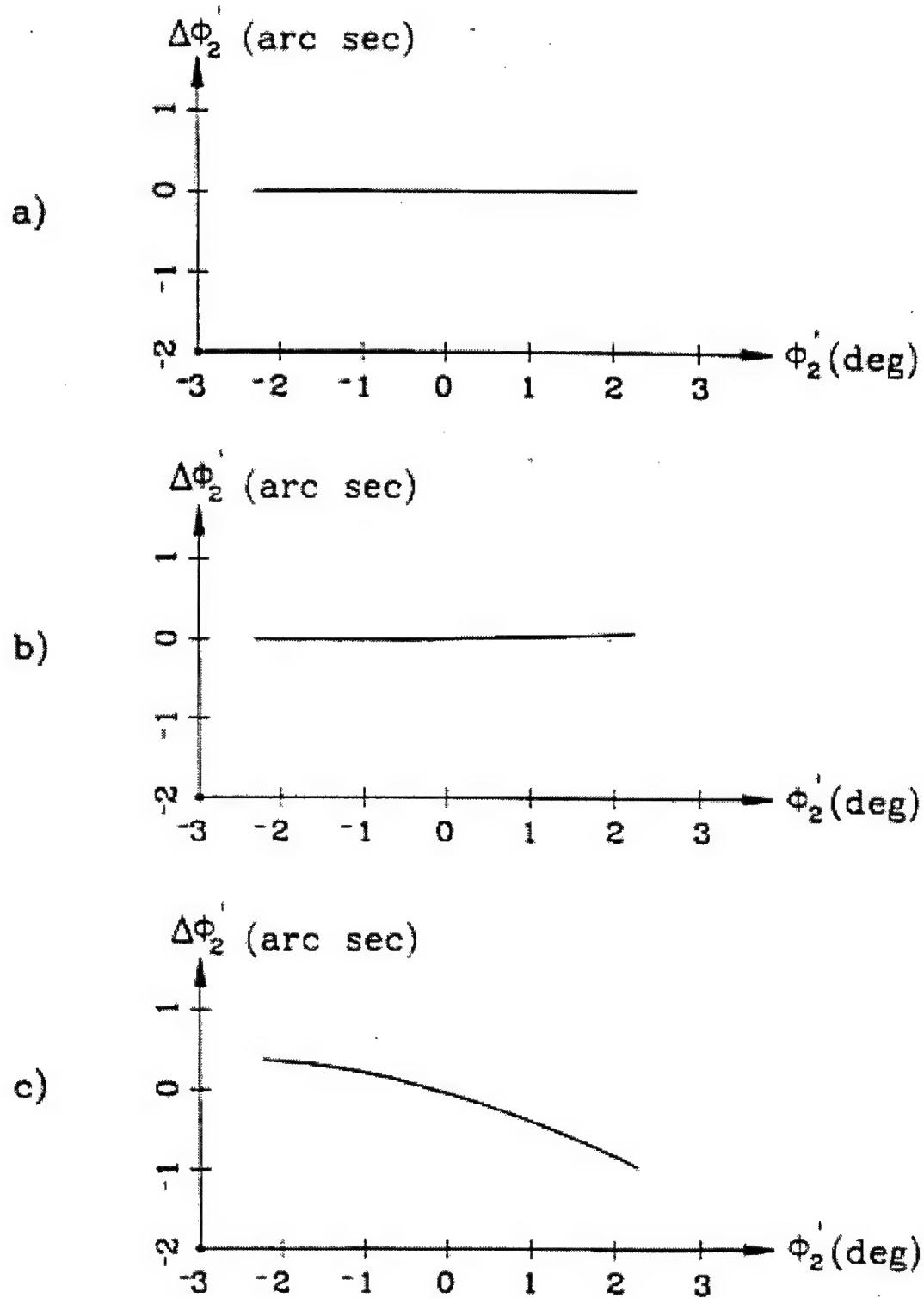
Fig. 1.9.4 Transmission errors of face-gear drive: (a) no misalignments, (b) ΔE = -0.05 mm, (c) $\Delta\gamma$ = -0.05 °
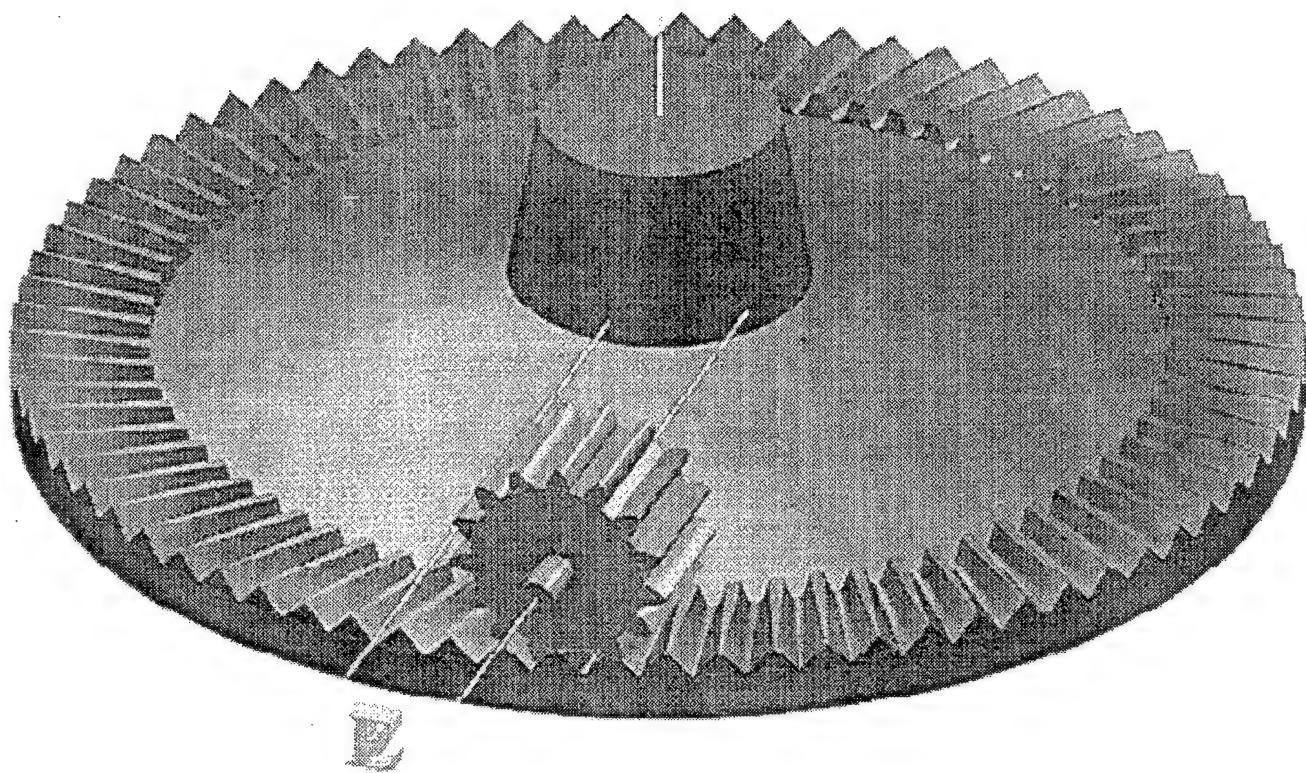
Fig. 2.1.1   Offset face-gear drive
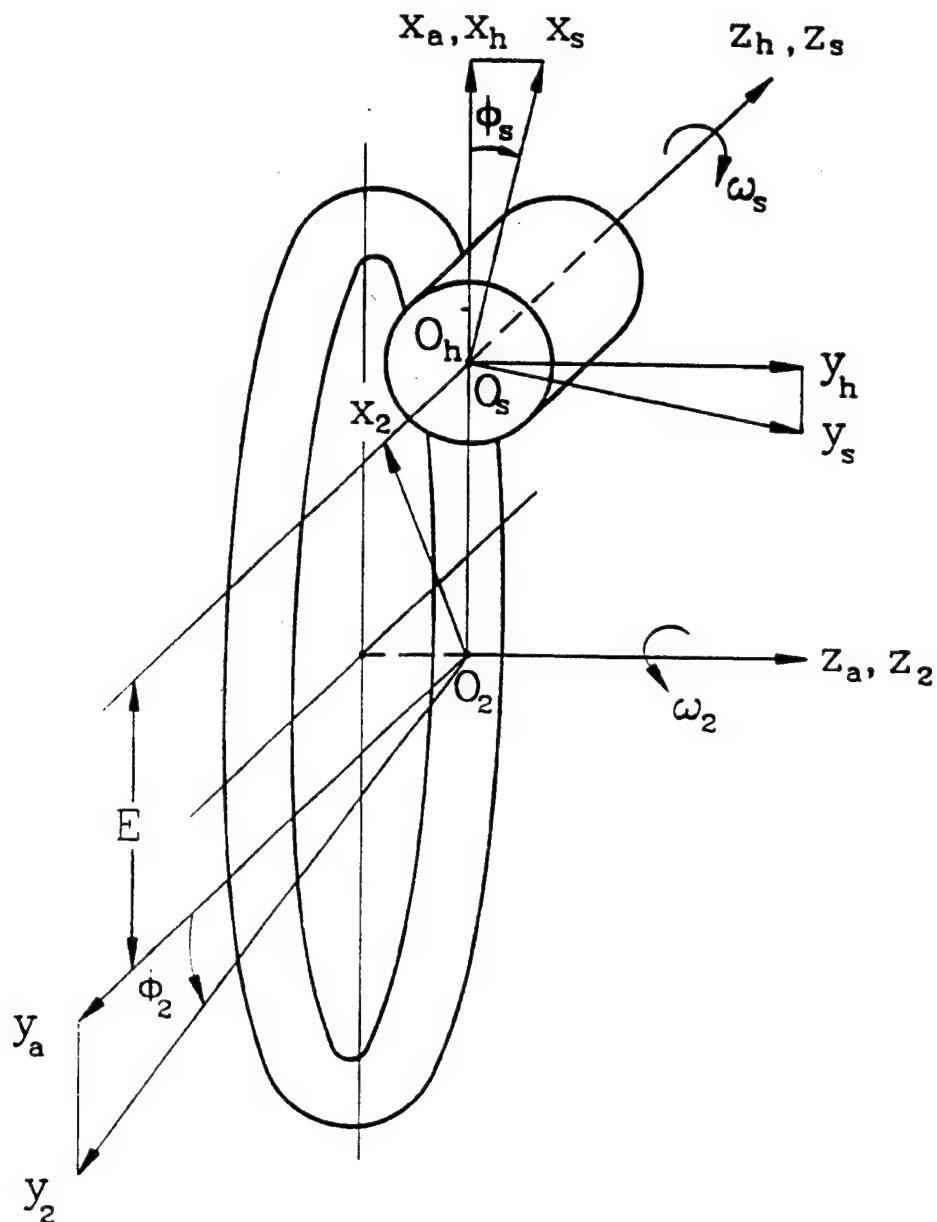
Fig. 2.1.2 Applied coordinate systems
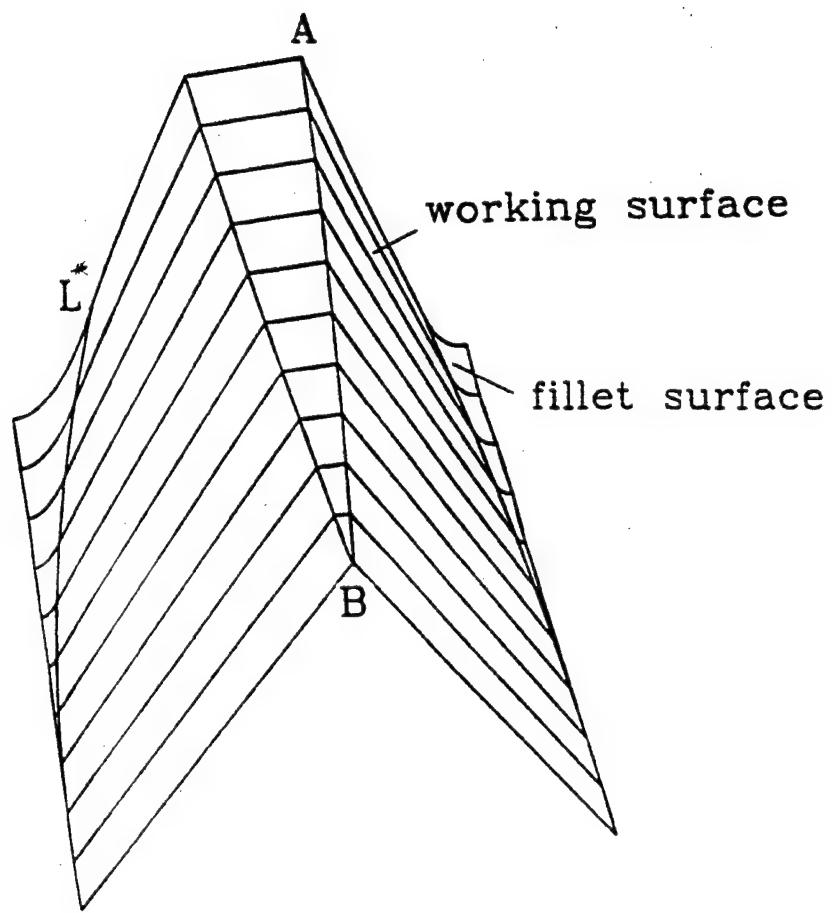
Fig. 2.1.3 Offset face-gear tooth (cross-sections of the working and fillet surface)
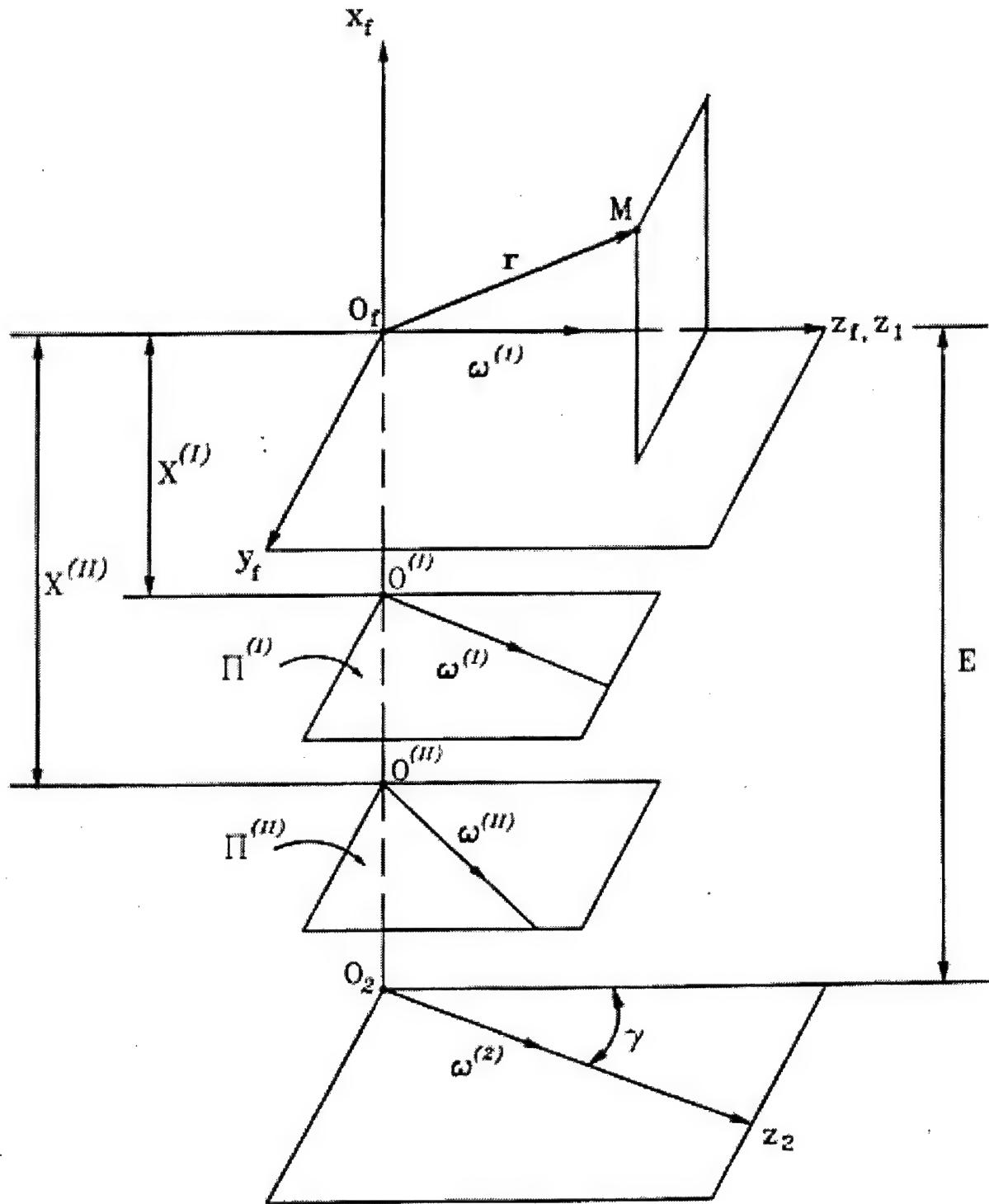
Fig. 2.2.1   For derivation of axes of meshing
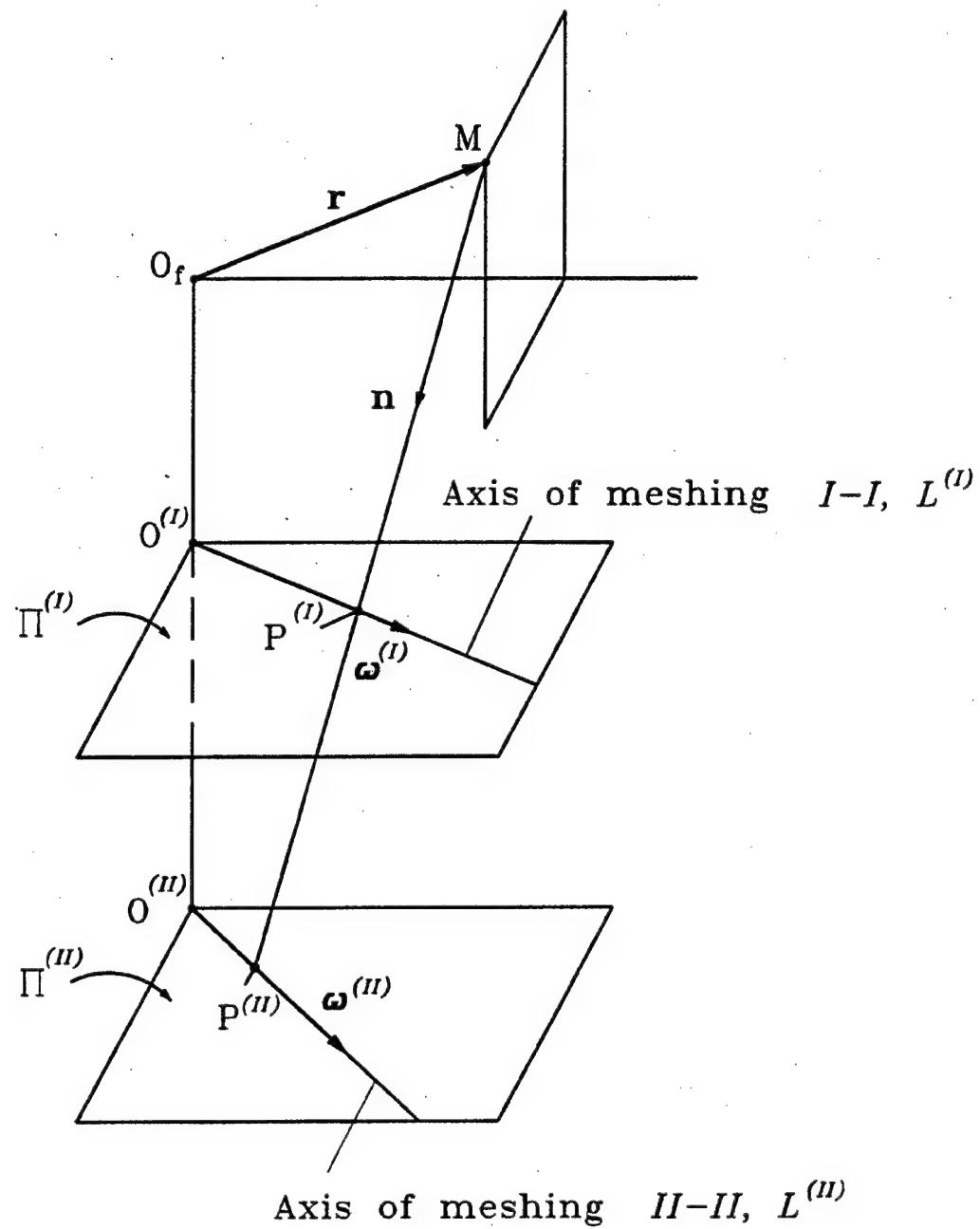
Fig. 2.2.2 Intersection of axes of meshing by the normal to the contacting surfaces
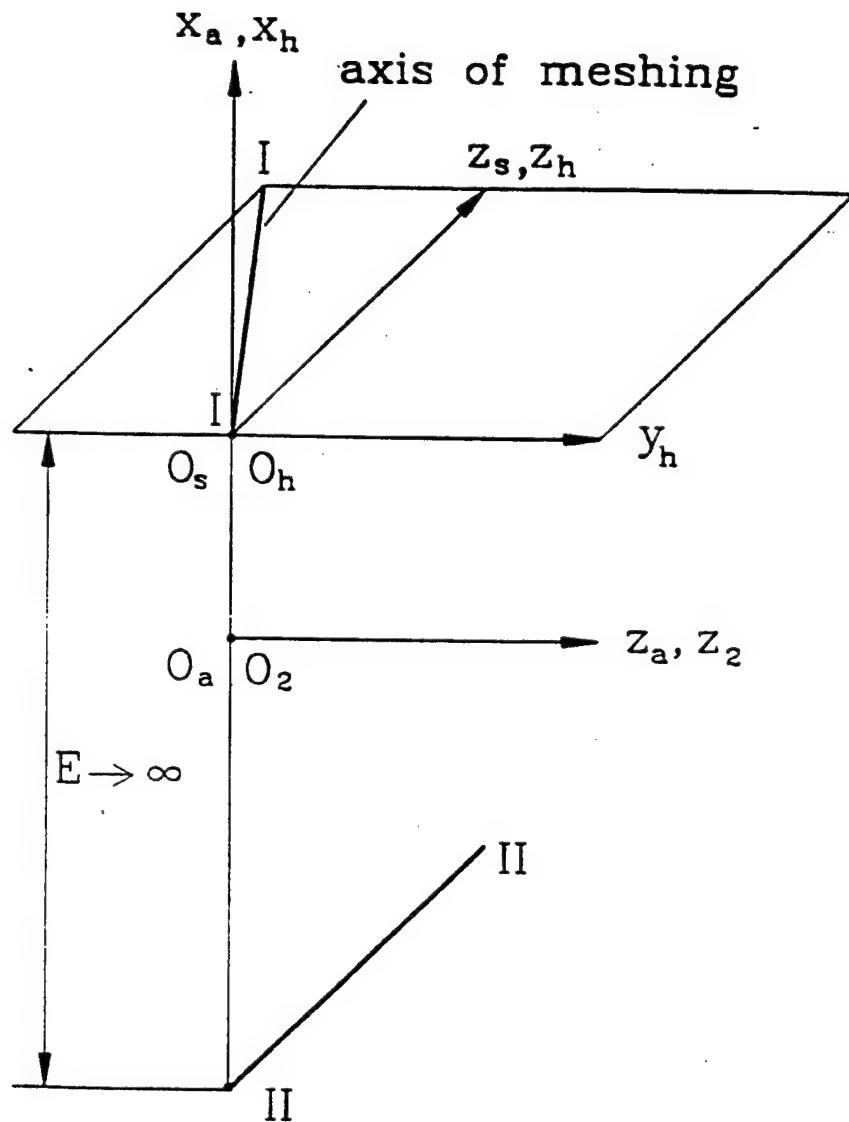
Fig. 2.2.3 Location and orientation of axes of meshing
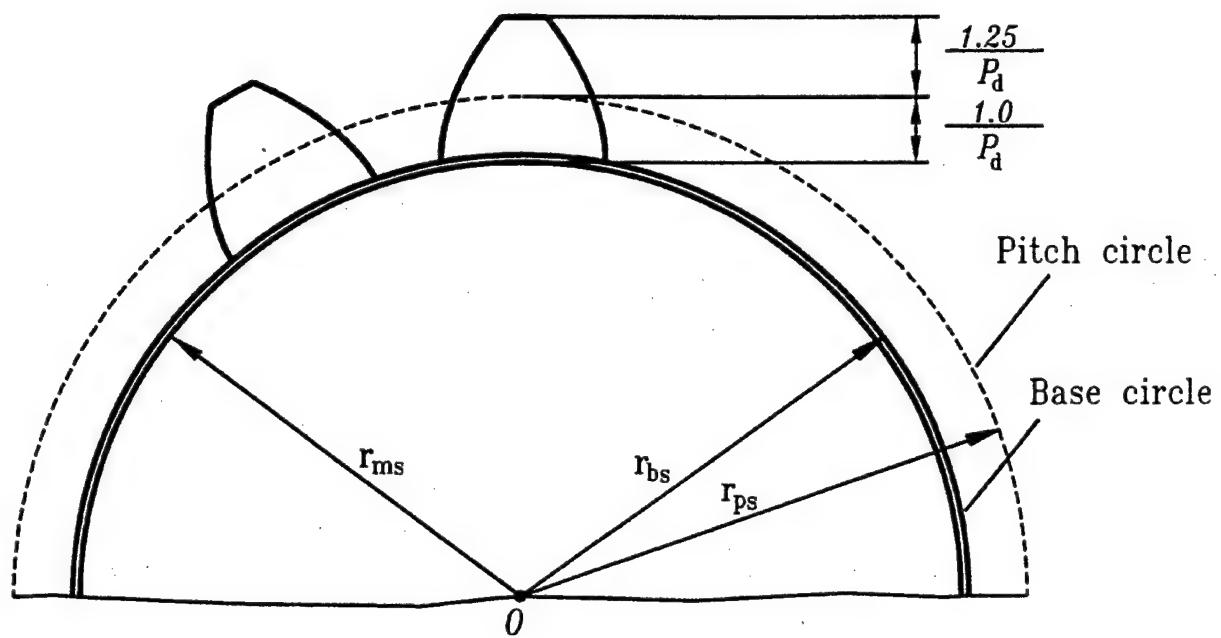
Fig. 2.3.1   Shaper tooth proportions

89
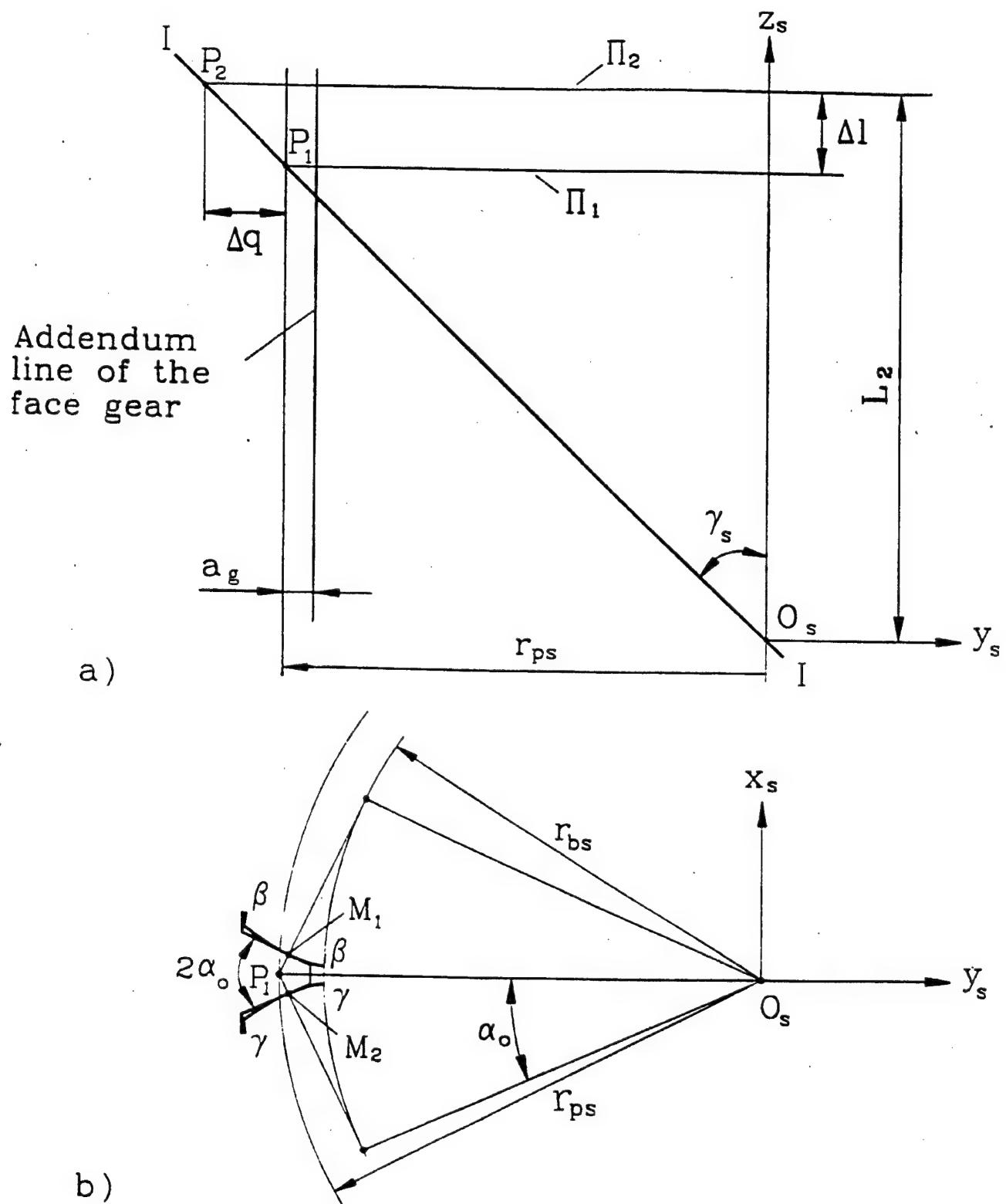
Fig. 2.3.2 Intersection of shaper tooth surface and axis of meshing *I-I* by planes Π_1 and Π_2
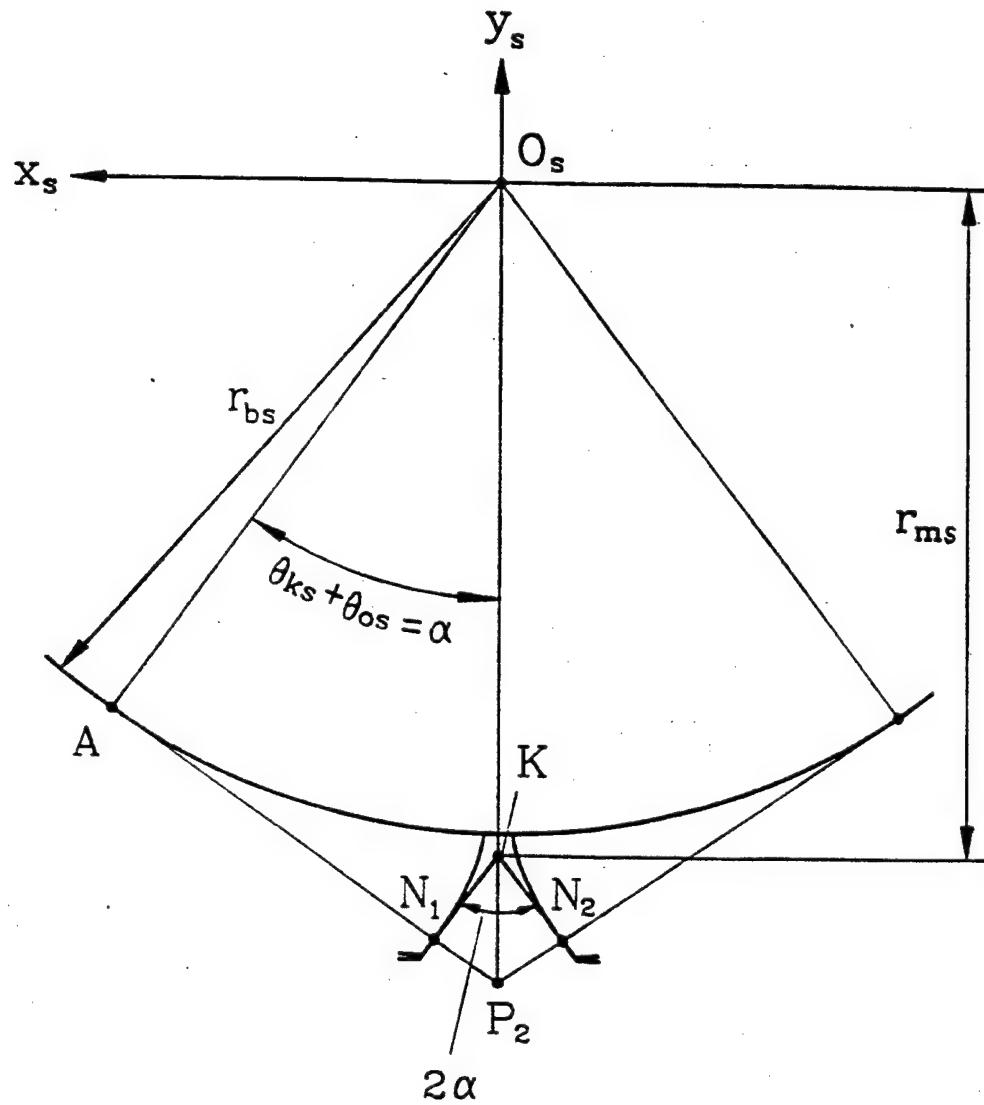
Fig. 2.3.3 Determination of angle α where pointing of the face gear occurs
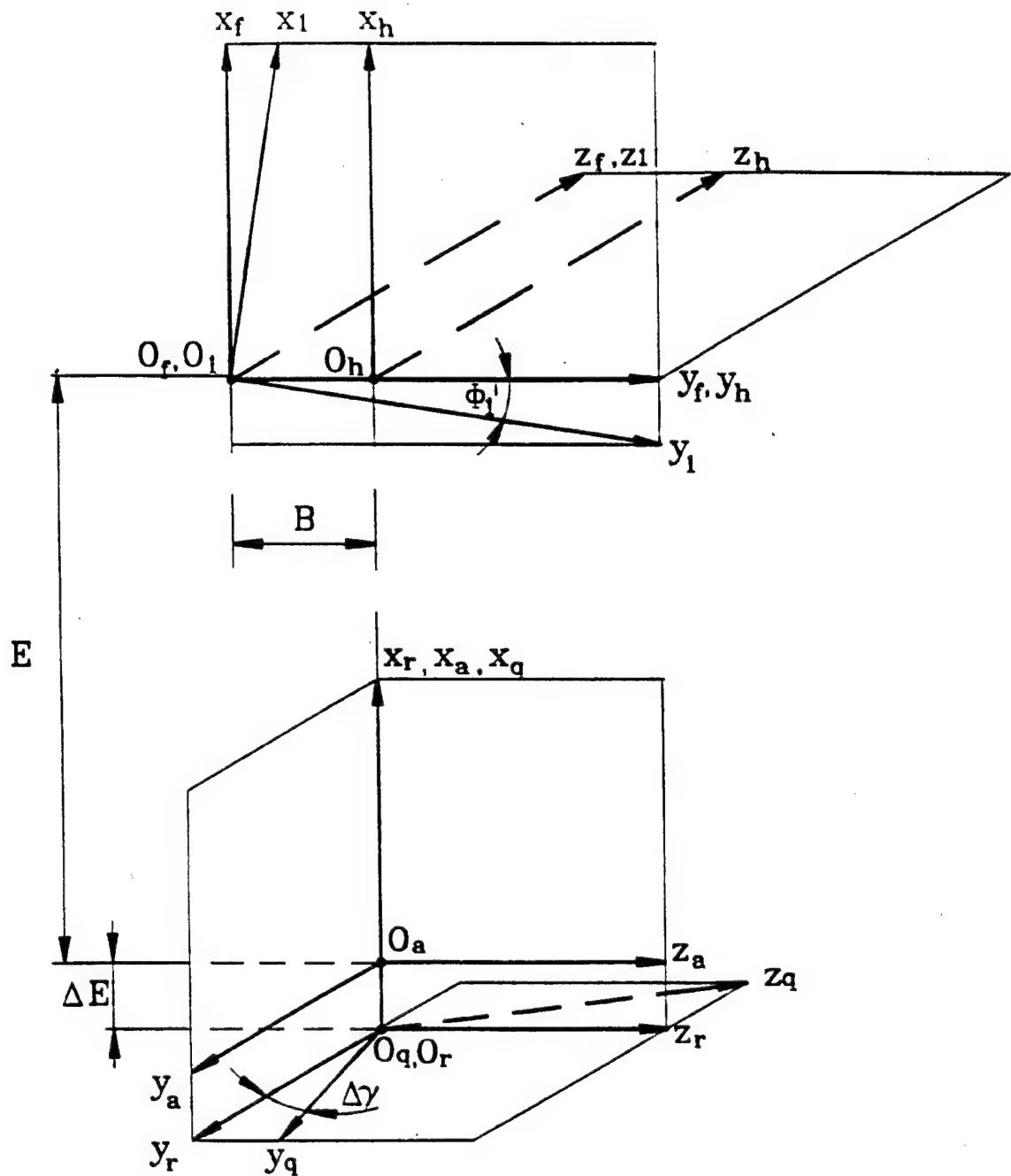
Fig. 2.4.1 (a) Applied coordinate systems for TCA (Approach 1)
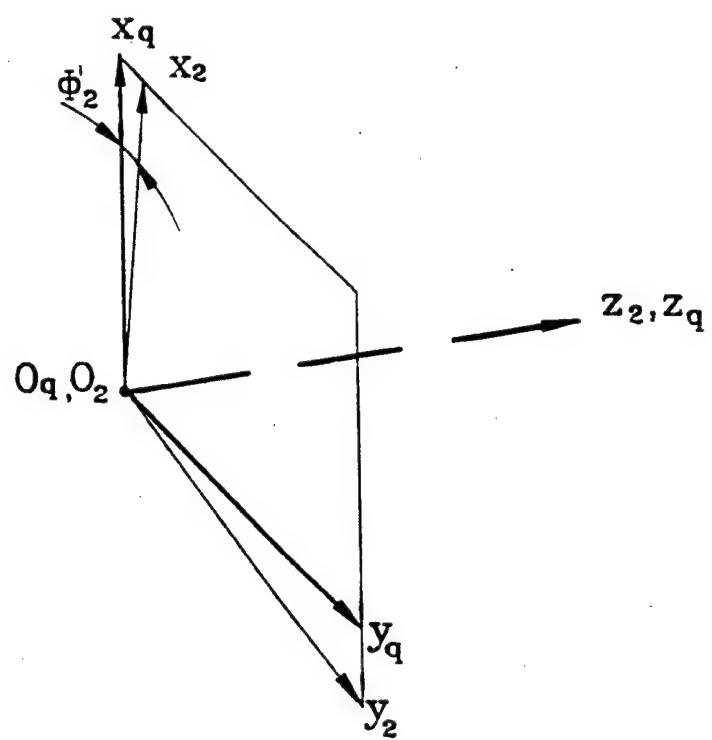
Fig. 2.4.1 (b)   Applied coordinate systems for TCA (Approach 1)
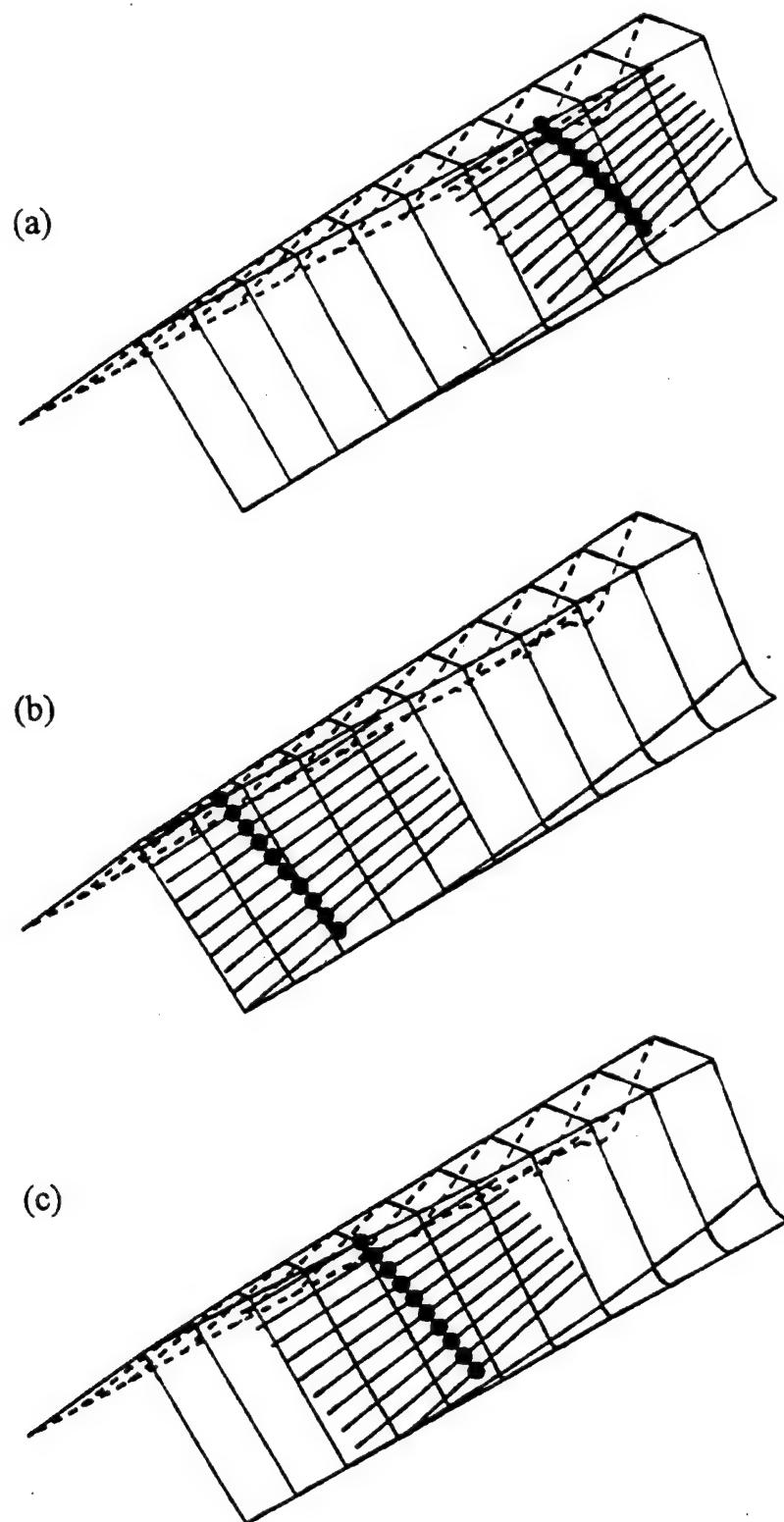
Fig. 2.4.2   Contact path on the face-gear tooth surface: (a) no misalignment,
(b) $\Delta E = 0.04$ mm, (c) $\Delta\gamma = -0.05°$
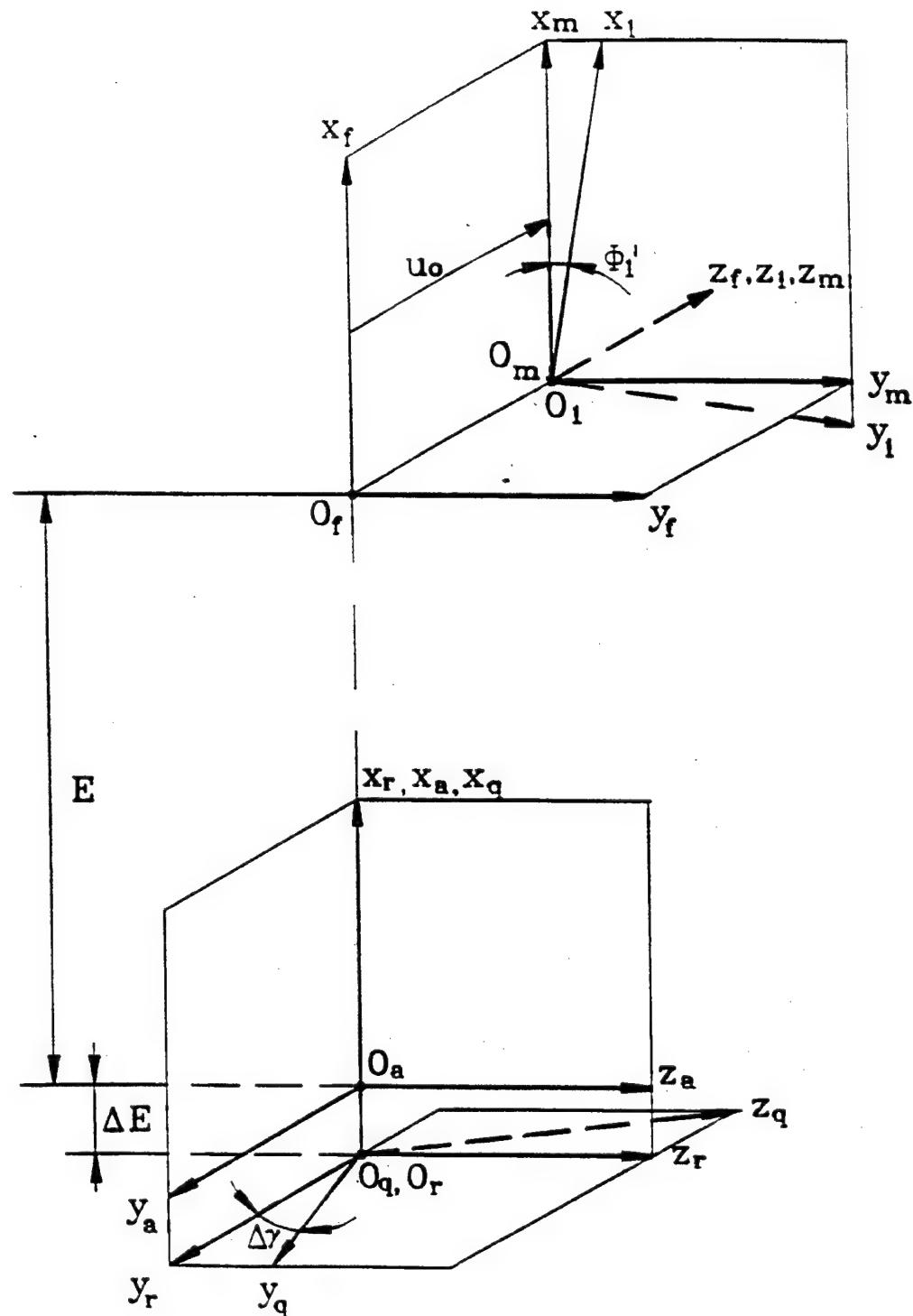
Fig. 2.4.3 (a)   Applied coordinate systems for TCA (Approach 2)
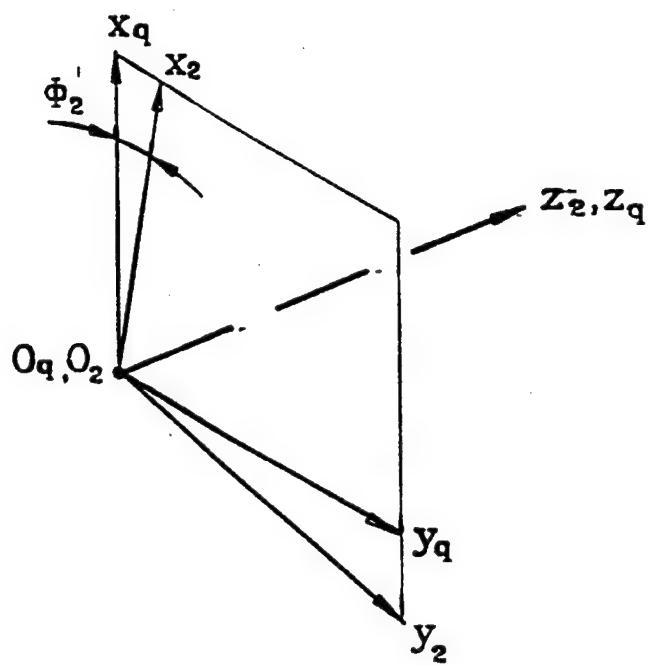
Fig. 2.4.3 (b) Applied coordinate systems for TCA (Approach 2)
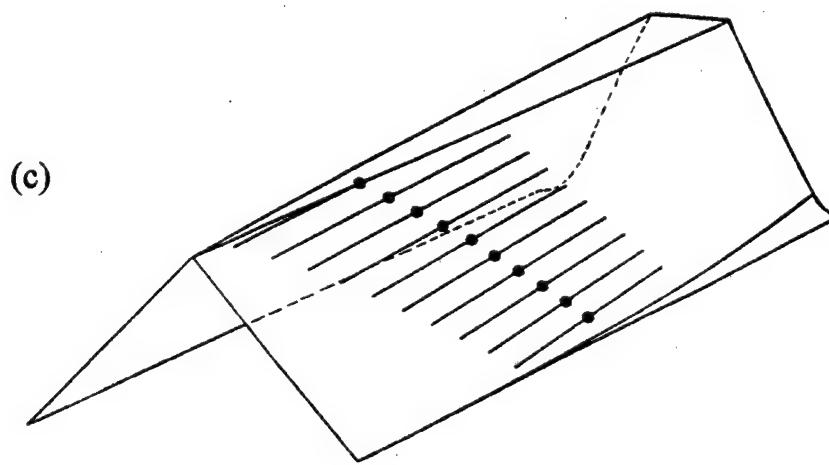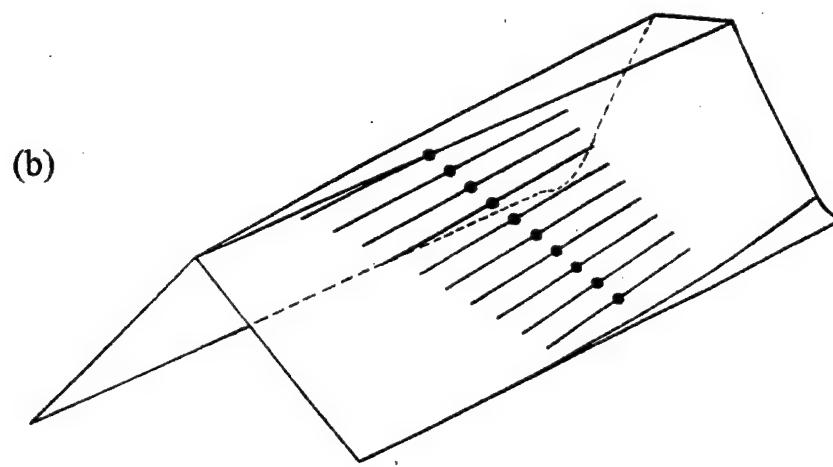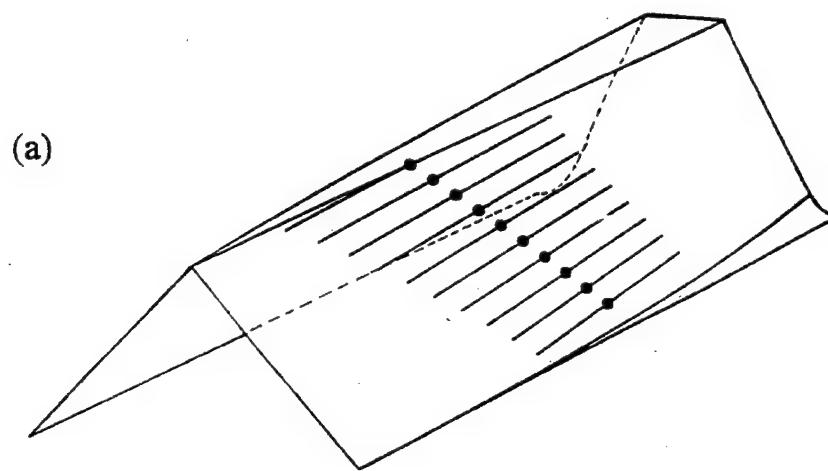
Fig. 2.4.4 Contact path on the offset face-gear tooth surface: (a) no misalignment,
(b) ΔE = -0.05 mm, (c) $\Delta\gamma$ = -0.05°
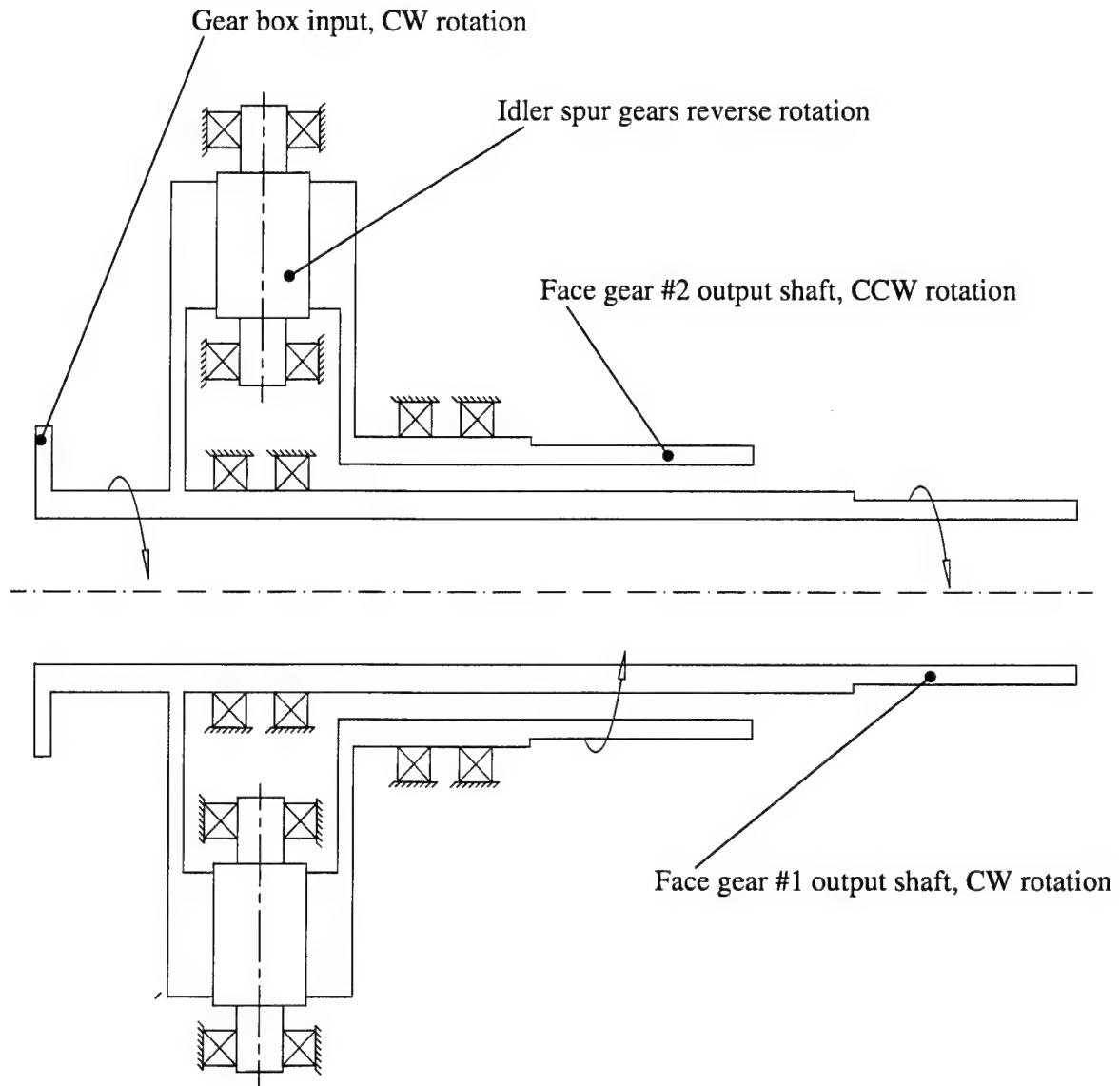
Fig. 3.1.1 Concentric face gears with dual counter-rotating output shafts

Tooth chamfer on I.D. of face gear

Tooth chamfer on O.D. of face gear
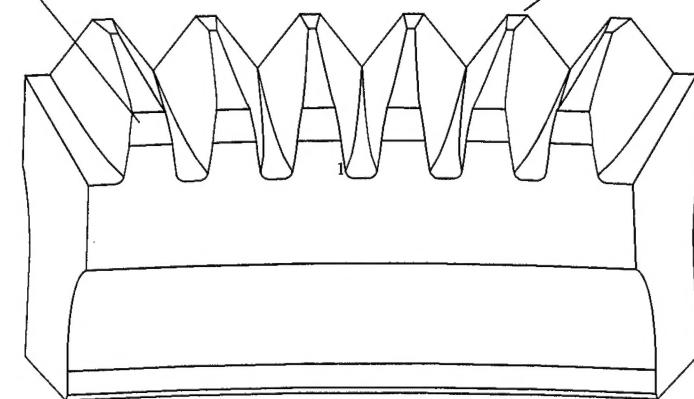
View of face gear teeth looking from I.D. to O.D.

Fig. 3.2.1   Face gear geometry showing tooth chamfering

Planetary carrier to output shaft

Ring gear

Planet gears

Idler spur gear (2)

Upper face gear / sun gear

Lower face gear

Input spur pinion (2)
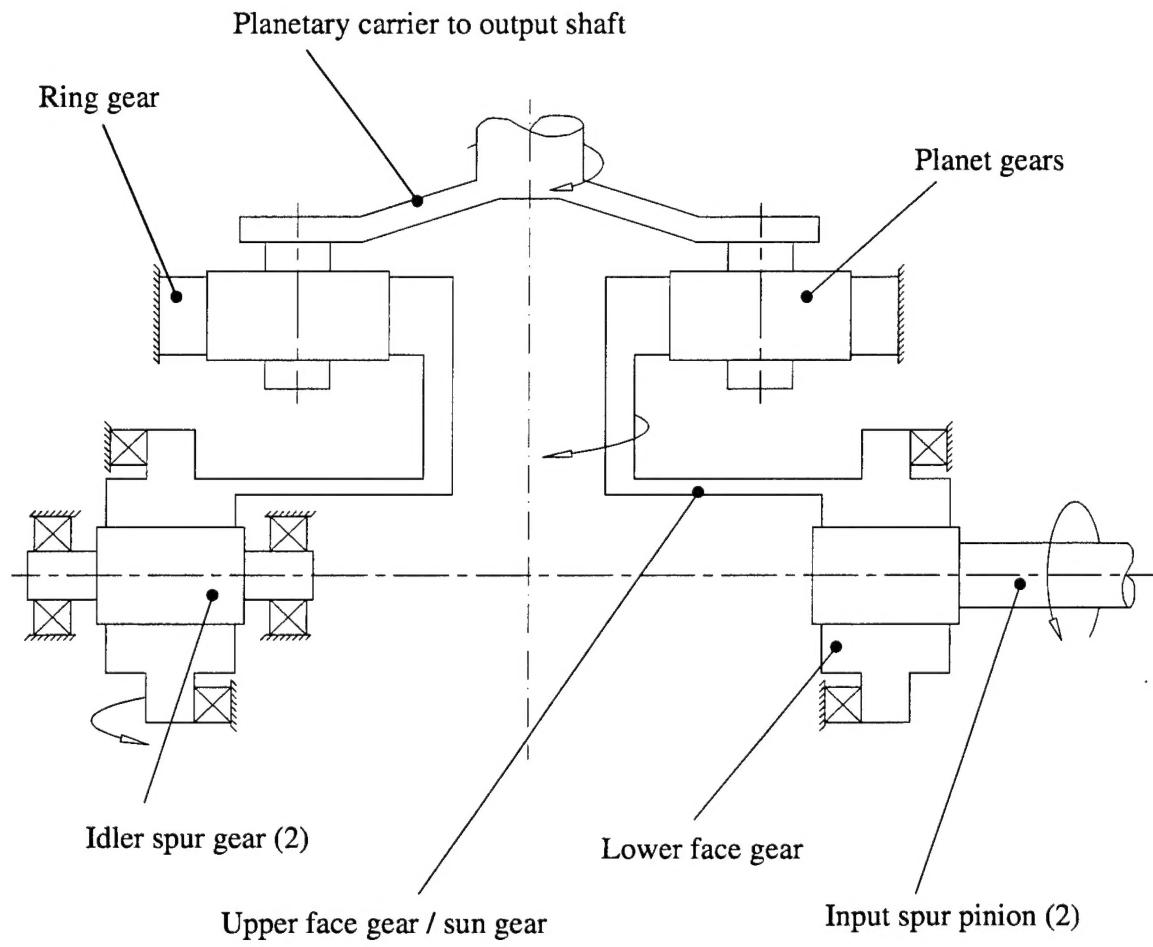
Fig. 3.3.1   Concentric face gear configuration with single output shaft
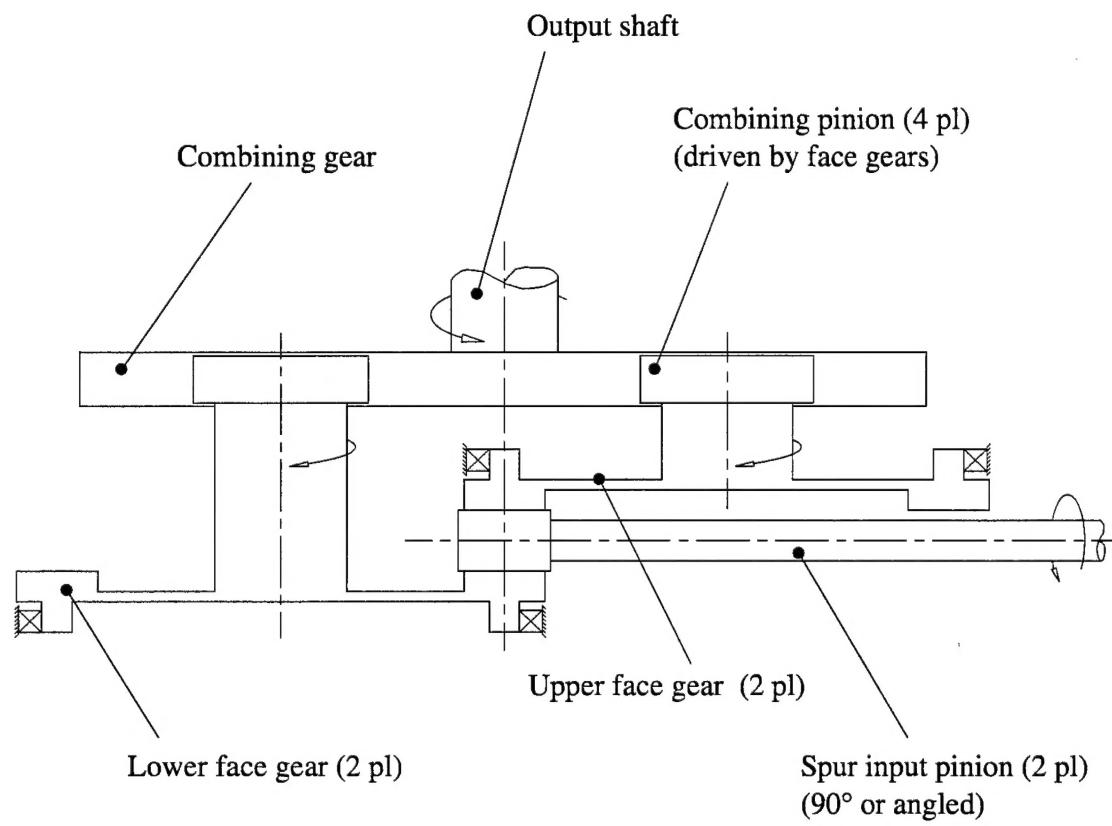
Fig. 3.3.2 Staggered (non-concentric) opposing face gear configuration

101

REPORT DOCUMENTATION PAGE

1. AGENCY USE ONLY (Leave blank)	2. REPORT DATE	3. REPORT TYPE AND DATES COVERED
	March 2000	Final Contractor Report

4. TITLE AND SUBTITLE

Handbook on Face Gear Drives With a Spur Involute Pinion

6. AUTHOR(S)

F.L. Litvin, A. Egelja, J. Tan, D.Y-D. Chen, and G. Heath

5. FUNDING NUMBERS

WU–581–30–13–00
NCC3–356
1L162211A47A

7. PERFORMING ORGANIZATION NAME(S) AND ADDRESS(ES)

University of Illinois at Chicago
Department of Mechanical Engineering
842 W. Taylor Street
Chicago, Illinois 60607

8. PERFORMING ORGANIZATION REPORT NUMBER

E–12127

9. SPONSORING/MONITORING AGENCY NAME(S) AND ADDRESS(ES)

U.S. Army Research Laboratory
Cleveland, Ohio 44135–3191

Defence Advanced Research
Projects Agency
Arlington, Virginia 22203–1714

NASA Glenn Research Center
Cleveland, Ohio 44135–3191

10. SPONSORING/MONITORING AGENCY REPORT NUMBER

NASA CR—2000-209909
ARL–CR–447

11. SUPPLEMENTARY NOTES

12a. DISTRIBUTION/AVAILABILITY STATEMENT

Unclassified - Unlimited
Subject Category: 37   Distribution: Standard

This publication is available from the NASA Center for AeroSpace Information, (301) 621–0390.

12b. DISTRIBUTION CODE

13. ABSTRACT (Maximum 200 words)

The use of face gears in power transmission and drive systems has a significant number of benefits. Face gears allow a variety of new transmission arrangements as well as high reduction ratio capability. This leads to drive system weight reduction and improvements in performance. In this work, basic information about the design and analysis of face gear drives is presented. The work considers face gears in mesh with spur involute pinions for both intersecting axes and offset drives. Tooth geometry, kinematics, generation of face gears with localized bearing contact by cutting and grinding, avoidance of tooth undercutting, avoidance of tooth pointing, tooth contact analysis, and algorithms for the simulation of meshing and contact are all topics which are discussed. In addition, applications of face gear drives are presented. Included are design uses in aerospace applications such as helicopter transmissions, split-torque face gear arrangements, comparisons of face gears with bevel gears, and general design considerations.

14. SUBJECT TERMS

Gears; Geometry; Contact; Design; Face-gears

15. NUMBER OF PAGES

107

16. PRICE CODE

A06

17. SECURITY CLASSIFICATION OF REPORT	18. SECURITY CLASSIFICATION OF THIS PAGE	19. SECURITY CLASSIFICATION OF ABSTRACT	20. LIMITATION OF ABSTRACT
Unclassified	Unclassified	Unclassified	